ROLE OF T-TYPE Ca^{2+} CHANNELS IN LYMPHATIC PACEMAKING

A Dissertation

presented to

the Faculty of the Graduate School

at the University of Missouri-Columbia

In Partial Fulfillment

of the Requirements for the Degree

Doctor of Philosophy

---

by

KIM HUNG THIEN TO

Dr. Michael J. Davis, Research Advisor

MAY 2017

The undersigned, appointed by the dean of the Graduate School, have examined the dissertation entitled

ROLE OF T-TYPE Ca^{2+} CHANNELS IN LYMPHATIC PACEMAKING

presented by KIM HUNG THIEN TO

a candidate for the degree of doctor of philosophy,

and hereby certify that, in their opinion, it is worthy of acceptance.

Professor Michael J. Davis

Professor Michael A. Hill

Professor Virginia H. Huxley

Professor Steven S. Segal

Professor Kevin D. Gillis

ACKNOWLEDGEMENTS

I am grateful to learn about gratitude. I feel thankful for the support that I received from many scientists at Mizzou. Their work in microcirculation has inspired me and has laid the foundation for the work on lymphatic vessels that I am about to report.

First, I am tremendously grateful to Dr. Michael John Davis (MJD), my mentor. He is constantly a leader in his field who has lived and leads by model. In my Master's, when performing femoral artery ligation, I believed that there were only a vein, an artery and a nerve, but not lymphatic vessels in the femoral bed. Knowing very little about the lymphatic vessels, I was fortunate to be allowed to work in Dr. Davis' laboratory and interact with many experienced and knowledgeable scientists, and experience the exponential growth of the lymphatic area. In this project, he also helped me with all the experiments on popliteal lymphatics from transgenic mice. He taught me to read and listen to scientific views with a grain of salt and to be ready to rigorously question and revisit the established concepts. He also let me go to many exciting professional conferences and introduced me to other renown scientists. Thanks to his mentoring, I have grown so much personally and professionally and there will be not enough words to describe the fortune I have received during my PhD training with Dr. Davis in his laboratory.

Second, I am also profoundly grateful for the interaction I get with my dissertation committee members, Dr. Virginia Huxley, Dr. Steven Segal, Dr. Michael Hill, Dr. Kevin Gillis and Dr. Alan Parrish. They have given me constructive feedback to help my project and me to grow professionally and provided me with examples of their working and living in science.

Third, I would like to thank the support from current and past members in Dr. Davis' laboratory. I treasure the opportunity to work as team in which I am the least experienced. Dr. Peichun Gui especially taught me how to digest collecting lymphatic vessels and patch-clamp technique. Dr. Min Li patiently showed me how to perform biomolecular techniques such as PCR and Western blot and how to maintain and develop transgenic mouse lines. Dr. Jorge A. Castorena-Gonzalez (JAC) kindly showed me how to use confocal microscopy with care and how to understand the application side of physics in biomedical science. I also enjoy the interaction with Dr. Scott D. Zawieja (SDZ) and he has provided me with many innovative ideas. I am also grateful to the interaction with Ms. Shan-yu Ho, our laboratory manager, who taught me about laboratory management by keeping the laboratory and its activities in an organized order. Finally, Dr. Joshua Scallan, a past member of Davis' laboratory, provided important guidance for my several first years of PhD training.

TABLE OF CONTENTS

LIST OF FIGURES

Figure **Page**

LIST OF TABLES

Table **Page**

LIST OF ABBREVIATIONS

Ach	acetylcholine
ACTB	β-actin
AP	action potential
B	brain
bp	base pair
BayK	Bay K8644
cGMP	cyclic guanosine monophosphate
CCBE-1	collagen and calcium-binding epidermal growth factor domain containing protein 1
CHO	Chinese hamster ovarian cell
CICR	calcium-induced calcium release
CPI-17	17-kDa protein kinase C-potentiated inhibitory protein
DAG	diacylglycerol
DAPI	4’,6-diamidino-2-phenylindole
DHP	dihydropyridine
DKO	double knock-out
DMSO	dimethylsulphoxide
ECM	extracellular matrix
EGTA	ethylene glycol tetraacetic acid
ERK	extracellular signal-regulated kinase
ESAM	endothelial cell-selective adhesion molecule
ET-1	endothelin 1

eNOS	endothelial nitric oxide synthase (NOS3)
FAK	focal adhesion kinase
Flt4	Fms-related tyrosine kinase 4
Fura 2-AM	fura 2-acetoxymethyl ester
GAP	GTPase activating protein
GAPD	glyceraldehyde-3-phosphate dehydrogenase
GI tract	Gastrointestinal tract
GJC	gap junction channel
GPCRs	G protein-coupled receptors
GTP	guanosine triphosphate
G-V	conductance-voltage relationship
HEK	human embryonic kidney cell
HEPES	4-(2-hydroxyethyl)-1-piperazineethanesulfonic acid
h	hour
HRP	horseradish peroxidase
K_{ATP}	ATP-sensitive K^+ channel
K_{Ca}	Ca^{2+}-activated K^+ channel
K_v	voltage-gated K^+ channel
K_{IR}	inward rectifier K^+ channel
IAL	inguinal-axillary lymphatic
ICC	interstitial cell of Cajal
iNOS	inducible nitric oxide synthase
i.p.	intraperitoneal

IP_3	inositol 1,4,5-triphosphate
IP_3R	inositol 1,4,5-triphosphate receptor
JAM-A	junctional adhesion molecule A
MLC-20	20 kDa myosin light chain
LEC	lymphatic endothelial cell
LSM	lymphatic smooth muscle
LV	lymphatic vessel
MAPK	mitogen-activated protein kinase
min	minute
MLCK	myosin light chain kinase
MLCP	myosin light chain phosphatase
mRNA	messenger ribonucleic acid
ms	millisecond
mTOR	mechanistic target of rapamycin
MYPT1	myosin phosphatase targeting subunit 1
NFAT5	nuclear factor of activated T-cells 5
NO	nitric oxide
PBS	phosphate buffered saline
PIP_2	phosphatidylinositol 4,5-bisphosphate
PKA	protein kinase A
PKC	protein kinase C
PKG	protein kinase G or cGMP-dependent protein kinase
PL	popliteal lymphatic

PLC	phospholipase C
PCR	polymerase chain reaction
PPS	physiological phosphate solution
RASA1	P120 RAS GTPase-activating protein 1, rasGAP or RAS p21 protein activator 1
RT	room temperature
ROCK	Rho-associated kinase
RyR	ryanodine receptor
SDS-PAGE	sodium dodecyl sulfate polyacrylamide gel electrophoresis
sec	second
SEM	standard error of the mean
SERCA	sarcoplasmic reticulum calcium transport ATPase
SMA	smooth muscle α-actin
rbU-SMC	rabbit urethra smooth muscle cell
SMMHC	smooth muscle myosin heavy chain
Sox18	Sex determining region of Y-chromosome-related HMG box
SR	sarcoplasmic reticulum
STD	spontaneous transient depolarization
TBST	Tris-buffered saline with Tween® 20
TMEM16A	transmembrane protein 16A
TRPM	transient receptor potential melastatin
VGCC	voltage-gated Ca^{2+} channel
v/v	volume/volume

VIP	vasoactive intestinal peptide
WT	wild-type
ZO-1	tight junction protein 1

ROLE OF T-TYPE Ca^{2+} CHANNELS IN LYMPHATIC PACEMAKING

Kim Hung Thien To

Dr. Michael J. Davis, Dissertation Supervisor

ABSTRACT

Lymphatic smooth muscle (LSM) contracts spontaneously, actively returning interstitial fluid through a network of lymphatic capillaries and collecting lymphatic vessels to the great veins. Dysfunctional lymphatic contractions can impair lymph transport in lymphatic-related diseases such as lymphedema. Understanding the pacemaking mechanism of LSM that underlies active lymph transport is essential for therapeutic targeting of lymphedema. Based on experiments using pharmacological inhibitors, current literature posits that T-type voltage-gated Ca^{2+} channels (T-channels) play a role in controlling the pacing of lymphatic contractions, i.e., the contraction frequency, while L-type voltage-gated Ca^{2+} channels (L-channels) play a role in controlling the strength of lymphatic contractions, i.e., the contraction amplitude. However, non-specific effects of currently available T-channel inhibitors, especially on L-channels, can confound the understanding of T-channel role in lymphatic pacemaking. Therefore, using transgenic mouse models as an alternative approach to test the role of T-channels, I hypothesized that genetic deletion of T-type Ca^{2+} channels would decrease the frequency of lymphatic contractions but not the amplitude. First, I tested for the presence of T-channels in lymphatic vessels from both rat and mouse, and then more specifically in isolated single mouse LSM cells; second, I tested the effects of commonly-used T-channel inhibitors on lymphatic pacemaking and/or contraction in both rat and mouse vessels; and finally, I

investigated the effect of genetic deletion of specific T-channel isoforms in mice on lymphatic pacemaking and contraction strength.

First, RT-PCR and immunostaining were performed on whole lymphatic vessels to test for the expression of T-channels at mRNA and protein levels. Rat mesenteric lymphatics, mouse popliteal lymphatic vessels (PLs) and mouse inguinal-axillary lymphatic vessels (IALs) showed the mRNA expression of $Ca_v3.1$ and 3.2, two of the three isoforms of T-channels, along with $Ca_v1.2$, the isoform of the L-channel prevalent in cardiac muscle and blood vessels. Likewise, in LSM cells isolated from mouse PLs and IALs, RT-PCR revealed the expression of $Ca_v3.1$ and 3.2. In mouse IALs, immunostaining consistently revealed the protein expression of T-channel isoforms $Ca_v3.1$ and 3.2 along with L-channel isoform $Ca_v1.2$ colocalized with the smooth-muscle α-actin (i.e., in LSM cells). Moreover, patch-clamp recordings in single LSM cells isolated from rat mesenteric, mouse PLs and IALs showed functional evidence of current through voltage-gated Ca^{2+} channels that was blocked by 1μM nifedipine, an L-channel inhibitor, along with a persistent nifedipine-insensitive current that had fast kinetics and was blocked by 1mM Ni^{2+}, a frequently used T-channel inhibitor.

Second, pharmacological inhibitors were tested on isolated, cannulated and pressurized *ex vivo* lymphatic vessels from rat and mouse. Consistent with the findings of Lee *et al.* (2014) on rat mesenteric lymphatics, mibefradil, another conventional T-channel inhibitor, inhibited the contraction frequency (IC_{50}=66nM) at a lower dose than that required to inhibit contraction amplitude (IC_{50}=423nM). However, in contrast to their findings, treatment of rat mesenteric lymphatics with Ni^{2+} inhibited both amplitude and frequency at similar doses (IC_{50}=248μM and 279μM, respectively). In wild-type (WT)

mouse IALs and PLs, increasing doses of Ni^{2+} progressively reduced contraction amplitude (IC_{50}=66μM and 110μM, respectively), while leaving the frequency unchanged until the contractions were completely inhibited. In WT PLs, TTA-A2, a more recently developed T-channel inhibitor, had only a modest effect on contraction amplitude (IC_{50}=1.3μM) without changing the contraction frequency. Similarly, treatment with nifedipine, a specific L-channel inhibitor, gradually attenuated contraction amplitude (IC_{50}=43.3nM), suggesting that the effect on amplitude of T-channel inhibitors Ni^{2+} and TTA-A2 could be due to off-target effects on L-channels.

Having established that pharmacologic inhibition of T-channels in this context is unreliable, I turned to genetic methods allowing deletion of specific T and L-channel isoforms. Surprisingly, smooth muscle-specific deletion of $Ca_v1.2$ (L-channels) rendered PLs and IALs quiescent without spontaneous lymphatic contractions, suggesting their potential contribution to both lymphatic frequency and contraction strength; no residual contractions were mediated by T-channels. In $Ca_v3.1$-null mice and $Ca_v3.2$-null mice, IALs exhibited no significant differences in functional contractile parameters (including frequency and amplitude) compared to WT vessels over a wide range of pressures. Likewise, PLs from $Ca_v3.1^{-/-}$ mice exhibited no significant defects in the contractile response to pressure, to the L-channel inhibitor nifedipine, or even to the endothelial-dependent inhibitor acetylcholine. These findings conflict with the currently established view that T-channels regulate the frequency of lymphatic pacemaking and that L-channels contribute only to the contraction strength.

In summary, I confirmed the functional expression of T-channels in both rat and mouse LSM, but selective genetic deletion of either $Ca_v3.1$ or $Ca_v3.2$ T-channel isoforms

did not produce a measurable functional defect in lymphatic vessel pacemaking or contraction. My findings conflict with the current established view that T-channels control lymphatic pacemaking and L-channels determine lymphatic contraction strength; a definitive role for T-channels in LSM function remains unknown.

CHAPTER 1: INTRODUCTION

1.1 Lymphedema

Lymphedema describes the swelling of a body part due to accumulation of protein-rich lymph fluid in the interstitial space when lymph transport is impaired (Lee *et al.*, 2011). As a consequence of lymph transport dysfunction, lymphedema reflects a severe imbalance between microvascular filtration rate to the interstitium and lymph transport, leading to tissue edema. Lymph transport refers to lymph uptake by peripheral lymphatic capillaries and active lymph pumping by the afferent and efferent collecting lymphatic vessels; the latter will be the focus of my dissertation. One of the main problems in lymphedema is the inefficiency of spontaneous lymphatic contractility driving the active lymph pump (Olszewski, 2008). The term lymphedema provides little information regarding the etiology of the condition and reflects a limited knowledge of the function or dysfunction of the underlying lymphatic system when compared with the detailed nomenclature of cardiovascular diseases (e.g., angina pectoris, diastolic cardiac dysfunction, systolic cardiac dysfunction, hypertension, atherosclerosis, etc.). Fortunately, there are now a growing number of studies on lymphedema, based on statistics found on pubmed.org for the period from 1935 to 2016. This recent emphasis on studies of the lymphatic system is predicted to have a transformative impact on the well-being of patients with lymphatic-related diseases in general and lymphedema in particular (Lee *et al.*, 2011).

1.1.1 Epidemiology

Lymphedema afflicts over 250 million people worldwide (Zuther, 2009). Since our understanding of lymphedema and lymphatic system is relatively limited, the number of

patients inflicted by lymphedema and lymphatic-related disorders, including lymphedema, is severely underestimated due to the lack of timely and objective diagnostics and adequate attention from health professionals. Filariasis is the most prominent cause of lymphedema in developing countries; while in Western countries, lymphedema is a common complication after surgical cancer treatment involving lymph node removal, biopsy and radiation. In the USA, more than 10 million patients suffer from lymphedema and this number is more than the number of patients with multiple sclerosis, Parkinson's disease, and AIDS combined (http://lymphaticnetwork.org/).

1.1.2 Classification

1.1.2.1 Primary lymphedema

Primary lymphedema, also called hereditary lymphedema, is caused by innate abnormalities in lymphatic structure and development due to genetic mutation. Primary lymphedema affects up to 1:6,000 live births (Rockson, 2008). The age at onset of the disease can vary; it can appear at birth or even late into adulthood. In other words, in some forms of hereditary lymphedema, a defect in the lymphatic system has appeared at birth, but due to the slow progression of the disease and the lack of proper diagnosis, lymphedema becomes visible only at a later stage of life. Although these innate lymphatic defects are considered uncommon, their study has contributed greatly in the scientific knowledge of normal lymphatic development and function. Primary lymphedema can be associated with mutation(s) in genes that are key in lymphatic development, such as FOXC2 (lymphedema–distichiasis), EphrinB2, FLT4 (Milroy disease), VEGF-C, PROX-1, CCBE1 (Hennekam disease), GJC2 (Cx47-Meige disease), GJA1 (Cx43-myelodentodigital dysplasia), SOX-18 (hypotrichosis–telangiectasia–lymphedema).

Furthermore, lymphatic developmental disorders can be associated with combined capillary malformation-arteriovenous malformation (Patel *et al.*, 2012). I now discuss three representative examples of primary lymphedema.

Milroy's disease is a congenital lymphedema transmitted in an autosomal dominant pattern. It is caused by a missense mutation in FLT4 (encoding VEGFR-3), which inactivates the tyrosine kinase domain and interferes with VEGFR-3 signaling (Karkkainen *et al.*, 2000). VEGFR-3 is expressed in lymphatic endothelium and is important for lymphangiogenesis. Milroy's disease is characterized by lower limb lymphedema (Brice *et al.*, 1993). $Flt4^{-/-}$ mice die in embryo. Transgenic mice, K14-VEGFR-3−Ig, in which dermal VEGFR-3 is specifically inhibited, develop lymphedema with swelling of the feet, fat accumulation and dermal fibrosis (Mäkinen *et al.*, 2001).

Lymphedema-distichiasis is an autosomal-dominant condition characterized by lower limb lymphedema, defects in lymphatic and venous valves, and an aberrant double row of eyelashes. It is caused by frameshift mutations of the forkhead transcription factor FOXC2. $Focx2^{-/-}$ mice, lacking lymphatic intraluminal valves, die embryonically (Petrova *et al.*, 2004). $Foxc2^{+/-}$ mice exhibit lymphatic hyperplasia and have at least some incompetent lymphatic valves (Kriederman *et al.*, 2003). Conditional deletion of Foxc2 in the lymphatic endothelium causes lymphatic valve regression, focal vascular lumen collapse and lethality (Sabine *et al.*, 2015). Patients with lymphedema distichiasis exhibit dysfunctional lymphatic and venous valves characterized by back flow during ultrasound imaging (Brice *et al.*, 2002).

Cantu syndrome is a complex multi-organ disorder with mild learning disability, skeletal muscle, cardiovascular abnormalities, and lymphedema. The underlying cause is a

gain-of-function mutation in K_{ATP} channels either the $K_{ir}6$ ion channel subunit or the sulfonylurea receptor. A portion of Cantu syndrome patients develops delayed lymphatic drainage accompanied by dilated lymphatic vessels (Grange *et al.*, 2014). Mice with gain-of-function mutations in K_{ATP} channels showed significant lymphatic contractile dysfunction due to chronically hyperpolarized LSM, which leads to inhibition of spontaneous lymphatic pumping (M. J. Davis and C. G. Nichols, unpublished data). This is the only reported instance of a primary lymphedema due to contractile dysfunction of LSM.

1.1.2.2 Secondary lymphedema

Secondary lymphedema makes up to 90% of lymphedema cases in the USA (Zuther, 2009). Secondary lymphedema refers to the acquired damage of the lymphatic system arising from surgical removal of lymph nodes, radiation, infection, filariasis and/or cancer. Filariasis, the most common cause of secondary lymphedema worldwide, refers to infection with parasites of the family Filariodidea. The worms migrate to and mature in the lymphatic vessels, causing lymphatic obstruction, initiating an immune response and activating vascular endothelial growth factors, therefore promoting lymphatic hyperplasia and inflammation. In Western countries, the most prevalent form of secondary lymphedema occurs after breast cancer treatment, especially after removal or biopsy of axillary lymph nodes. Furthermore, trauma and chronic venous diseases can also cause secondary lymphedema (Lee *et al.*, 2011). All cancer survivors, such as those treated for melanoma, head, neck, breast, prostate and ovarian cancers, are susceptible to developing lymphedema. Among breast cancer survivors, the incidence of upper extremity swelling is up to 56% two years after surgical intervention (Paskett *et al.*, 2007). 100% of patients

treated for head and neck cancers will develop lymphedema (http://lymphaticnetwork.org/). Upper-extremity lymphedema usually occurs after axillary lymph node dissection in breast cancer treatment. Lower-extremity lymphedema usually occurs after inguinal lymph node dissection in melanoma as well as in cancers in the lower half of the body, such as prostate and ovarian cancers. The extent of surgery, i.e., number of lymph nodes affected and severity of tissue damage correlates with the risk of developing lymphedema (Lee *et al.*, 2011). Lymphedema can occur early on but also up to 30 years after the surgical procedures (Brennan & Weitz, 1992). Patients with secondary lymphedema have reduced lymph pumping compared to healthy individuals (Unno *et al.*, 2010). Furthermore, lymphedema is usually more prevalent in women than men. This consistent difference may point to a potential role of sex hormones or sex differences in the development of lymphedema (Cambria *et al.*, 1993; Greene *et al.*, 2015). Chronic venous insufficiency in the lower extremities can also compromise lymphatic function and lead to lympho-venous edema (Rasmussen *et al.*, 2016).

1.1.3 Clinical symptoms

Lymphedema usually affects a localized body region such as an upper or lower extremity. The onset of lymphedema is often neglected. However, it can be suddenly initiated by an inflammatory incident such as local infection or injury (https://www.cancer.gov/about-cancer/treatment/side-effects/lymphedema/lymphedema-hp-pdq). At-risk patients are recommended to be evaluated for cellulitis because this inflammatory condition can further damage the lymphatic system and leading to the onset of lymphedema (Quirke *et al.*, 2016).

Table 1. Classification of lymphedema severity

Stage	Clinical Presentation
I	Pitting edema that resolves with elevation
II	Pitting edema that does not subside with elevation alone
III	Nonpitting edema with overlying skin changes

(Adapted from (Cuzzone *et al.*, 2014))

The progression of lymphedema can be divided into three or more different stages as formulated by the International Society of Lymphedema (Table 1; Cuzzone *et al.*, 2014). Early stages of lymphedema manifest with pitting edema that attenuates during recumbence and worsens toward the end of the waking day (Thomas-MacLean *et al.*, 2005). Over time, the swelling becomes permanent, with changes in underlying tissue architecture such as fibrosis and adipose tissue deposition. The skin and subcutaneous tissue become thick and firm, developing non-pitting edema with a peau d'orange (orange peel) appearance (Bergan *et al.*, 2011). The hallmark of lymphedema is dilated collecting lymphatics (mega-lymphatics), however the delayed length of time between the first sign of mega-lymphatics/lymphatic remodeling and the first clinical sign of lymphedema is unknown. Patients with lymphedema are susceptible to recurrent episodes of infection and inflammation, which can be part of a vicious cycle where dysfunction in lymphatic system impairs lymph return and the immune response, as illustrated in Figure 1.

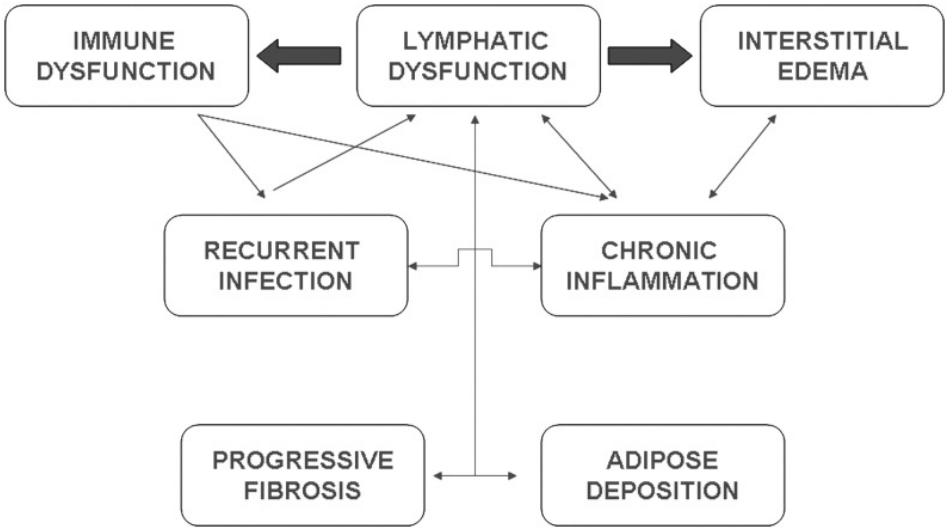

Figure 1. Vicious cycle in lymphedematous tissue. In lymphedematous tissue, lymphatic dysfunction can lead to fluid accumulation in the interstitial space (interstitial edema) along with immune cells causing immune dysfunction. Immune cells cannot travel to lymph nodes for antigen presentation, but rather they are trapped locally and initiate local excessive inflammation. When inflammation is chronic, the affected region is prone to recurrent infection, inducing progressive fibrosis and adipose deposition. Accumulation of fibrotic and adipose tissue can further impede lymphatic function and impair the role of lymphatics in lymph return and immune surveillance (Rockson, 2013).

Mechanistically, lymphedema is initiated by impaired lymphatic transport, leading to lymph stagnation, an overactivated local immune response, tissue swelling and fibrosis. After lymphatic transport becomes dysfunctional, fluid and accompanying proteins and immune cells accumulate in the interstitial space. As a result, oncotic pressure in the interstitial compartment increases, leading to retention of more fluid. The accumulated interstitial fluid and macromolecules such as lipids, sugars and proteins create a favorable environment for pathogens and bacteria, attracting and activating immune cells. Further,

overactivated immune cells that are trapped in the interstitial space can cause damaging inflammation (Rockson, 2013). The events occurring in lymphedematous limbs reflect a crucial role of lymph transport in the immune response and removal/clearance of lymph contents.

1.1.4 Imaging diagnostics

The common diagnoses of lymphedema are based on volume measurement of the affected body region, including circumferential tape measurement, water displacement volumetry, infrared arm perometry and bioelectrical impedance spectroscopy (Gaw *et al.*, 2011; Bundred *et al.*, 2015). Imaging diagnostics can be used alongside physical examination to detect mega-lymphatics, dermal backflow and lymph/diagnostic tracer clearance. In parallel with the search for lymphedema therapeutics, the development of imaging techniques for assessing lymphatic function is necessary for a deeper understanding of lymphatic transport mechanisms and for evaluating therapeutic effectiveness *in vivo* and in clinical settings. Common imaging modalities are lymphography, radionuclide lymphoscintigraphy, and indocyanine near-infrared fluorescence angiography (Munn & Padera, 2014).

Lymphography is an imaging method for lymphatic vessels similar to angiography, which uses a contrast medium such as iodinated ethyl ester and iodinated glycerol ester, to fill the lymphatic vascular network (Guermazi *et al.*, 2003). Lymphography can highlight all structures of the lymphatic network: lymphatic capillaries, lymphatic collectors and lymph nodes. In contrast to angiography, where the contrast agent can be injected in any major artery/vein and will be spread to the entire blood circulatory tree, in lymphography the contrast agent is required to be injected at multiple sites near peripheral lymphatic

capillaries, downstream of the lymphatic tree, and can only spread locally. This method used to be the standard diagnostic to detect lymphatic leaks, obstructions and structural abnormalities in cancers such as Hodgkin's lymphoma, as well as to detect disorders of lymph flow. However, the use of this invasive and time-consuming technique has been curtailed because of its association with inflammation, scarring, and atrophy of the remaining healthy lymphatic vessels (Guermazi *et al.*, 2003; Morrell *et al.*, 2005).

Lymphoscintigraphy is the current gold standard imaging modality for lymphedema diagnostics in clinical settings to measure lymph transport, lymphatic anatomy and possible obstruction (Weiss *et al.*, 2014). It utilizes a gamma radiation camera to detect a radioactive tracer such as ^{99m}-technetium injected intradermally into lymphadematous tissue and a control region to visualize the difference in the structure of lymphatic network, tracer clearance rate and potential dermal backflow. However, the radioisotope used in lymphoscintigraphy is teratogenic and is contraindicated for women during pregnancy (Unno *et al.*, 2008).

Near-infrared (NIR) fluorescence angiography is a new non-invasive and inexpensive method, which is less time-consuming than previous methods and is the only method that can directly capture the phasic contractions of collecting lymphatic vessels. Infrared light can penetrate tissue better than visible light because penetration depth increases when the illumination wavelength increases. However, low penetration depth (i.e., up to several millimeters into soft tissues) remains the major limitation of this optical imaging technique due to tissue absorption and light scattering (Sevick-Muraca *et al.*, 2014). Furthermore, the FDA-approved dye indocyanine green, the most common NIR fluorescent tracer, has potential negative effects on lymphatic contractility (Gashev *et al.*,

2010; Aldrich *et al.*, 2012). However, novel inert PEG-conjugated NIR dyes have been introduced recently to study mouse lymphatic contractions *in vivo*. The application of NIR imaging modalities, enabling capture of real-time, high resolution images of the lymphatic system, potentially can be applied in lymphedema diagnostics as well as in *in vivo* lymphatic research (Chong *et al.*, 2016).

1.1.5 Current treatments

Currently available treatments for lymphedema are palliative and indirect, merely acting to alleviate symptoms and limit its progression and inflammatory complications rather than improving lymphatic function directly. Depending on the stage and severity of lymphedema, treatments will range from compression therapy, surgical intervention, and pharmacological approaches.

The gold standard treatment for lymphedema is combined decongestive therapy using compression garments/devices that apply high external pressure, up to 120 mmHg (Lee *et al.*, 2011) to passively and extrinsically increase lymph transport. This approach can be counterproductive as the applied pressure exceeds lymphatic intraluminal pressure, which is inherently low, causing further lymph obstruction (Modi *et al.*, 2007). The treatment is composed of an intensive initial phase and then a maintenance phase. The first stage usually requires a hospital visit and can involve pneumatic sequential pumps in combination with multilayer bandaging, manual lymphatic drainage, decongestive exercise, elevation of the affected limb, skin care. This initial stage attempts to reduce the size of the lymphedematous limb, and undo any reversible fibrosis and tissue remodeling. Overall, this stage can increase the mobility of the lymphedema patient. A long-term second stage is important to maintain the achievement of the initial treatment and prevent

the progression of lymphedema, its relapse and complications (Olszewski, 2011). A second phase of self-treatment with the above-mentioned techniques at a lower, maintenance-level intensity requires the purchase of expensive medical devices and compression garments (Lee *et al.*, 2011; Godoy *et al.*, 2010).

Patients unresponsive to the above-mentioned compression treatments may benefit from more invasive treatments such as reconstructive surgery (lymphaticovenous anastomosis), excisional surgery (vascularized lymph node transfer), and liposuction to reduce adipose accumulation and hypertrophy (Brorson, 2012). In patients with end-stage lymphedema (i.e., stage III in Table 1), especially when the major structural change in lymphedematous regions is expansion of adipose tissue rather than fluid accumulation, liposuction can be used as part of a treatment combination to alleviate lymphedema progression and improve quality of life. The possible disruptive effects of liposuction on lymphatic networks have not been studied.

Recently, there are several pharmacological candidates to treat lymphedema and lymphatic-related diseases including: topical tacrolimus (Gardenier *et al.*, 2015), rapamycin (Ando *et al.*, 2013), VEGF-C (Jin *et al.*, 2009) and benzo-pyrones such as coumarin and flavonoid derivatives (Badger *et al.*, 2004). Furthermore, topical or prophylactic antibiotic treatment is also administered at the earliest signs of infection, as minor as a cut or a wound, to prevent the risk of infection relapse and expansion. Cellulitis, an acute inflammation of the dermis and subcutaneous areas, can also be prevented with antibiotics (Swartz, 2004). None of the above-mentioned drugs directly target collecting lymphatic vessel function or are FDA-approved for lymphedema treatment, suggesting that

a deeper understanding of lymphatic transport might provide a therapeutic target to directly improve lymphatic function to resolve lymphedema.

In summary, both function and dysfunction of lymphatic system remain poorly understood. Lymphatic-related disorders lack efficient diagnoses for early detection and direct therapeutics. Therefore, a deeper understanding of lymphatic transport mechanisms may contribute to the development of therapeutics to improve the lymphatic function.

1.2 Lymphatic transport

The lymphatic system is composed of a blind-ended lymphatic vessel network and interconnected lymph nodes densely located across the body. Lymph nodes are small, bean-shaped glands that filter lymph transported by lymphatic vessels. The lymph nodes and lymphoid organs are major sites of antigen presentation and activation of T- and B-lymphocytes. Lymphatic capillaries and collecting lymphatic vessels actively transport lymph containing interstitial fluid, protein and immune cells centrally through a chain of lymph nodes and back to the great veins of the blood circulatory system (Aspelund *et al.*, 2015). After a meal, the mesenteric lymphatic vessels are also the main route to transport chylomicrons from the intestinal villi to the blood circulation (Hall & Guyton, 2015).

The lymphatic system has three primary roles — immune surveillance, lipid transport and fluid homeostasis — that interact highly with each other. Failure of one component sequentially entrains failure in the other two, analogous to a domino effect. For example, in lymphedema patients, failure of lymph transport and an imbalance in fluid homeostasis leads to lipid accumulation in the affected region and a weakened immune defense (Unno *et al.*, 2010). In lipedema patients suffering from chronic fat deposition in lower extremities, lymph flow slows and is accompanied by an

abnormal lymphoscintigraphic pattern (i.e., abnormal lymph flow pattern), suggesting a connection between pathological lipid deposition and lymphatic function (Bilancini *et al.*, 1995). Obese individuals have reduced lymph transport and retrograde lymph flow (Weitman *et al.*, 2013). ApoE$^{-/-}$ mice, with genetic deletion of apolipoprotein E, are born with chronically high cholesterol levels (Pendse *et al.*, 2009). With long-term exposure to elevated circulating free fatty acid and lipoproteins, the collecting lymphatics degenerate and muscle cell coverage becomes sparse, thereby hampering lymph transport (Lim *et al.*, 2009). As a result, the lymphatic role in immunity is compromised, leaving the periphery with an accumulation of dendritic cells, other immune cells and macromolecules, and therefore resulting in systemic inflammation (Lim *et al.*, 2009). Similarly, obese mice fed a high fat diet show defective lymph transport, apparently the consequence of architectural changes in collecting lymphatics (Weitman *et al.*, 2013; Blum *et al.*, 2014). Mice engineered to have abnormal immune responses, e.g., to induce rheumatoid arthritis (Liang *et al.*, 2015) or inflammatory bowel disease (Cromer *et al.*, 2015), also have reduced lymph flow. These mouse models correspond to human patients with rheumatoid arthritis (Grillet and Dequeker, 1987) and inflammatory bowel disease (Monk and Mortimer, 1999) that are prone to developing lymphedema.

The focus of this dissertation will be on contractile function of collecting lymphatic vessels, a critical determinant of lymph transport. In the following section I will concentrate on describing the role of the lymphatic system in fluid homeostasis, and will not discuss its roles in immune surveillance and fat absorption further.

During nutrient and oxygen exchange between capillaries and surrounding tissues, a fraction of blood plasma constantly percolates into the interstitial space through the

semipermeable blood capillaries and post-capillary venules. The network of lymphatic vessels, including initial and collecting lymphatic vessels, has an important role in the uptake of interstitial fluid and its transport back to the blood circulatory system. It is estimated that in an average 65kg-male, a total plasma volume of around 3L (Hall and Guyton, 2015) extravasates from the blood vasculature every 9 hours (Levick & Michel, 2010). As a result, in a day, the lymphatic network returns 8-12L of fluid and 20-30g of protein back to the blood circulatory system (Renkin, 1986). Contrary to information commonly found in textbooks, the majority of the extravasated interstitial fluid and macromolecules are re-absorbed by the lymphatic capillaries rather than by post-capillary venules, except in the kidney and the intestinal mucosa where venous fluid re-absorption is maintained by local epithelia (Levick & Michel, 2010). Thus it is not surprising that lymphatic developmental defects in mice cause massive embryonic edema and prenatal death (Wigle & Oliver, 1999; Karkkainen *et al.*, 2004; François *et al.*, 2008).

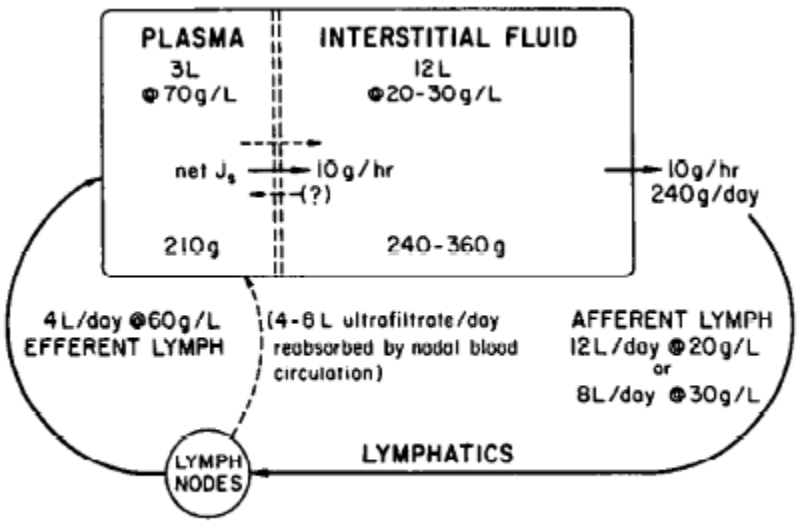

Figure 2. Lymph movement in an average human

Reprint with permission from Renkin, 1986

1.2.1 Initial lymphatic vessels

Initial lymphatic vessels, also called lymphatic capillaries, are formed by blind-ended tubes of flattened lymphatic endothelial cells (LECs) lacking a muscle layer. The thinness of the initial LEC layer enhances the permeability of lymphatic capillaries to immune cells and macromolecules (Scallan *et al.*, 2010) and lymph formation. Initial LECs have an oak-leaf shape and are slightly overlapped at their edges, forming a primary valve system. The borders of LECs are linked by button-like junctions that are rich in tight-junction-associated proteins such as ZO-1 (zonula occludens-1), occludin, claudin-5, JAM-A, ESAM, along with vascular endothelial cadherin (VE-cadherin) at adherens junctions (Kakei *et al.*, 2014; Baluk *et al.*, 2007). The tips of the lymphatic capillaries have zipper-like junctions with similar tight-junction protein profiles with the above-mentioned button-like junctions. The high permeability of initial lymphatics is dictated by their special features: a thin monolayer of LECs, button-like junctions between adjacent LECs, a discontinuous basement membrane, and a lack of muscle cell coverage.

1.2.2 Collecting lymphatic vessels

Lymphatic capillaries coalesce into larger collecting lymphatic vessels, where lymphatic vessels transit from a role of taking up lymph to a role of transporting lymph. Therefore, the anatomy of collecting lymphatic vessels is accordingly different from that of lymphatic capillaries. Collecting lymphatics have both LECs and LSM cells. The LEC layer is invested with at least one layer of smooth muscle cells with tight, zipper-like junctions and a continuous basement membrane (Baluk *et al.*, 2007). This special anatomical structure of the collecting lymphatics ensures their role in active lymph transport with minimal leakage to surrounding interstitial space. The pumping action of the

LSM provides active driving force to push lymph uphill against the gravitational pressure gradient.

When collecting lymphatics transport lymph centrally, pressure gradients throughout lymphatic tree are not favorable for lymph movement (Zawieja, 2009). Although the lymphatic system is usually referred as a drainage system (Aspelund *et al.*, 2016), the process of returning lymph against a hydrostatic pressure gradient is active rather than passive. In many tissues, interstitial fluid pressures are subatmospheric (slightly negative) to atmospheric (near 0cmH_2O) (Aukland & Reed, 1993). These negative pressures facilitate capillary exchange while opposing lymph formation. Textbook explanations emphasizing post-capillary venous reabsorption as the main source of interstitial fluid reuptake (Hall & Guyton, 2015), based on the Starling principle, have been tested vigorously but are challenged by more recent literature that lymphatic vessels are responsible for substantial fluid and solute uptake and thus critical for tissue fluid balance (Levick & Michel, 2010). Only a few pressure measurements in the initial and collecting lymphatic vessels in large animals, such as in cat and cow lymphatics (Zweifach & Prather, 1975; Ohhashi *et al.*, 1980) have been reported, due to challenges of making accurate pressure measurements in the lymphatic microvasculature. In most cases, the lymphatic intraluminal pressure is slightly positive. This pressure gradually rises up to ~10cmH_2O (Scallan *et al.*, 2016) as the lymphatics approach lymph nodes (Zweifach & Prather, 1975). Therefore, passive draining of lymph is not adequate to transport lymph uphill. How does the body override the opposing pressure gradient in the lymphatic network? A longstanding model (Levick & Michel, 2010), well supported by solid data, is that episodic changes in interstitial fluid pressure and lymphatic intraluminal pressure will produce a transient

positive pressure gradient in favor of central lymph movement. Extrinsic compression closes the primary valves and pushes lymph into the collecting lymphatic vessels. Additionally, active contractions of LSM also create a suction effect aiding lymph to move uphill. The adverse pressure gradient in the lymphatic tree is aggravated in large animals by the additional influence of larger gravitational forces on the lymph pressure. In an average human who spends almost two-thirds of his/her time in upright position, there is a potential hydrostatic pressure gradient of around 150cmH_2O between the feet and the subclavian veins, where the thoracic duct returns lymph to the blood circulatory system (Zawieja *et al.*, 2011). This pressure challenge is overcome in two ways: 1) segmentation of hydrostatic columns by secondary valves, and 2) lymph pumping machinery.

At regular spaces, two LECs form secondary bicuspid valves that only allow one-way, central lymph transport (Trzewik *et al.*, 2001). The functional unit of the collecting lymphatic between two consecutive secondary bi-leaflet valves is called a lymphangion. The hydrostatic column of lymph is thereby segmented by a series of unidirectional secondary valves to divide gravitational force up into smaller values. In human leg lymphatics, under a physiological hydration state, there are only a few milliliters of lymph in some lymphangions, while many others remain empty. Therefore, hydrostatic pressure is near zero in the lymphatics of an extremity even in the upright position (Olszewski, 2003). Intraluminal lymphatic valve opening and closing are closely regulated by pre- and post-valve pressures (Davis *et al.*, 2011). Once the output pressure rises above input pressure, the backsides of two LEC leaflets bulge inward to oppose each other and close the valves. The secondary valve system, therefore, normally allows lymph fluid to move

only in one direction, preventing backflow. The other determinant of lymph transport, i.e., lymph pump will be discussed in the next section.

1.3 Pump function of collecting lymphatic vessels

The active lymph pump that drives lymph through the lymphatic tree is composed of two components. One comes from rhythmic contractions of LSM cells in the walls of collecting lymphatic vessels, termed the intrinsic lymph pump. The other comes from cyclical compression and expansion movements of the surrounding tissues, termed the extrinsic pump. On average, the intrinsic pump accounts for 2/3 of the lymph driving force, and the extrinsic pump for the remaining 1/3 (Engeset *et al.*, 1977). Depending on body regions and the characteristics of surrounding tissues, the proportion of intrinsic and extrinsic pump contributions may vary across the lymphatic vascular tree. The extrinsic force is more important in the lymphatics of the heart, skeletal muscle, thorax and gut wall, while the intrinsic pump is crucial in other lymphatic vascular beds. Efficient lymph transport in some tissues may require both intrinsic and extrinsic pumps at a balanced ratio (Zawieja *et al.*, 2009). Thus, an excessive increase in external pressure, e.g., as occurs during lymphatic compression therapy, can be counterproductive, shifting this ratio out of the optimal balance, and potentially worsening lymphedema. Impairment of the intrinsic pump was observed in the legs of lymphedema patients (Olszewski, 2002). However, the current therapeutics for lymphedema do not target the intrinsic pumping mechanism of LSM. For example, the pneumatic pump or manual lymph drainage targets only on the extrinsic pumping mechanism. Thus, understanding of the intrinsic pumping machinery could provide a novel therapeutic target to enhance lymph transport, especially in lymphedema with dysfunctional collecting lymphatic contractions. Therefore, my

dissertation focuses on investigating the ionic mechanism of the intrinsic pump. Details of the intrinsic pump by LSM will be further described in the next section.

1.4 Function of lymphatic smooth muscle cells

Since collecting lymphatic vessels perform both pumping and conduit function, LSM has both rapid, phasic contractile activity similar to cardiac muscle, and a slower, tonic contraction similar to blood vascular smooth muscle. LSM possess a maximal shortening velocity of >2.0 lengths (L)/s, in between that of vascular smooth muscle (0.48L/s) and cardiac muscle (0.6-3.3L/s) (Zhang *et al.*, 2013). This functional property correlates with the finding that lymphatic smooth muscle expresses both striated and smooth muscle components (Muthuchamy *et al.*, 2003).

1.4.1 Functional similarities to arterial smooth muscle

LSM expresses smooth muscle myosin heavy chain (SMMHC), myosin light chain (MLC) and actin, characteristic of smooth muscle (Wang *et al.*, 2009; Muthuchamy *et al.*, 2003). Normally, lymphatic basal tone ranges from 10-20%, relatively lower than the average tone of arterioles (40-50%). Experimentally, like arterioles, collecting lymphatics develop a slow tonic contraction when warmed to body temperature in physiological solution. The lymphatics lose this tonic contraction in Ca^{2+} free solution, indicating that lymphatic tone depends on extracellular Ca^{2+}, as in arterioles. The tone of lymphatic vessels (i.e., basal tone) can be evaluated by calculating the difference between the diameter at the end of diastole and the maximal dilated diameter as a percentage of the maximal dilated diameter in Ca^{2+}-free physiological solution (Zawieja *et al.*, 2009).

In collecting lymphatics, as in arterioles, basal tone is maintained by a low basal level of intracellular Ca^{2+} that maintains a set balance of MLC kinase/MLC phosphatase

activity in response to physical and chemical stimulation in the surrounding milieu (Wang et al, 2009). In LSM, MLC and two forms of phosphorylated MLC: MLC-P and MLC-2P are expressed (Nepiyushchikh *et al.*, 2011). Inhibition of MLC kinase decreases tonic lymphatic contraction (Wang *et al.*, 2009; Nepiyushchikh *et al.*, 2011). Activation of MLC phosphatase can deactivate MLC and relax LSM. Rho kinase can inactivate MLC phosphatase by phosphorylation at the regulatory subunit MYPT-1 to promote tonic lymphatic contraction (Kurtz *et al.*, 2014).

Similar to arterioles, LSM also exhibits a myogenic response. In arterioles, myogenic tone is the phenomenon of decreasing vessel diameter in response to increasing stretch on the vessel wall, as would occur with an increase in intraluminal blood pressure. The myogenic tone of arterioles regulates peripheral resistance, blood pressure and blood flow. This mechanism protects downstream capillaries from changes in blood pressure to maintain proper capillary filtration rate. In lymphatic vessels, tonic contraction decreases lymphatic diameter, increases downstream lymphatic resistance, and decreases lymph flow out of a lymphatic vascular bed. Compared to arteriole tone, which is augmented with an increase in intraluminal pressure and vice versa (Meininger and Davis, 1992), the level of tone in lymphatics seems stable regardless of the intraluminal pressure level (Zawieja *et al.*, 2009). However, during a sudden step pressure increase, collecting lymphatics show myogenic constriction when they quickly expand and then regain a portion of tone over the course of one to two minutes (Davis *et al.*, 2009).

LSM also exhibits a myogenic constriction when output pressure of a two-valve segment is rapidly and selectively elevated: the segment upstream of the valve, which is protected from any change in pressure, progressively constricts in proportion to the rise in

output pressure, at least over a certain range. This lymphatic myogenic constriction appears to be important for proper valve closure to protect downstream lymphatic capillaries from retrograde lymph flow (Scallan *et al.*, 2013) and for preventing excessive lymphatic dilation when intraluminal pressure rises during inflammation or edema (Davis *et al.*, 2009).

1.4.2 Functional similarities to cardiac muscle

Similar to the heart, LSM expresses troponin I, T and C and cardiac actin (Muthuchamy *et al.*, 2003; Muthuchamy & Zawieja, 2008; Zolla *et al.*, 2015). LSM cells phasically contract as a muscle syncytium and fire repetitive action potentials (APs) like cardiac cells. The LSM cells are tightly connected by gap junctions (Kanady and Simone, 2012). When one of these cells is excited, the electrical signal will be propagated along the vessel length (Gui *et al.*, 2015).

Similar to cardiac muscle, the contraction of lymphatic muscle is driven by rhythmic firing of APs. Every lymphatic phasic contraction is preceded by an AP. A typical AP is preceded by a slow and gradual diastolic depolarization. Once membrane potential reaches threshold, a sharp 100ms potential spike from -40 to +5mV occurs, followed by a gradually declining 0.5-1ms plateau at -20mV and a small after-hyperpolarization of around 5mV. The diastolic depolarization slope is sensitive to pressure change, HCN inhibitors and KCNQ channel modulators (MJD unpublished observations). The AP spike is sensitive to TTX and nifedipine, implicating the importance of both voltage-gated Na^+ and Ca^{2+} channels in the AP (MJD unpublished). The LSM cell network functions as a syncytium, with entrained depolarizations and APs that trigger nearly-simultaneous global increases in intracellular calcium in the smooth muscle layer. The entrained global calcium

rise leads to the shortening of LSM cells (Imtiaz *et al.*, 2007). A contraction wave is thus propagated along the lymphatic wall and generates pulses of lymph flow, moving lymph from one lymphangion to the next.

Historically, lymphatic contractions have been analyzed using cardiac contractile parameters (as illustrated and further described in Figure 9). The diameter at which the lymphatic vessel develops basal tone, as mentioned earlier, is called the end diastolic diameter. In a lymphangion with two valves, the input valve opens during diastole, creating suction and allowing lymph to fill the pumping unit. The end diastolic pressure created by the fluid volume in the lymphangion from the input up to the output valve is equivalent to preload in the heart. Afterload is the pressure at the beginning of systole and determines the load against which the lymphangion must pump. During systole, lymphatic diameter is decreased to an end systolic diameter. The contraction generates a pressure to overcome the output pressure, opening the output valve, and ejecting lymph to the next lymphangion. The difference between the end diastolic diameter and the end systolic diameter is the contraction amplitude. The number of contractions in a minute is counted as the contraction frequency. Amplitude and frequency have an interrelationship. An increase in frequency decreases the filling time and therefore reduces the amplitude of the next contraction. Stroke volume is the volume of lymph propelled during each contraction cycle and is the difference between end diastolic volume and end systolic volume. Ejection fraction is the proportion of end diastolic volume ejected during a contraction cycle. Fractional pump flow, a theoretical index of lymph flow per unit time, is the product of ejection fraction and contraction frequency. Contractility is a term that is commonly used to indicate the ability

of LSM to shorten its length and pump stroke volume forward at a given level of preload and afterload.

Both tonic and phasic contractions are required to ensure lymphatic transport efficiency. Phasic contractions work as an intrinsic pump, creating a favorable pressure gradient to move lymph uphill. Tonic contraction acts as one of the regulators of valve movement allowing adequate pressure build-up during diastole, and preventing retrograde movement of lymph. Together, they are hallmarks of a "good" isolated lymphatic vessel preparation that recapitulates a normal physiological state. In undamaged collecting lymphatics, tonic and phasic contractions usually develop in parallel. Additionally, tone development during the warming and equilibration period is one of the signs of a healthy lymphatic vessel which will subsequently develop phasic contractions.

1.5 Ca^{2+} signaling

Ca^{2+} is important in many different roles in physiology such as, but not limited to, second messenger signaling, vascular remodeling, proliferation, triggering of electrical events in muscle contraction and cardiac and lymphatic pacemaking (Imtiaz, 2012). In contrast to other cations that control electrical activities across cellular membranes such as Na^{+} and K^{+}, Ca^{2+} has a large variability across cell compartments, which is the reason for its versatility in cellular function. Extracellular [Ca^{2+}] is ~1.8mM, [Ca^{2+}] in the sarcoplasmic reticulum (SR) varies from 300μM to 2mM, and intracellular [Ca^{2+}] at resting state is ~0.1μM and can increase up to 7-10-fold during cell activation, such as in smooth muscle contraction (Bose *et al.*, 2015).

Elevations of intracellular [Ca^{2+}] can come from different Ca^{2+} sources. Ca^{2+} release from the SR can initiate Ca^{2+} spark release via ryanodine receptors, Ca^{2+} puff release

via inositol 1,4,5-triphosphate (IP_3) receptors, and waves through calcium-induced calcium release. In contrast, Ca^{2+} influx from the extracellular space can be detected as rapid Ca^{2+} transients, spontaneous local Ca^{2+} sparklets, and an increase in global Ca^{2+} (e.g., flashes through voltage-gated Ca^{2+} channels) (Hill-Eubank *et al.*, 2011). In vascular smooth muscle cells, global Ca^{2+} elevation induces tonic constriction mainly via opening of voltage-gated Ca^{2+} channels (VGCCs). Other, more localized Ca^{2+} events can modulate contraction by indirectly trigger global Ca^{2+} elevation (Berridge, 2006).

Among these Ca^{2+} sources, Ca^{2+} through voltage-gated Ca^{2+} channels greatly contribute to the upstroke of spontaneous APs in smooth muscle cells. VGCCs open when membrane potential is depolarized above their threshold of activation. These types of channels can be activated rapidly and drastically change the intracellular [Ca^{2+}]. This class of homologous proteins is divided into three families: Cav1.x, 2.x and 3.x. The cardiovascular system predominantly expresses two of them, which are the L-type Ca^{2+} channels: $Ca_v1.x$, and the T-type Ca^{2+} channels: $Ca_v3.x$. My dissertation will focus only on T and L-channels (Figure 3).

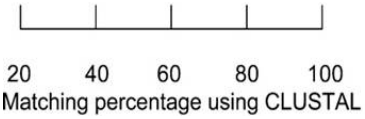

Protein	Gene	Chromosome	Primary tissues	Calcium current
$Ca_v1.1$ (a_{1S})	*CACNA1S*	1q32	skeletal muscle	L-type
$Ca_v1.2$ (a_{1C})	*CACNA1C*	12p13.3	heart smooth muscle brain, heart, pituitary, adrenal	L-type
$Ca_v1.3$ (a_{1D})	*CACNA1D*	3p14.3	brain, pancreas, kidney, ovary, cochlea	L-type
$Ca_v1.4$ (a_{1F})	*CACNA1F*	Xp11.23	retina	L-type
$Ca_v2.1$ (a_{1A})	*CACNA1A*	19p13	brain, cochlea, pituitary	P/Q-type
$Ca_v2.2$ (a_{1B})	*CACNA1B*	9q34	brain, nervous system	N-type
$Ca_v2.3$ (a_{1E})	*CACNA1E*	1q25-31	brain, cochlea, retina, heart, pituitary	R-type
$Ca_v3.1$ (a_{1G})	*CACNA1G*	17q22	brain, nervous system	T-type
$Ca_v3.2$ (a_{1H})	*CACNA1H*	16p13.3	brain, heart, kidney, liver	T-type
$Ca_v3.3$ (a_{1I})	*CACNA1I*	22q12.3-13-2	brain	T-type

Figure 3. Classification and nomeclature of VGCC isoforms. Figure shows the three subfamilies of VGCCs: $Ca_v1.x$, $Ca_v2.x$ and $Ca_v3.x$ and their evolutionary relationship. Reprint with permission from Jurkat-Rott and Lehmann-Horn, 2004.

The general structure of VGCCs is composed of four different types of subunits: a main pore-forming α_1, associated with other auxiliary subunits: $\alpha_2\delta$, β_{1-4}, γ. Differences in the pore-forming α_1 subunit structure divide the VGCC class into different subclasses: $Ca_v1.2$ (α_{1C}), $Ca_v1.3$ (α_{1D}), $Ca_v3.1$ (α_{1G}), $Ca_v3.2$ (α_{1H}), $Ca_v3.3$ (α_{1I}).

The α_1 subunit consists of four linked membrane-spanning domains DI-IV. The intracellular amino-and carboxyl termini are both intracellular. Each domain has six transmembrane segments S1-6, in which S4 acts as a voltage sensor. With membrane depolarization, S4 moves outward and rotates creating a conformational change to open the channel pore. Between S5 and S6 lies a pore-forming loop (P-loop). The cytoplasmic loops linking the four domains DI-IV are crucial for channel gating, and for interactions

between α_1 and second messengers, the β subunit, and scaffolding proteins. β and $\alpha_2\delta$ subunits are essential for most types of VGCCs with respect to channel regulation, membrane expression optimization, and gating kinetics (Perez-Reyes, 2003). Figure 4 illustrates the interactions between VGCC subunits.

The pharmacological susceptibility to inorganic antagonists of VGCCs such as dihydropyridines (DHPs) is attributed to the α_1 subunit. The binding of DHPs to the pore-forming α_1 subunit is determined by the S5-6 extracellular linker, segment S6 of subunit III and IV, and two amino acid residues on segment S5 of subunit III on α_1 subunit (Sandmann and Unger, 1999). The mouse α_1 subunit of $Ca_v1.2$ is a large construct containing 49 exons in which at least 20 exons are alternative splicing sites (Hofmann *et al.*, 2014). The smooth muscle L-channel variant (i.e., $Ca_v1.2b$) is more sensitive to DHP inhibition compared to the variants in the heart (i.e., $Ca_v1.2a$). The 190-250kDa pore-forming α_1 is also important for other functional properties of VGCCs such as voltage sensitivity, Ca^{2+}-dependent inactivation, and Ca^{2+} permeability (Catterall, 2011).

A

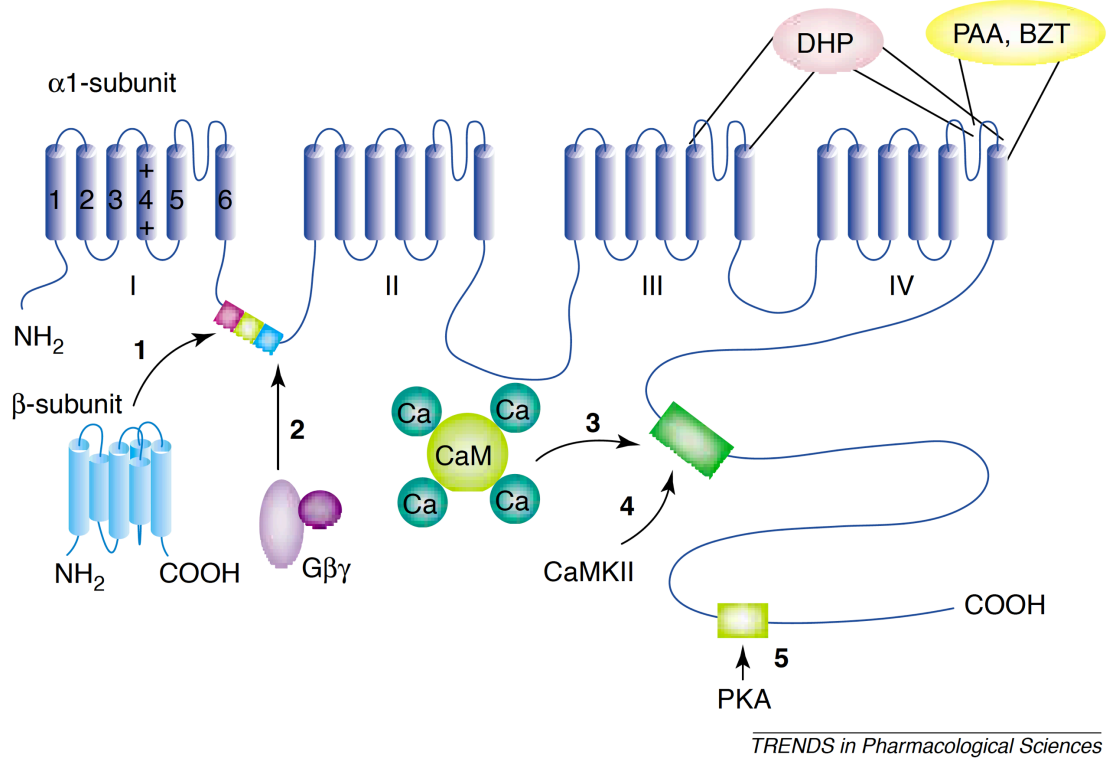

B

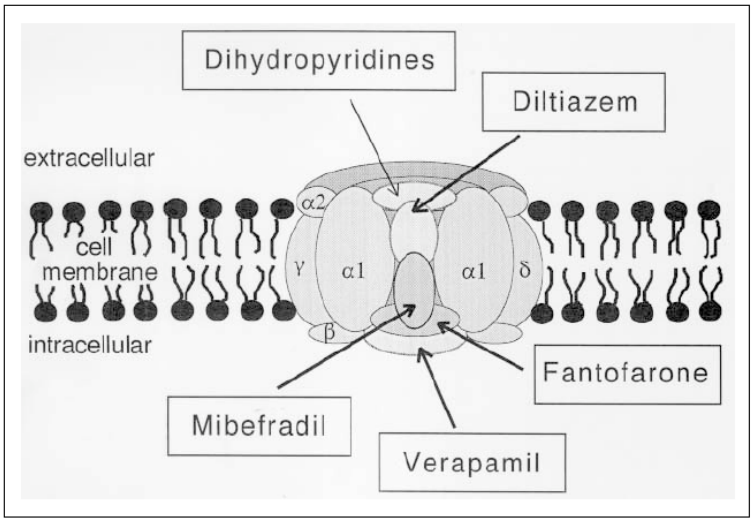

Figure 4. The structural map of the alpha 1 subunit of the calcium channels and its interaction with regulatory components and inhibitor binding sites. A: the 2D-structure of the pore forming subunit alpha 1 of VGCCs, its interaction with regulatory signaling such as PKA, Ca^{2+}-Calmodulin, auxiliary subunits, and the conceptual binding sites for

VGCC inhibitors such as dihydropyridines (e.g., nifedipine, nicardipine), phenylalkalamines-PAAs (e.g., verapamil), and benzothiazepine-BZT (e.g., diltiazem). B: the 3D-structure of the alpha 1 subunit and the conceptual binding site for the T-channel inhibitor mibefradil. Reprinted with permission from Muth *et al.*, 2001 (A) and Sandmann and Unger, 1999 (B).

The most used method in the literature to functionally differentiate between vascular T and L-channels and between different vascular T-channel isoforms is their susceptibility to pharmacological agents. L-channels can be blocked by nanomolar concentrations of DHPs, while T-channels are theoretically insensitive to DHPs (Perez-Reyes, 2003). The well-established pharmacological approach to inhibit T-channels is to use a low dose of Ni^{2+} to target the vascular isoform $Ca_v3.2$ (i.e., ~50μM inhibits 60% of $Ca_v3.2$ but not $Ca_v3.1$ or $Ca_v1.2$, El-Rhahman *et al.*, 2013). However, the IC_{50} for $Ca_v3.1$, $Ca_v3.3$ and $Ca_v1.2$ closely overlap (see Table 3). The high sensitivity of $Ca_v3.2$ to Ni^{2+} is regulated by a histidine on S3-S4 loop on the extracellular side: histidine 191 (Kang *et al.*, 2005). $Ca_v1.2$ and $Ca_v3.1$ are blocked at much higher concentrations of Ni^{2+} (Table 2) by pore occlusion at a shared site deep in the pore. However, the rate for blocking $Ca_v3.1$ is faster than that for blocking $Ca_v1.2$ (Obejero-Paz *et al.*, 2008). Genetic manipulation technology currently offers the most accurate method to study and distinguish the roles between different VGCC families (L vs. T-channels), as well as between different T-channel isoforms (e.g., $Ca_v3.1$ vs. $Ca_v3.2$) (Hansen, 2015).

Table 2. IC_{50} values of currently available VGCC blockers

Inhibitor	Assay system	Ca^{2+} channel	Isoform	IC_{50} (μM)
Ni^{2+}	Oocyte	T-type	$Ca_v3.1$	167
			$Ca_v3.2$	5.7
			$Ca_v3.3$	87
		L-type	$Ca_v1.2$	127.6
	HEK293	T-type	$Ca_v3.1$	250
			$Ca_v3.2$	12
			$Ca_v3.3$	216
	rbU-SMC	L-type		324
Ni^{2+}	selectivity		$Ca_v3.2$>>3.3>1.2>3.1	
Mibefradil	HEK293	T-type		0.87
		L-type		1.4
Mibefradil	selectivity		T-type>L-type	
TTA-A2	HEK293	T-type	$Ca_v3.1$	4.1
			$Ca_v3.2$	5.3
			$Ca_v3.3$	3.7
TTA-A2	selectivity		$Ca_v3.1$~3.2~3.3	
Nifedipine	tSA-201	T-type	$Ca_v3.1$	109
	HEK293		$Ca_v3.2$	1.2
	CHO	L-type	Cardiac $Ca_v1.2$ ($\alpha_{1C\text{-}a}$)	0.47
			Vascular $Ca_v1.2$ ($\alpha_{1C\text{-}b}$)	0.01
Nifedipine	selectivity	Vascular>	Cardiac $Ca_v1.2$> Ca_v 3.2	>Ca_v 3.1

*CHO: Chinese hamster ovary; HEK: human embryonic kidney; rbU-SMC: rabbit urethra smooth muscle cells. (Kraus *et al.*, 2010; Jensen and Holstein-Rathlou, 2009; Lee *et al.*, 2006; Shcheglovitov *et al.*, 2005; Bradley *et al.*, 2004; Lee *et al.*, 1999; Morel *et al.*, 1998; Zamponi *et al.*, 1996)

Different vascular beds have different profiles of T- and L-channel expression depending on their specific physiological function. Resistance arteries, subjected to lower pressure (40-80mmHg), such as rat cerebral arterioles, express both T- and L-channels (Abd El-Rahman *et al.*, 2013). T-channels are also thought to underlie pacemaker activities

in some veins exhibiting spontaneous contractions such as dog saphenous vein (Yatani *et al.*, 1987), rat portal vein (Loirand *et al.*, 1989), and rabbit pulmonary vein (Chen *et al.*, 2004). The next section will focus on highlighting the current strategies about how to differentiate between T- and L-channels.

1.5.1 L-channels

The activation of L-channels is rapid, lasting and voltage-dependent. L-channels are activated at relatively more depolarized membrane potentials compared to T-channels: e.g., around 10mV more positive in mouse tibialis arteries (Moosmang *et al.*, 2003). L-channels have a long-lasting activation, and therefore allow a relatively larger amount of Ca^{2+} ions to pass into the intracellular compartment. In vascular smooth muscle, the L-channel isoform $Ca_v1.2$ predominates (Catterall, 2011). When intraluminal pressure increases, vascular smooth muscles exhibit myogenic reactivity by depolarizing the membrane potential and opening $Ca_v1.2$ channels (Jaggar *et al.*, 1998). Intracellular Ca^{2+} complexes with calmodulin, resulting in myosin light-chain kinase activation and vascular smooth muscle shortening.

Patch-clamp experiments typically use high [Ba^{2+}] as charge carrier to study L and T-type Ca^{2+} channels because $Ca_v1.2$ is two to three times more permeable to Ba^{2+} than Ca^{2+} (Perez-Reyes, 2003). In addition, since Ca^{2+} signaling involves many cellular processes, a higher concentration of Ba^{2+} is less likely to change the intracellular Ca^{2+} homeostasis than a high concentration of Ca^{2+}. The higher permeability for Ba^{2+} results in longer activation because the conductance for Ba^{2+} is not subject to Ca^{2+}-independent inactivation. Furthermore, the pore has a high affinity for Ca^{2+} and is particularly sensitive to low extracellular concentrations of Ca^{2+} (10^{-6}M). However, this affinity also makes Ca^{2+}

obstruct its own influx, therefore allowing Ca^{2+} to permeate more slowly than Ba^{2+} (Sather and McCleskey, 2003). L-channels have a large conductance for Ba^{2+}; in 110mM Ba^{2+} the conductance of L-channels (25pS) is three times higher than that of T-channels (8pS) (Bkaily, 1994). Patch-clamp recordings substituting a high concentration of Ba^{2+} (10-20mM) for physiological [Ca^{2+}] of 1.8mM reported an approximately 10-mV depolarized shift in the current-voltage relationship (Abd El-Rahman *et al.*, 2013). This depolarized shift was explained by Ca^{2+} binding strongly to the hydrophilic part of the lipid bilayer membrane, referred as surface charge screening. Like some other K^+ and Na^+ channels, patch-clamp recordings of L-channels are also prone to rundown/washout phenomena, where the channel activity decreases when the contact between cytosol and membrane is disrupted during patch formation. These effects can be slowed by addition of ATP, Mg^{2+} and cAMP to the pipette solution to increase recording stability (Fedulova *et al.*, 1985; Hille, 2001). Rundown can also be reduced by addition of protease and phosphatase inhibitors.

L-channels (i.e. $Ca_v1.2$) play an important role in myogenic tone, smooth muscle contraction and therefore regulation of blood pressure. Global $Ca_v1.2$ deletion is embryonically lethal. Inducible smooth muscle-specific $Ca_v1.2$ deletion using the SM-22-Cre promoters reduces blood pressure, blunts the myogenic response in arteries/arterioles and is eventually lethal around 21st day after Cre-induction (Moosmang *et al.*, 2003).

1.5.2 T-channels

Since their original discovery in 1975, T-type VGCCs have been shown to be activated at more hyperpolarized membrane potentials compared to the activation potential threshold of other VGCCs: thus, they are also called low-voltage activated Ca^{2+} channels

(Hagiwara *et al*., 1975). Compared to L-channels, T-channels have a faster, more *t*ransient activation and inactivation. Different from L-channels, the range of voltage where T-channels opens (-65 to -44.7mV, also called window current) is more hyperpolarized than the window current for L-channels, (-40mV to -30mV) (Cheng *et al.*, 2009; Satoh, 1995).

Furthermore, the window current of the channels expressed in smooth muscle has a depolarized shift compared to that of neuronal T-channels (Kuo *et al.*, 2014). This shift could be possibly caused by 1) predominant expression of smooth-muscle T-channel splice variants with a more positive activation potential; 2) possible interaction with a) other components of the cell membrane, e.g., other ion channels; b) auxiliary subunits; c) intracellular second messengers (Kuo *et al.*, 2014). Moreover, substitution of Ba^{2+} for Ca^{2+}, as is common practice in patch-clamp experiments to enhance current flowing through VGCCs, does not shift the current-voltage relationship for T-channels as it does for L-channels (Perez-Reyes, 2003).

The small depolarization caused by Ca^{2+} entry through T-channels was shown to be required for activation of high-voltage activated Ca^{2+} channels, specifically L-channels in some cardiovascular contexts (Perez-Reyes, 2003). Furthermore, given that T-channels also have faster voltage-dependent inactivation (Hille, 2001), their characteristics are suited for initiating repetitive action potentials by depolarizing membrane potential to the AP threshold.

T-channels have also been shown to play a role in tone regulation in resistance arteries (Abd El-Rahman *et al.*, 2013). Indeed, the T-channel/L-channel ratio has been shown to be higher in small vessels compared to large vessels (Ball *et al.*, 2009). In the cardiovascular system, $Ca_v3.1$ and $Ca_v3.2$ are the two main subtypes, while the $Ca_v3.3$

isoform is thought to be limited to expression in the central nervous system, in particular to the reticular neurons of thalamus (Vinogradova *et al*., 2009; Perez-Reyes, 2003). However, in a recent publication, $Ca_v3.3$ was found to play the same role in human cerebral arteries as $Ca_v3.1$ plays in rat cerebral arteries (Harraz *et al.*, 2015). Studies in resistance vessels, such as smaller branches of mesenteric arteries and cerebral arteries, show a functional role for T-channels (Abd El-Rahman *et al.*, 2013). Ca^{2+} entry through T-channels, in particular $Ca_v3.2$, has been shown to contribute to the global Ca^{2+} increase and the development of myogenic tone at low intravascular pressures in cerebral and mesenteric arteries (Harraz *et al.*, 2015; Abd El-Rahman *et al.*, 2013; Kuo *et al.*, 2010). In contrast, $Ca_v3.1$ has been shown to play a role in the myogenic tone of retinal arterioles (Fernández *et al.*, 2015).

Vascular T-channel splice variants have a more depolarized window current corresponding to V_m of vascular smooth muscle ~ -40mV. The α_1 subunit of $Ca_v3.1$ contains at least 15 alternative splicing sites among which the splice variants of exon 25 and 26 determine the shift in voltage sensitivity. The isoform $Ca_v3.2$ also has 12-14 splicing sites between exons 25 and 26 (Kuo *et al.*, 2014). For example, the splice variant 25bc at the III-IV linker region predominates in high-order cerebral, mesenteric and renal arteries, while the variant 25a is mainly expressed in the brain and determines altered membrane firing in various forms of epilepsy (Zhong *et al.*, 2006).

1.6 Role of L and T- type Ca^{2+} channels in cardiac pacemaking

Ca^{2+} signaling is an important component of pacemaking in cardiac muscle. It has two major roles: an electrogenic role as in the Hodgkin-Huxley cycle of electrical excitation, and a regulatory role as a second messenger. In parts of the cardiovascular

system such as cardiac pacemaker cells of the sino-atrial node (SAN) and atrio-ventricular node (AVN), the Hodgkin-Huxley cycle can be applied to Ca^{2+} entry through VGCCs as follows: T-channels are activated initially and temporally, contribute to the transient upstroke, therefore depolarizing the membrane potential to the activation potential of L-channels; L- channels then are activated and maintain a long-lasting Ca^{2+} influx, along with contributing a substantial change in intracellular [Ca^{2+}]. As T-channels are inactivated the membrane potential is brought back to the resting level by K^+ outflow, getting the cell ready for the next excitation cycle. The pacemaking cycle is often regulated by a diastolic depolarization (DD). The voltage-gated T and L-channels are proposed to contribute to the DD slope (Maltsev and Lakatta, 2008). VGCCs provide an important Ca^{2+} input regulating the pacemaker in the heart. L and T-channel currents have been recorded in both SAN and AVN cells (Mesirca *et al.*, 2014).

T-channels have been suggested to contribute to pacemaker potentials in the heart, with the highest density in pacemaker and conduction cells. T-channels are suggested to contribute to the mid-late diastolic depolarization, leading to the activation of L-channels, and contributing to the global Ca^{2+} rise (Maltsev and Lakatta, 2008). In mice lacking $Ca_v3.1$, T-current is completely abolished in sino-atrial nodal cells (Mangoni *et al.*, 2006), atrio-ventricular conduction is delayed and the beating rate is decreased by 30% (Mangoni *et al.*, 2008; Chen *et al.*, 2003). However, selectively inhibiting $Ca_v3.2$ with 40 μM Ni^{2+} only decreases the beating rate by 10% (Hagiwara *et al.*, 1988). In contrast, $Ca_v3.2$KO mice have a normal heart rate, suggesting that $Ca_v3.2$ is not crucial for cardiac pacemaking.

Therefore, $Ca_v3.1$, but not $Ca_v3.2$, contributes cardiac pacemaking. Could $Ca_v3.1$ also play a role in lymphatic pacemaking?

1.7 Hypotheses of lymphatic pacemaking

Currently, there are three schools of thoughts about the possible pacemaking mechanism underlying spontaneous contractions LSM.

1.7.1 Spontaneous transient depolarizations (STDs)

Lymphatic electrical pacing is similar in some respects to that observed in mesenteric veins and gastrointestinal (GI) smooth muscle (McHale *et al.*, 2006). As in the GI tract (Kito *et al.*, 2009), LSM displays spontaneous transient depolarizations (STDs), small fluctuations in membrane potential preceding the AP firing, as recorded by intracellular electrodes (Van Helden, 1993). STDs are defined as a 1-2mV deflections in V_m that produce no constriction and correlate with Ca^{2+} puffs-small oscillations in Ca^{2+} release from IP_3R (Imtiaz *et al.*, 2007). In the current literature, STDs are hypothesized to summate into pacemaking potentials and take the membrane potential up to the AP threshold to initiate AP firing. They are also observed in blood vessels such as rat mesenteric, irideal and basilar arteries (Haddock & Hill, 2005). The ionic mechanism underlying STDs is thought to be spontaneous transient inward currents (STICs) evoked by the activation of Ca^{2+} activated Cl^- channels downstream to a spontaneous Ca^{2+} release from the sarcoplasmic reticulum through IP_3 receptors (von der Weid *et al.*, 2008); in guinea pig LSM STDs do not depend on ryanodine receptors. However, several unpublished findings from our laboratory suggest otherwise: 1) ryanodine receptor inhibition increases the lymphatic contraction frequency (SDZ unpublished data); 2) STDs are occasionally present, but their activity is not required for AP firings (SDZ unpublished

data in Tmem16a knockout mice); 3) selective inhibition of IP_3 receptors by xestopongin (Miyamoto *et al.*, 2000) does not reduce the lymphatic contraction frequency (MJD and JAC's unpublished data). Therefore, the hypothesis of STDs being critical for pacing lymphatic contractions is supported by some data, but those data can be questioned due to their sole reliance on pharmacological modulators.

1.7.2 Ion channels located on the plasma membrane of lymphatic smooth muscle cells

Similar to cardiac muscle, there is a close overlap of the contribution of different ion channels in lymphatic pacemaking (Maltsev & Lakatta, 2008). In the literature, the roles of different ion channels in lymphatic pacemaking have been assessed only with pharmacological tools. L-channels are the main driving force for the AP upstroke (Beckett *et al.*, 2007). Nifedipine application stops both AP firing and spontaneous contractions (Souza-Smith *et al.*, 2015). K^+ channels such as K_{ATP}, K_{ir}, K_V, K_{Ca}, Erg are expressed in LSM from human (Telinius *et al.*, 2014), guinea pig (von der Weid, 1998), sheep (Cotton *et al.*, 1997) and mouse lymphatic vessels (MJD unpublished data). K^+ channels are responsible for the repolarization post-AP and regulate the resting membrane potential (Telinius *et al.*, 2014). Hyperpolarization-activated cyclic nucleotide-gated channels, responsible for funny current in the heart (DiFrancesco, 2010), are suggested to play a role in lymphatic pacemaking in rat (Negrini *et al.*, 2016) and sheep (McCloskey *et al.*, 1999). In rat (Lee *et al.*, 2014) and sheep (Cotton & McHale, 1997), T-channels are also implicated in a pacemaking role, contributing to the initial DD, and depolarizing the membrane potential toward the AP threshold, to the point where membrane potential increases exponentially. Non-selective cation channels are also suggested to be activated by lymphatic wall stretch and to trigger the next contraction after diastole (Lee *et al.*, 2014).

A Ca^{2+}-activated Cl^- channel was identified in sheep LSM (Beckett *et al.*, 2007), and proposed to set the resting membrane potential, modulate the AP frequency and the responses to stretch in rat, mouse and human (Zawieja *et al.*, 2016 abstract). Na^+ channels are postulated to contribute to the AP upstroke in LSM from sheep (Hollywood *et al.*, 1997; Beckett *et al.*, 2007) and human (Telinius *et al.*, 2015). Roles for the Na^+/Ca^{2+} exchanger in reverse mode also have been suggested to contribute to Ca^{2+} influx along with VGCCs (Allen *et al.*, 1986). Table 5 summarizes the ion channels known to contribute to lymphatic pacemaking.

Table 5. Contribution of ion channels to lymphatic contraction mechanism

Ion	Species	Ref	Channel	Channel modulator(s)
K^+	Human thoracic duct	Telinius *et al.*, 2014b	K_{ATP}, K_{ir}, K_v, K_{Ca}	Glibencamide (10μM), pinacidil* (1μM), TEA (1mM), paxillin (10μM), 4-AP (40μM-1mM), KPSS (10mM)
	Rat mesenteric lymphatics	Gui *et al.*, 2014	KCNQ, K_v7.1 ERG	XE991, linopiridine (1-10μM) flupirtine (10μM)* E-4031 (2-6μM)
	Sheep mesenteric lymphatics	Beckett *et al.*, 2007	BK	Penitrem-A (100nM), 4-AP (5μM)
	Rat mesenteric lymph microvessels	Mizuno *et al.*, 1999	K_{ATP}	Glibencamide# (100nM and 1μM), pinacidil* (100nM and 1μM), TEA# (100μM and 1mM), iberiotoxin (1-10nM)
Na^+	Human thoracic duct and mesenteric lymphatics	Telinius *et al.*, 2015	Na_v1.3 Reverse-Na^+/Ca^{2+} exchanger	TTX (1nM-1μM), veratridine* (0.1-30μM), ranolazine (1μM) KB-R7943 (3μM)
	Sheep mesenteric lymphatics	Beckett *et al.*, 2007	Na_v	TTX (0.5-1μM)
	Guinea pig mesenteric LVs	von der Weid *et al.*, 2015	TRPM4	Phenantrol (IC_{50}=1.2μM)
Ca^{2+}	Rat mesenteric lymphatics	Lee *et al.*, 2014a	L and T-channels	Ni^{2+} (100μM), mibefradil (100nM), nifedipine (100 and 200nM)
	Rat mesenteric lymphatics	Souza-Smith *et al.*, 2007	L-channels	Nifedipine (100nM)
	Human thoracic duct and mesenteric lymphatics	Telinius et al, 2014a	L -channels	Nifedipine (10nM)
	Sheep mesenteric LVs	Beckett *et al.*, 2007	L and T-channels	Ni^{2+} (100μM), nifedipine (1μM)
	Sheep mesenteric LVs	Hollywood *et al.*, 1997	L-channels	Nifedipine (1μM)
Cl^-	Sheep mesenteric LVs	Toland *et al.*, 2000	Cl^- channels	9-AC (1mM), Cl^- substitution by glutamate or I^-

HCN	Rat diaphragmatic LVs	Negrini *et al.*, 2016	HCN1-4	Ivabradine (300μM), ZD-7288 (200μM), Cs^{+} (10mM)

* indicates an activator, the rest are inhibitors; # indicates no significant effect

1.7.3 Interstitial cells of Cajals (ICCs)

A specialized network of pacemaker cells, known as interstitial cells of Cajal (ICCs), have been found in the gastrointestinal (GI) smooth muscle layers as well as in many hollow organs including bladder, urethra, and fallopian tubes (Sergeant *et al.*, 2006). These pacemaker cells are speculated to exhibit pacemaking related to Ca^{2+} release and are also expected to show rhythmicity even at low IP_3 concentration (Imtiaz *et al.*, 2007). However, the LSM layer of many strongly contracting lymphatics such as mouse popliteals contains only a single layer of LSM, in contrast to the GI tract wall which has many layers of GI smooth muscle (i.e., longitudinal, circular muscle layers and four ICC networks). c-Kit, a prototypical marker for ICCs, co-localizes with Ca^{2+}-activated chloride channels TMEM16A (Sanders *et al.*, 2014)in the GI tract. c-Kit immuno-positive cells have been identified in lymphatic vessels based on anatomical evidence, but without any support for a functional role in electrical pacemaking (McCloskey *et al.*, 2002; Imtiaz *et al.*, 2007; Briggs Boedtkjer *et al.*, 2013). Unpublished experiments in our laboratory on Kit-GFP reporter mice reveal that the only c-Kit positive cells in most lymphatic vessels are rounded, non-interconnected mast cells along the outer adventitia of the vessel wall. Additionally, TMEM16A immunostaining and TMEM16A-GFP reporter mice reveal signal in every LSM cell rather than in a confined ICC network. Dual intracellular recordings in pairs of LSM cells reveal that action potentials fire in both cells with one cell consistently leading the other (MJD unpublished observation). Injection of hyperpolarizing current into the lead cell alters the conduction direction and reduces the pacemaking rate.

This observation suggests that the lymphatic pacing frequency is controlled by the LSM cell with the highest intrinsic depolarization rate rather than relying on a network of pacemaking cells such as ICCs (Gui *et al.*, 2015 abstract). In brief, the hypothesis of an ICC network in lymphatic vessels is contradicted by preliminary data from our laboratory that suggests pacemaking is initiated by LSM cells.

1.7 Role of L and T-channels in the lymphatic pacemaking

Similar to blood vascular and cardiac muscle, Ca^{2+} signaling in LSM is regulated by two main Ca^{2+} sources: Ca^{2+} entry through VGCCs and release from internal Ca^{2+} stores. VGCC-mediated Ca^{2+} influx is proven to be crucial for LSM contraction across different species: in bovine mesenteric lymphatics (Atchison and Johnston, 1997), in sheep mesenteric lymphatics ((Beckett *et al.*, 2007), and in rat mesenteric lymphatics (Souza-Smith *et al.*, 2015)Lee *et al.*, 2014a). However, pharmacological modulation is the only approach that has been used to test the functional role of VGCCs in lymphatic pacemaking.

T and L-type Ca^{2+} channels are the two VGCC families expressed in LSM at the mRNA and protein levels (Lee *et al.*, 2014a). The current established view suggested distinct roles for T and L-channels, in which L-channels regulate lymphatic amplitude and T-channels regulate lymphatic frequency. However, currently available T-channel inhibitors are not specific, make these results inconclusive.

Some of the evidence for T-channels in lymphatic contraction/pacemaking could be explained by partial blockade of L-channels by T-channel inhibitors (Cotton & McHale, 1997; Beckett *et al.*, 2007; Lee *et al.*, 2014), because the IC_{50}s of T-channels and L-channels closely overlap, except for $Ca_v3.2$, which can be inhibited at low micromolar concentrations (Hansen, 2013; Jensen and Holstein-Rathlou, 2009) (Table 2). Lee *et al.*,

2014a and Beckett *et al.*, 2007 intentionally used low doses of pharmacological agents for T-channels (100μM Ni^{2+}), expecting to only inhibit the T-channel isoform $Ca_v3.2$ (Ni^{2+} IC_{50}=12μM for $Ca_v3.2$) without affecting L-channels (Ni^{2+} IC_{50}=324μM) (Jensen and Holstein-Rathlou, 2009). However, the lymphatic pacemaker eventually stopped, reducing both lymphatic AP amplitude and frequency to zero (Figure 5); this result suggests that L-channels could have already been affected by 100μM Ni^{2+}. Furthermore, the other T-channel isoform in lymphatic vessels $Ca_v3.1$, has an IC_{50} (Ni^{2+} IC_{50}=250μM) very close to that of L-channel (Table 2). Therefore, it is necessary to have an alternative approach to inhibit T-channels more specifically than can differentiate T-channels from L-channels as well as between the two T-channel isoforms, $Ca_v3.1$ and $Ca_v3.2$.

A. Lee *et al.*, 2014a (100µM Ni^{2+})

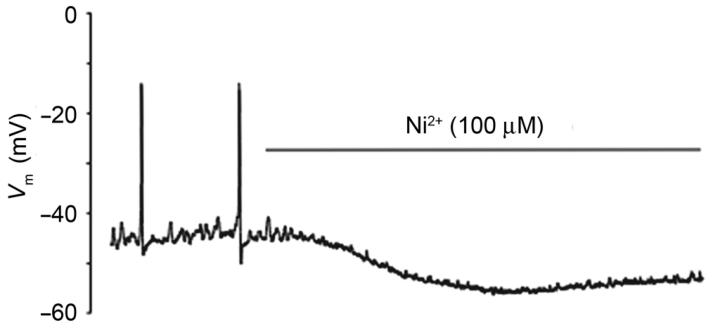

B. Beckett *et al.*, 2007 (100µM Ni^{2+})

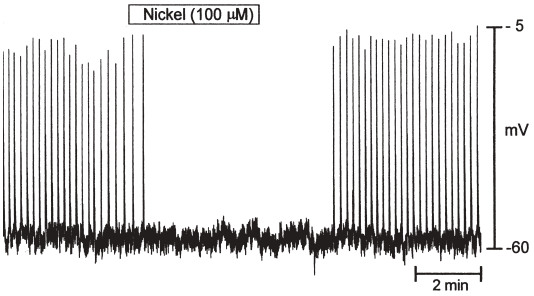

Figure 5. Published records of Ni^{2+} effects in rat and sheep mesenteric lymphatic vessels. A: Intracellular recording in an unstretched rat mesenteric lymphatic vessel treated with 100µM Ni^{2+} showed that eventually AP firing stopped (Lee *et al.*, 2014a). B: Intracellular recording in a sheep mesenteric vessel (wire myograph) treated with 100µM Ni^{2+} showing a slight decrease in AP frequency before AP firing ceased (Beckett *et al.*, 2007). Reprinted with permission from Lee *et al.*, 2014a and Beckett *et al.*, 2007.

1.8 Translational implications of increased knowledge of T-channels in the lymphatic smooth muscle

A lack of functional lymphatics can lead to debilitating and incurable diseases such as lymphedema. As with many other bodily functions, lymphatic function degenerates with age (Zolla *et al.*, 2015; Bridenbaugh, 2013) and becomes impaired in many inflammatory conditions (Liang *et al.*, 2016; Thangaswamy *et al.*, 2012). Lymphatic dysfunction may

also contribute to other chronic diseases such as metabolic syndrome (Chakraborty *et al.*, 2015) or hypertension (Wiig *et al.*, 2013). Moreover, many forms of lymphatic dysfunction are left undiagnosed and untreated without direct, mechanism-based therapeutics. In lymphedema, lymphatic vessels in the affected region are dilated and have impaired contractions, or no contractions, and are unable to generate positive lymph flow (Olszewski, 2012). Understanding how lymphatic vessels contract can provide a therapeutic target to improve lymphatic function in lymphatic-related diseases, and therefore patients' health and quality of life. Thus, the aim of my study is to seek a deeper understanding of the ionic mechanism of lymphatic phasic contractions.

1.9 Rationale, significance and hypothesis

In the field of studying ion channels in lymphatic pacemaking/contraction, the only approaches used to date are with pharmacologic inhibition. This is especially problematic for the understanding of ion channels, such as T-channels, that lack specific pharmacological modulators. Recently, robust development of transgenic technology in mice, as acclaimed by the Nobel Prize 2007 to Mario R. Capecchi, Martin J. Evans and Oliver Smithies, has provided an option to test the established hypothesis of lymphatic pacemaking using selective deletion of specific ion channel isoforms. However, one challenge of applying this approach is that viable mouse lymphatic vessels are difficult to isolate. Fortunately, Dr. Davis and Dr. Scallan, a former post-doc in Dr. Davis' laboratory, developed methods to isolate, cannulate and study single mouse collecting lymphatic vessels using pressure myography (Scallan and Davis, 2013a). After joining Davis' laboratory, I was able to use lymphatic vessels isolated from mice deleted of specific T-channel isoforms to test the role of T-channels as critical components of the lymphatic

pacemaker. I utilized three well-established transgenic mouse models $Ca_v3.1^{-/-}$, $Ca_v3.2^{-/-}$ and smooth-muscle-specific $Ca_v1.2^{-/-}$ to investigate for the role of T-channels in lymphatic pacemaking.

In accord with the previous findings of Lee *et al.*, 2014a, I hypothesized that genetic deletion of T-channel isoforms $Ca_v3.1$ and/or $Ca_v3.2$ would reduce the pacemaking frequency, but not the amplitude, of spontaneous lymphatic contractions.

CHAPTER 2: MATERIALS AND METHODS

2.1 Animals

Experiments testing the role of T-channels were conducted on mature male Spargue-Dawley rats (180-250g), male C57BL/6 wild-type (WT) mice, male and female Cav3.1$^{-/-}$ (Lee *et al.*, 2004) mice, and male $Ca_v3.2^{-/-}$ (Chen *et al.*, 2003) mice (8- to 10-week-old, 18-25 g), with the latter two mice bred more than ten generations onto the C57BL/6 background.

$Ca_v3.1^{-/-}$ mice were obtained from Dr. Jeff Molkentin's laboratory at Cincinnati Children's Hospital Medical Center. Due to the presence of parvo- and hepatoviruses in those mice, sperm from them was obtained and the line was rederived locally (IDEXX Laboratories, Columbia, MO). Sperm was used to generate embryos by *in vitro* fertilization, which were then implanted in three newly purchased C57BL/6 wild-type females. $Ca_v3.1^{-/-}$ mice were obtain after two generations. Rat, C57BL/6, and $Ca_v3.2^{-/-}$ (B6;129-*Cacna1h*^{tm1Kcam}/J) mice were purchased from Jackson laboratory (Bar Harbor, MA).

Other studies were conducted in mice with smooth-muscle-specific deletion of $Ca_v1.2$ ($Ca_v1.2$ global KO is lethal). SMMHC-CreER^{T2} (B6.FVB-Tg(Myh11-cre/ERT2)1Soff/J) were obtained from Steffan Offermanns, $Ca_v1.2^{fl/fl}$ (*Cacna1c*^{tm3Hfm}/J) mice were purchased from Jackson laboratory (Bar Harbor, MA). Subsequently, $Ca_v1.2^{fl/fl}$ mice were bred with SMMHC-CreER^{T2} mice to allow inducible and specific deletion of $Ca_v1.2$ in smooth muscle.

To image lymphatic vessels *in vivo*, Prox1-GFP mice were obtained from Dr. Young-Kwon Hong, University of Southern California. To visualize fluorescent LSM

cells, α-SMA-DsRed^{P} mice were obtained from Dr. Tim Padera, Massachusetts General Hospital, and SMMHCCre-eGFP mice were purchased from Jackson Laboratory (Bar Harbor, MA). All animal procedures were approved by the University of Missouri Animal Care and Use Committee, and conformed to the National Institutes of Health's *Guide for the Care and Use of Laboratory Animals (8th edition, 2011)*.

Table 3. Summary of mouse lines used

Genotype	Purpose	Source
C57BL/6	Control	Jackson laboratory
$Ca_v3.1^{-/-}$	Global KO	Jeff Molkentin
$Ca_v3.2^{-/-}$	Global KO	Jackson laboratory
$Ca_v1.2^{fl/fl}$	To breed with SMMHC-CreER^{T2}	Jackson laboratory
SMMHC-CreER^{T2}	To breed with $Ca_v1.2^{fl/fl}$	Steffan Offermanns
SMMHC-CreER^{T2}; $Ca_v1.2^{fl/fl}$	Smooth-muscle specific KO	Breeding
Prox1-GFP	To image lymphatics *in vivo*	Young-Kwon Hong
α-SMA-DsRed^{P}	To visualize red fluorescent smooth muscle	Tim Padera
SMMHCCre-eGFP	To visualize green fluorescent smooth muscle	Jackson laboratory

2.2 Lymphatic vessel isolation

Animals were anesthetized with pentobarbital sodium (Nembutal; mouse: 60mg*kg^{-1}, rat: 100mg*kg^{-1}, intraperitoneal injection). Surgery for lymphatic vessel excision proceeded after the animals became unresponsive to toe pinch. After completion of lymphatic vessel excision, animals were euthanized by intracardial injection of 1mL of 200mM KCl.

Rats were placed in the supine position and an incision was made at the abdominal midline to expose the gastrointestinal tract. Loops of intestine were pinned down to facilitate the visualization of mesenteric lymphatic vessels that usually ran in parallel with

mesenteric veins and arteries. Mesenteric lymphatic vessels were excised along with surrounding tissues such as fat and the adjacent mesenteric vein and transferred to room temperature albumin-supplemented Krebs buffer.

An anesthetized mouse was placed in the prone position and an incision was made in either flank from the inguinal node to the axillary node (to access the inguinal-axillary lymphatics) or at the outer margin of either leg from the ankle toward near the groin region (to access the popliteal afferent lymphatics). After either excision, the inguinal-axillary or popliteal lymphatic was placed in warm Krebs' buffer supplemented with albumin.

The lymphatic vessel was pinned on a Sylgard platform (Sylgard® 184, Dow Corning, Midland, MI) and subsequently isolated from the surrounding connective tissue and fat cells. A segment of a cleaned lymphatic vessel (e.g., inguinal-axillary vessels with inner diameter 100-150μm, containing at least one valve), was then transferred to a 3mL chamber where it was cannulated and pressurized on two micropipettes (outer diameter of 40-80μm) at the two ends. The bath was exchanged at a rate of 0.4ml/min; and equilibrated at 37ºC in preparation for pressure myograph experiments, as previously described (Scallan *et al.*, 2013a).

Krebs buffer contained (in mM): NaCl, 146.9; KCl, 4.7; $CaCl_2$, 2; $MgSO_4$, 1.2; $NaH_2PO4.H_2O$, 1.2; $NaHCO_3$, 3; Na-HEPES, 1.5; D-glucose, 5 (pH 7.4, 37ºC). Krebs with 0.5% BSA was used for vessel isolation and cannulation and to fill the pipette system and vessel lumen.

2.3 Pressure myograph

Each vessel was equilibrated for 30-60 minutes at 2-3cmH_2O and tested for contractile function using pressure steps 0.5-8cmH_2O (for inguinal-axillary lymphatics)

and 0.5-10cmH_2O (for popliteal lymphatics). The inner diameter was tracked by computer from a video image (Davis *et al.*, 2011) to record the change in diameter of each spontaneous contraction. The vessel was only included in the data analysis if 1) spontaneous contractions and tone developed within the first 60 minutes; 2) contraction amplitude was more than 30% at 1cmH_2O. Subsequently, the vessel was treated with pharmacological inhibitors at the pressure that produced the largest contraction amplitude (usually 2-3cmH_2O). To test the potential for a role of T-channels in lymphatic contractions using pharmacological approaches, increasing concentrations of the inhibitors Ni^{2+} (15μM-2mM), nifedipine (1nM-10μM), TTA-A2 (100nM-100μM), or mibefradil (0.2nM-2μM) were added to the bath solution with the perfusion halted. In some protocols acetylcholine (1-300nM) was added to test the ability to activate eNOS. Bay K8644 (1μM) was added to test residual $Ca_v1.2$ activity in vessels from tamoxifen-induced SMMHC-Cre; $Ca_v1.2^{fl/fl}$ mice. Mibefradil was dissolved in warm double-distilled water. TTA-A2, Bay K8644 and nifedipine were dissolved in DMSO. Ni^{2+} and acetylcholine were dissolved in warm Krebs buffer without BSA. The contraction response was recorded for 3 min before the next dose was applied. At high concentrations of pharmacological inhibitors such as nifedipine and Ni^{2+}, small, irregular changes in inner diameter of less than 5μm were not considered as contractions. At the end of every pressure myograph experiment the lymphatic vessels were superfused with Ca^{2+} free Krebs buffer solution to obtain the passive diameter (Davis *et al.*, 2011).

2.4 Single lymphatic smooth muscle cell isolation

Cleaned collecting lymphatics were pre-heated in low-Ca^{2+}-digestion solution at 37^{o}C for 10 minutes, and then went through two digestion steps: 1) in 1mg/ml

dithioerythritol (Sigma, D8161-5G) and 1.5mg/ml (rat) or 1mg/ml (mouse) papain (Sigma, P4762-1G); 2) in 0.5mg/ml collagenase H (Sigma, C8051-1G), 0.7mg/ml collagenase F (Sigma, C7926-1G) and 1mg/ml soybean trypsin inhibitor II (Sigma, T9128-1G). The digestion cocktails were diluted and aliquoted in physiological salt solution (PSS) containing (in mM): 144 NaCl; 5.6 KCl; 1.0 $MgSO_4$; 0.42 $Na_2HPO_4.H_2O$; 0.44 $NaH_2PO_4.H_2O$; 4.17 $NaHCO_3$; 10 HEPES; 5 D-glucose (pH 7.4 adjusted with NaOH, 25ºC). The digestion process occurred in a low-Ca^{2+}-digestion solution, which is PSS supplemented with $CaCl_2$ and BSA, containing (in mM): 144 NaCl; 5.6 KCl; 0.1 $CaCl_2.2H_2O$; 1.0 $MgSO_4$; 0.42 $Na_2HPO_4.H_2O$; 0.44 $NaH_2PO_4.H_2O$; 4.17 $NaHCO_3$; 10 HEPES; 5 D-glucose; 1mg/ml BSA (pH 7.4 adjusted with NaOH, 25ºC). After digestion, the remaining vessel fragments were rinsed with an ice-cold digestion solution and triturated with a fire-polished Pasteur pipette to release single cells. Isolated muscle cells were stored in ice-cold solution to stop enzymatic digestion and used within 4-6h (Harraz and Welsh, 2013). The resulting LSM cell homogenates were used either for Ca^{2+} current recording using the patch-clamp technique or collection of single LSM cells for mRNA detection for Ca^{2+} channels and related controls that will be discussed in the subsequent PCR section. For LSM cell collection, the cell suspension was placed in a chamber at room temperature and a 30µm-pipette was used to collect single, spindle-shaped cells. For patch-clamp experiments, the cell suspension was placed in a recording chamber perfused with Ca^{2+} 1.8mM physiological solution at room temperature and current through VGCCs were recorded as described in the following section.

2.5 Patch-clamp recordings

The smooth muscle cells resulting from the digestion of lymphatic vessels were placed in a recording chamber under an inverted microscope and perfused with 1.8mM-Ca^{2+} physiological solution containing (in mM) 110 NaCl, 1 CsCl, 1.8 $CaCl_2$, 1.2 $MgCl_2$, 10 HEPES, 10 D-glucose (pH was adjusted to 7.4 with NaOH). Whole-cell patch-clamp recordings were performed using a pipette solution containing (in mM): 135 CsCl (stock 1M), 10 HEPES (stock 1M), 10 EGTA (stock 100mM), 5 GTP·Mg (stock 1M) (Sigma, A-9187-1G), with pH was adjusted to 7.2 with CsOH 1M and a bath solution contained (in mM) 110 NaCl (stock 2M), 1 CsCl (stock 1M), 10 or 20 $BaCl_2$ (stock 1M), 1.2 $MgCl_2$ (stock 1M), 10 HEPES (stock 1M), 10 D-glucose (stock 1M), with pH was adjusted to 7.4 with NaOH. Cs^+ and Mg^{2+} were added into the pipette solution to block K^+ channels. Mg^{2+} along with GTP was added to prevent Ca^{2+} channel run down. The use of GTP is preferred over the use of ATP in studies of T-channels because ATP can activate PKA, and therefore have an indirect activating effect on T-channels (Harraz and Welsh, 2013).

LSM cells were distinguished from other cell types (endothelial cells and neural cells) in the homogenate based on the cell size and morphology. LSM cells had either a bean or spindle shape and were significantly larger than endothelial cells which were round and small. Whole-cell patch-clamp recording of current through VGCCs was performed using an EPC9 amplifier controlled by Pulse software (HEKA instruments, Bellmore, NY). Recording electrodes (resistance from 3-5MΩ) were back-filled with a pipette solution containing (in mM): 135 CsCl (to block K^+ channels), 10 HEPES, 10 EGTA, 5 GTP·Mg (pH adjusted to 7.2 with CsOH). Pipette movement was controlled with a hydraulic manipulator (MO-102, Narishige, Tokyo, Japan). After the cell and its gigaseal (>1GΩ)

stabilized in 1.8mM-Ca^{2+} physiological solution, all subsequent recordings were performed using Ba^{2+} as the charge carrier; the solution contained (in mM) 110 NaCl, 1 CsCl, 10 or 20 $BaCl_2$, 1.2 $MgCl_2$, 10 HEPES, 10 D-glucose (pH was adjusted to 7.4 with NaOH). Cell capacitance, an indication of cell membrane surface area, ranged from 9-25pF. The recorded current value (pA) was normalized to cell capacitance (pF) to obtain current density (pA/pF). The holding potential was -70mV. This is a more hyperpolarized potential compared to the resting membrane potential of LSM cells under physiological conditions recorded intracellularly with electrode impalement (-45 to -35mV).

I subsequently performed two voltage clamp protocols: 1) a voltage ramp, from -100 to +80mV at 1mV/ms to generate directly and rapidly current-voltage relations (Figure 6); 2) voltage steps from a holding potential of -70mV with a prepulse to -90mV for 200ms, then steps to a range of voltages from -80 to +40mV (10mV-increment, 2s each), and a final step back to the holding potential; this protocol provided a measurement of current kinetics at different voltage steps (Figure 7).

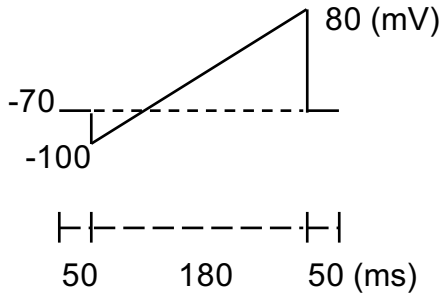

Figure 6. Ramp protocol used in patch-clamp experiments. The ramp protocol used to instantaneously elicit Ca^{2+} current in response to a voltage gradient: from the holding potential -70mV, the membrane potential is hyperpolarized to -100mV to relieve

inactivation of VGCCs. From -100mV the membrane potential is progressively depolarized to 80mV to obtain a pseudo-instantaneous I-V relationship.

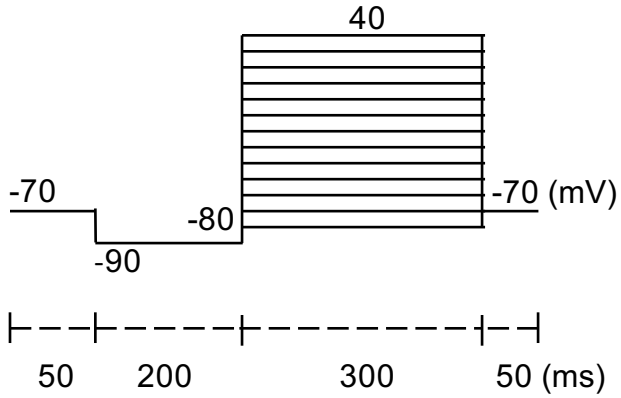

Figure 7. Step protocol used in patch-clamp experiments. From a holding potential voltage of -70mV, Vm was hyperpolarized with a prepulse to -90mV for 200ms, then stepped to a range of voltage from -80 to +40mV (10mV increment, 2s each), and finally stepped back to the holding potential (Davis *et al.*, 1992).

2.6 Immunostaining

Inguinal-axillary lymphatic vessels were isolated and pressurized at ~8cmH_2O and slightly stretched axially to remove slack. Pressurized lymphatics were fixed in 2% paraformaldehyde (v/v) (19943-1L, Affymetrix, Cleveland, OH) for 30 minutes. The vessels were then washed in Phosphate Buffered Saline (PBS, 21600-010, Thermo Fisher Scientific, Waltham, MA), permeabilized with 0.3% Triton-X (v/v) (32737-1000, Acros Organics, Thermo Fisher Scientific, Springfield Town, NJ) for 30 minutes, and blocked with 5% donkey serum (v/v) for 1 hour at RT. The vessels were incubated in α-actin primary antibody (Sigma, -A2547) (1:200) and one of the primary antibodies for Ca^{2+} channels (Alomone, Jerusalem, Israel): $Ca_v3.1$ (ACC-021), $Ca_v3.2$ (ACC-025), $Ca_v3.3$ (ACC-009) and $Ca_v1.2$ (ACC-003) (1:100) diluted into PBS containing 5% donkey serum

(017-000-121, Jackson ImmunoResearch Laboratories, West Grove, PA) and 0.1% Triton-X (AC2156825000, Thermo Fisher Scientific, Waltham, MA). The vessels were washed with PBS for at least 3 times for 20 min (a total of 2 hours), and incubated in secondary antibodies diluted 200-fold in PBS containing 5% donkey serum and 0.1% Triton-X for 1h at RT. The secondary antibodies used were goat anti-mouse antibody Alexa Fluor 647 (A21241, Invitrogen, Carlsbad, CA) and donkey anti-rabbit Alexa Fluor 448 (A21206, Invitrogen, Carlsbad, CA). The vessels were subsequently washed again with PBS for at least 3 times for 20 min (a total of 2 hours). Subsequently, ProLong® Gold Antifade Reagent with DAPI (P36931, Thermo Fisher Scientific, Waltham, MA) was used to stain for the nuclei and mount the vessels onto imaging slides. The mounted vessels were allowed to cure overnight and sealed the following day by painting nail polish around the edges of the slides. $Ca_v1.2$ staining served as a positive control and α-actin co-staining was used to outline the structure and location of LSM cells. Negative controls included omission of the Ca^{2+} channel primary antibody or primary antibody pre-absorption using the corresponding Alomone antigens. Fluorescence emission was imaged using an Olympus IX81 microscope equipped with a Nippon spinning disk confocal microscopy and Hamamatsu Flash 4.0 camera (Hamamatsu Photonics, Shizuoka, Japan), illumination was controlled by Andor diode lasers (Andor, Belfast, Northern Ireland) under Metamorph (Nashville, TN, USA). Images were processed with NIH ImageJ.

2.7 PCR

2.7.1. End-point PCR

End-point PCR experiments are performed to detect the presence of VGCCs in rat mesenteric LVs, mouse whole PL, IAL vessels and their freshly isolated LSM cells.

Vessels used for PCR were dissected at 4ºC. The freshly isolated lymphatic vessels or collected cells were directly transferred to RNAlater solution (Qiagen, Hilden, Germany) and stored at -80ºC. RNA from 6-16 lymphatic vessels or five hundred LSM cells from more than three mice was extracted using the Arcturus PicoPure RNA Isolation Kit (Life Technology, Carlsbad, CA, USA). cDNA then was synthesized using the Superscript III first Strand synthesis system (Invitrogen, Carlsbad, CA, USA). PCR using primers listed in Table 4 and 6 was subsequently performed using GoTaq Flexi Reverse Transcriptase (M8291, Promega, Madison, WI, USA) or Biotool Universe Hot Start High-Fidelity 2x PCR mix (B22100, Biotool, Jupiter, FL, USA). Nested PCR was performed for weak signals such as $Ca_v3.1$, $Ca_v3.2$ and $Ca_v3.3$. Nested PCR used a second internal set of primers to amplify the PCR product of the first external set of primers. PCR were performed with a Biorad thermal cycler (Type C1000 Touch™, Biorad, Hercules, CA, USA). Following a five-min initial step at 95ºC were 35 cycle of [95ºC, 30 sec denaturation; 58ºC, 30 sec annealation; 72ºC, 20 sec extension) and a final extension at 72ºC for 5 min. The PCR products were then cooled down to 12ºC. The amplified PCR products along with a 100-bp DNA ladder (15628-019, Invitrogen) were loaded in to 1.5-2% Agarose gel (Invitrogen) + Gel Red (1:10000, Biotum, Fremont, CA, USA) and the gel was run at 70-80V for 60-90 min. The gel was subsequently imaged by a ChemiDoc XRS+ digital system (Biorad).

2.7.2. Genotyping PCR

1 to 2-mm pieces of tails were collected from 3-week-old transgenic mice for genotyping. Scissors were cleaned with 70% ethanol before each sample collection to disinfect and prevent DNA contamination from previous sample. For DNA extraction, tail

biopsies were incubated in base solution (25mM NaOH and 0.2mM, pH~12) at 95º for 45 min until the tail pieces were completely dissolved. The digestion reaction was stopped by adding equal amount of neutralization solution (40mM Tris-HCl, pH~5). The samples were subsequently centrifuged (3 min; 13,000 rpm) to collect the supernatant containing genomic DNA. DNA samples were mixed with 2x Conquest™ PCR mix (D911, Lambda Biotech) and genotyping PCR primers listed in Table 5. After an initial 5 min pre-incubation step at 94ºC, PCR were amplified using initial 10 cycles of [94ºC, 20 s; 65ºC, 15 s; 68ºC, 30 s] and subsequent 28 cycles of [94ºC, 15 s; 60ºC, 15 s; 72ºC, 30 s]. The final step was at 72ºC for 5 min before the products were cooled down to 12ºC.

Table 4. Primers targeting rat T-type Ca^{2+} channels and control genes used in end-point PCR

Target	Accession number	Primer sequence (5' to 3')	Size	Reference
$Ca_v3.1$	AF027984	F: 5'-TCT TCC AGG ACA GGT GGA AC-3'	501bp	Abd El-Rahman *et al.*, 2013
		R: 5'-TCA GCA CGA AGG ACA CAA AG-3'		
$Ca_v3.2$	AF290213	F: 5'-AGT TTC CTC TTT GGG GGC TA-3'	402bp	Abd El-Rahman *et al.*, 2013
		R: 5'-CAG GAA AAC CCA AAC CTG AA-3'		
$Ca_v3.3$	AF086827	F: 5'-CCC TGG AGA TGA TCC TGA AA-3'	501bp	Abd El-Rahman *et al.*, 2013
		R: 5'-AGT TGC CAA AGG TCA TGA GG-3'		

Table 5. Genotyping primers targeting $Ca_v3.1$ and $Ca_v3.2$

Target	Primer type	Primer sequence (5' to 3')	Size	Reference
$Ca_v3.2$	WT Forward	5'-ATT CAA GGG CTT CCA CAG GGT A-3'	Mutant: 330bp WT: 480bp Heterozygote: 330 and 480bp	Jackson Laboratory site
	Mutant Forward	5'-GCT AAA GCG CAT GCT CCA GAC TG-3'		
	Common	5'-CAT CTC AGG GCC TCT GGA CCA C-3'		
$Ca_v3.1$	WT Forward	5'-CGAAGGCCTGACGTAGAAAG-3'	Mutant: 385bp WT: 288bp Heterozygote: 288 and 385bp	Kim *et al.*, 2001
	Mutant Forward	5'-CTGACTAGGGGAGGAGTAGAAG-3'		
	Common	5'-ATACGTGGTTCGAGCGAGTC-3'		

Table 6. Primers targeting mouse Ca^{2+} channels and control genes used in end-point PCR

Target	Accession number	Primer sequence (5' to 3')	Size	Reference
$Ca_v3.1$ external	NM_009783	F: 5'-TGT GGA AAT GGT GAA GA-3'	150bp	Li *et al.*, 2012
		R: 5'-ACT GCG GAG AAG CTG ACA TT -3'		
$Ca_v3.1$ internal		F: 5'-GAT GGT CGC TTT GGG TAT CT-3'	131bp	Designed with PrimerQuest Tool
		R: 5'-ACT GCG GAG AAG CTG ACA TT-3'		
$Ca_v3.2$ external	NM_021415	F: 5'- TTC ATT GTC ATG GCT GGC AT-3'	289bp	Lin *et al.*, 2014
		R: 5'- TCA GGT TGT TGT TCC TGA CG-3'		
$Ca_v3.2$ internal	NM_021415	F: 5'-TAC TCT CTG GAC GGA CAC AA-3'	262bp	Designed with PrimerQuest Tool
		R: 5'-TCA GGT TGT TGT TCC TGA CG-3'		
$Ca_v3.3$ external	NM_001044308	F: 5'-GAT CCT GCA GGT CTT TGA TGA-3'	239bp	Designed with Primer BLAST
		R: 5'-GAA CAC GGT TGA TGG CTT TG-3'		
$Ca_v3.3$ internal		F: 5'-TGG GCA TTT TTG GCA AGA A-3'	129bp	Li *et al.*, 2012
		R: 5'-CAG TGC GGA TGG CTG ACA-3'		

$Ca_v1.2$	NM_00159533	F: 5'- CAG GAG GTG ATG GAG AAG CCA -3'	315bp	Xu *et al.*, 2003
		R: 5'-CTG CAG GCG GAA CCT GTT GTT-3'		
$Ca_v1.3$ external	NM_028981	F: 5'- TGC TGT GAG GAC GAC AGC TCT CCC A -3'	342bp	Maddala *et al.*, 2013
		R: 5'- TAG GCC TGC AAC GGC CAT GAT CTG C -3'		
$Ca_v1.3$ internal		F: 5'- CAG CTC CAT GGA CTT TGA GAG -3'	117bp	Designed with PrimerQuest Tool
		R: 5'- TAG GCC TGC AAC GGC CAT GAT CTG C -3'		
α-actin	NM_007392	F: 5'-GTG AAG AGG AAG ACA GCA CAG-3'	146bp	Chow *et al*., 2016
		R: 5'-GCC CAT TCC AAC CAT TAC TCC-3'		
eNOS	NM_008713	F: 5'-CTG CCA CCT GAT CCT AAC TTG-3'	143bp	Chiplunkar *et al.*, 2013
		R: 5'-CAG CCA AAC ACC AAA GTC ATG-3'		

2.8 Western blotting

Brain, a tissue expressing T and L-channels abundantly, from WT and $Ca_v3.2^{-/-}$ mice was excised and ground in liquid nitrogen using a mortar and pestle. Total proteins were extracted with ice-cold RIPA lysis buffer containing protease inhibitor cocktail (Thermo Fisher Scientific, Waltham, MA). The resulting homogenates were centrifuged to separate the protein-containing supernatant from the solid matter. Protein concentrations in the supernatants were determined using a BCA kit (Pierce, Rockford, IL, USA) and measured by Nanodrop 2000c (ThermoFisher Scientific, Waltham, MA, USA). Approximately 50µg of protein was loaded on 4-20% sodium dodecyl sulfate (SDS) polyacrylamide gel (Biorad) and total proteins were separated into different molecular masses in an electric field using a SDS-polyacrylamide gel electrophoresis (SDS-PAGE) system. The gel was electro-transferred to a nitrocellulose membrane for 16h at 4ºC. Non-specific binding on the membrane was blocked by incubation in 5% non-fat dry milk dissolved in TBST (0.1% Tween 20) for 2h. The membrane then was incubated overnight in rabbit polyclonal anti-$Ca_v3.2$ antibody (Alomone, Jerusalem, Israel) and mixed in the blocking solution (1:800) overnight at 4ºC. The membrane was washed with TBST (0.05% Tween 20). After that, the membrane was incubated in horseradish peroxidase-conjugated goat anti-rabbit secondary antibody (Cell signaling, Danvers, MA) and diluted in blocking solution (1:4000) for 2h at RT. After washing with TBST (0.05% Tween 20), immunoreactive protein bands were detected using SuperSignal Pico Extended Duration Substrate (ThermoFisher Scientific), and imaged by a ChemiDoc XRS+ digital system (Biorad).

2.9 Alcein blue staining

Tracheal segments were dissected from 10-week old WT and $Ca_v3.2^{-/-}$ mice to confirm one of the major phenotypes of $Ca_v3.2^{-/-}$ mice (Lin *et al.*, 2014). The tissue was fixed for 18h in 4% paraformaldehyde and washed in PBS. The cartilage ring structure was stained with 1% Alcein blue in 3% acetic acid to detect tracheal stenosis as described in Lin *et al.*, 2014. The dye then was washed and, dyed tissue was immersed in 2% KOH for 24h. The stained tracheas were kept in glycerol until ready for imaging.

2.10 Validation of transgenic mouse models lacking specific T-type Ca^{2+} channel isoforms

Although we obtained knock-out mice from reliable sources ($Ca_v3.2^{-/-}$ from Jackson Laboratory and $Ca_v3.1^{-/-}$ from Jeffrey Molkentin's laboratory), I tested the expression of L- and T-channels to confirm the deletion of the specific T-channel isoforms in the respective knock-out mice.

2.10.1 Validation of global $Ca_v3.2^{-/-}$ mice

To validate the $Ca_v3.2^{-/-}$ mouse model, I first tested the mRNA expression of $Ca_v3.2$ in brain harvested from $Ca_v3.2^{-/-}$ mice (Figure 8A) using primers published in the original paper that described phenotypes of the first generation of global $Ca_v3.2^{-/-}$ mice (Chen *et al.*, 2003). Although Chen *et al.* 2003 showed no $Ca_v3.2$ mRNA expression in $Ca_v3.2^{-/-}$ mice, I was still able to amplify the amplicon targeted by their same primers in $Ca_v3.2^{-/-}$ brain. The positive $Ca_v3.2$ mRNA expression in $Ca_v3.2^{-/-}$ brain was further confirmed with western blotting, detecting positive $Ca_v3.2$ protein expression (Figure 8A) using rabbit polyclonal anti-$Ca_v3.2$ (cat#ACC-025, Alomone, Jerusalem, Israel) in contrast to from the original report showing negative $Ca_v3.2$ protein expression. We contacted the authors of

the original paper (Dr. Campbell and Dr. Chen) who suggested we use an alternative set of primers (Lin *et al.*, 2014), (Figure 8D). The absence of $Ca_v3.2$ mRNA expression was further confirmed with a narrowed tracheal phenotype consistent with that described by Lin *et al.*, 2014 (Figure 8E).

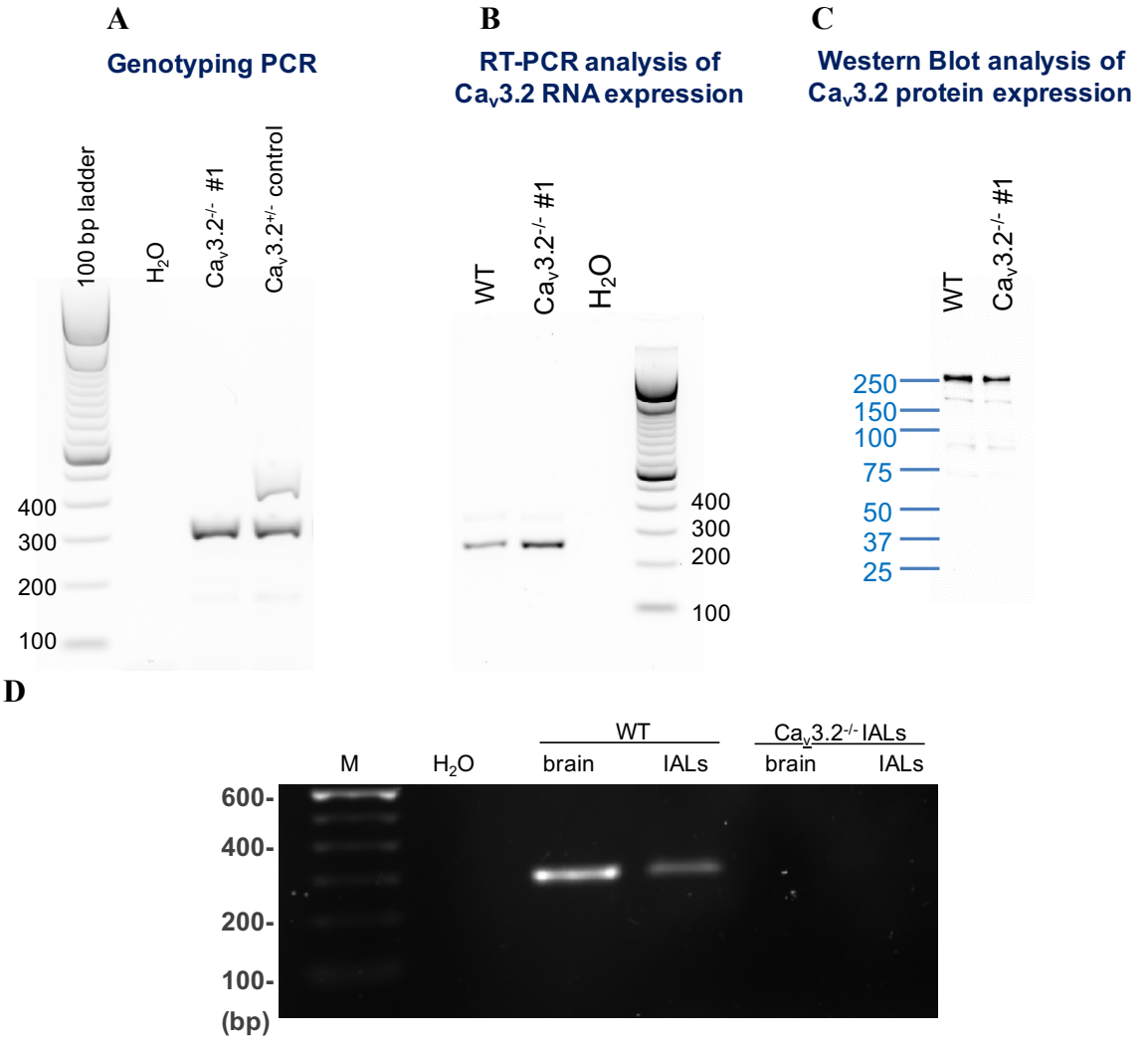

E

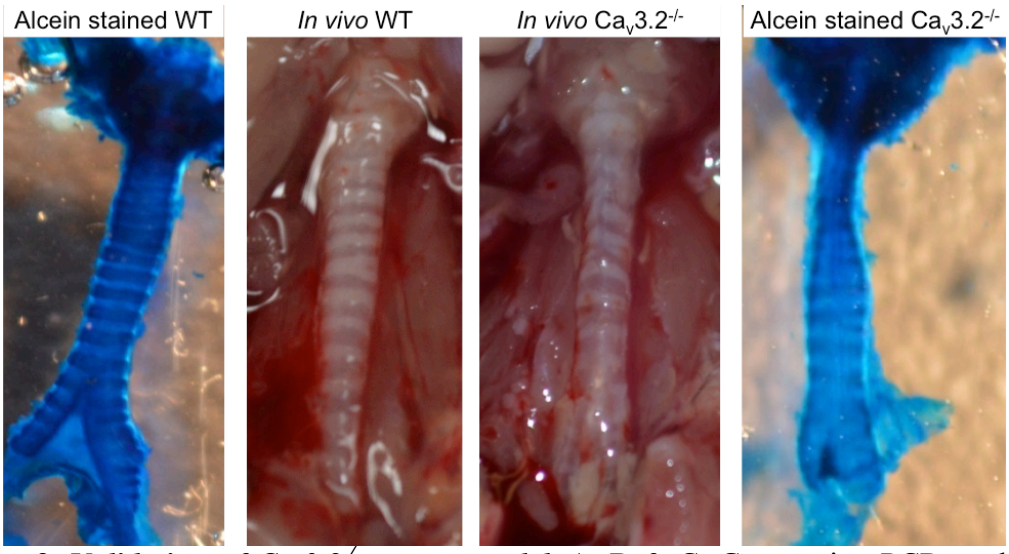

Figure 8. Validation of $Ca_v3.2^{-/-}$ mouse model. A, B & C: Genotyping PCR, end-point PCR and western blot results of brain sample from a representative $Ca_v3.2^{-/-}$ mouse (#1) indicate the presence of both mRNA (n=3) and protein expression (n=1) of $Ca_v3.2$ in $Ca_v3.2^{-/-}$ mice using PCR primers previously used in Chen *et al.* 2003 and rabbit polyclonal anti-$Ca_v3.2$ (cat#ACC-025, Alomone, Israel). D: end-point PCR detecting $Ca_v3.2$ in $Ca_v3.2^{-/-}$ mice using a newer set of PCR primers recently used by Chen's group (Lin *et al.*, 2014) showed the absence of $Ca_v3.2$ mRNA expression. E: The lack of Cav3.2 mRNA expression was further confirmed by a typical tracheal phenotype in 10-week old $Ca_v3.2^{-/-}$ mice (n=3).

2.10.2 Validation of global $Ca_v3.1^{-/-}$ mice

To validate the $Ca_v3.1^{-/-}$ mouse model, I tested the mRNA expression of $Ca_v3.1$ in brain harvested from $Ca_v3.1^{-/-}$ mice. I confirmed the absence of $Ca_v3.1$ mRNA expression in brain harvested from $Ca_v3.1^{-/-}$ mice.

2.11 Chemicals

Unless otherwise stated, all chemicals were obtained from Sigma (St. Louis, MO), except for BSA (US Biochemicals; Cleveland, OH), $MgSO_4$, HEPES (Fisher Scientific; Pittsburgh, PA, USA), and TTA-A2 (Alomone, Jerusalem, Israel).

2.12 Data analysis

All data were analyzed using Prism 5 (Graphpad, La Jolla, CA, USA) and JMP 8 (SAS institute, Cary, NC, USA). A one-way ANOVA was performed to compare contraction parameters before and after pharmacological treatments in the same lymphatics. A two-way ANOVA was performed to compare contractile function parameters between transgenic and WT mice. P-values less than 0.05 were considered significant. The data are expressed as mean ± standard error of the mean.

CHAPTER 3: RESULTS

3.1 Representative contraction pattern recording using pressure myograph

I used pressure myography to functionally assess the contraction patterns of isolated collecting lymphatic vessels from rat, WT mice, and transgenic mice with selective genetic deletion of Ca^{2+} channel isoform(s) in the presence of voltage-gated Ca^{2+} channel modulators and acetylcholine. A representative recording of inner diameter shows the contraction patterns of a cannulated and pressurized collecting lymphatic vessel (Figure 9A). The technique of pressure myography simulates the physiological pressure conditions experienced by the collecting lymphatics in the body. I routinely used vessel segments containing at least one intraluminal valve, thus enabling pressure control throughout the segment. Frequency is the number of spontaneous contractions in a minute; in the example below (Figure 9A), there are eleven contractions/min. Inner diameter is tracked to record end diastolic diameter (EDD) and end systolic diameter (ESD). ESD is the lymphatic diameter where the lymphatic vessel contracts maximally during the spontaneous contraction cycle. EDD is the diameter at the end of the contraction cycle. Amplitude is the difference between EDD and ESD. Maximal diameter (MaxD) was recorded at each pressure at the end of the experiment when the vessel was perfused with Ca^{2+}-free Krebs. Tone, ejection fraction, and fractional pump flow were calculated to comprehensively describe lymphatic contractile function (Scallan *et al.*, 2013a). To compare between two groups, amplitude can be normalized to MaxD if their EDD values significantly differ. For pressure steps, frequency can be normalized to the maximal frequency value over the different pressure steps. The maximal frequency value usually occurs at pressure 8 or

10cmH_2O, but it can sometimes occur at lower pressure steps. For dose response curves to pharmacological agents, frequency can be normalized to the control value prior to inhibitor/agonist application (Figure 9C).

A

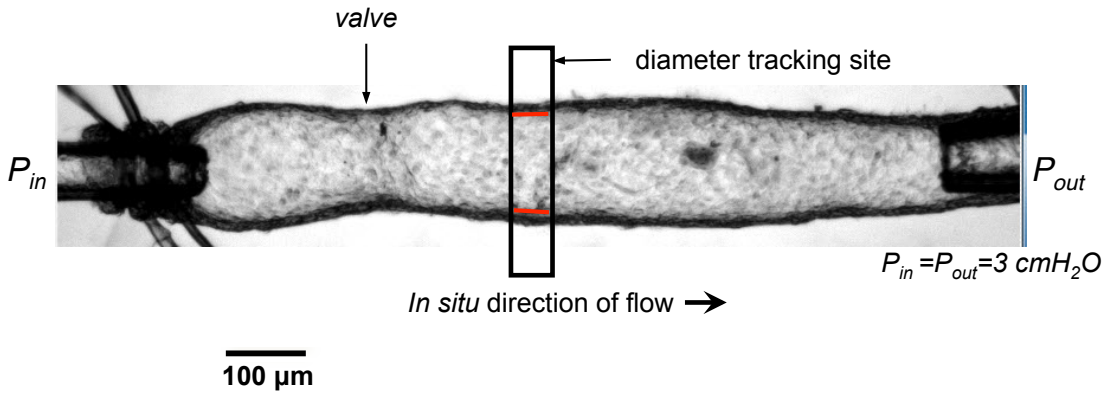

B

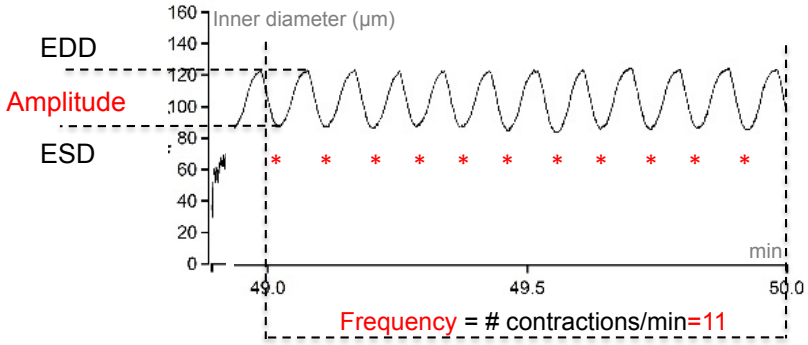

C

$$AMP = EDD - ESD \quad (1)$$

$$\%\ Tone = [(MaxD - EDD)/MaxD] \times 100 \quad (2)$$

$$Ejection\ fraction\ (EF) = (EDD^2 - ESD^2)/EDD^2 \quad (3)$$

$$Fractional\ pump\ flow\ (FPF) = FREQ \times EF \quad (4)$$

$$Normalized\ AMP = (AMP/MaxD) \times 100 \quad (5)$$

$$Change\ in\ EDD = EDD - EDD_{avg} \quad (6)$$

$$Change\ in\ \%\ Tone = \%Tone - \%Tone_{avg} \quad (7)$$

$$Normalized\ FREQ = (FREQ/FREQ_{avg}) \times 100 \quad (8)$$

Figure 9. Example of a pressure myography recording. A: An inguinal-axillary lymphatic vessel (inner diameter=120µm) is cannulated and pressurized at two ends onto two glass micropipettes for pressure control. B: Representative diameter recording characterizing the

contraction patterns of an *ex-vivo* pressurized inguinal-axillary lymphatic vessel; C: Formulas used to calculate the contractile parameters to assess the lymphatic contractile function (Scallan *et al.*, 2013a).

3.2 Rationale for the study of different lymphatic vascular beds

I tested the expression of T-type Ca^{2+} channels in LSM cells at the mRNA, protein, and electrophysiological levels and then assessed their functional role in lymphatic pacemaking in rat and/or mouse using pressure myography. Rat mesenteric lymphatics were used initially to compare my work with other published lymphatic contractile studies. Subsequently, due to the lack of transgenic rat models, I shifted to mouse transgenic models to allow tests of contractile function after deletion of specific VGCC isoforms (Chen *et al.*, 2003; Moosmang *et al.*, 2003; Lee *et al.*, 2001). While mesenteric lymphatics in rat and most other species show strong contraction patterns (Telinius *et al.*, 2014a; Gashev *et al.*, 2009, von der Weid *et al.*, 2008, and Beckett *et al.*, 2007), mouse mesenteric lymphatics do not (Scallan *et al.*, 2015). Therefore, I used two other types of lymphatic vessels exhibiting rhythmic and spontaneous contraction patterns at different locations in the mouse: 1) the inguinal-axillary lymphatic vessel (IAL), which is both an efferent vessel draining the inguinal node in the flank and an afferent vessel entering the axillary node group, and 2) the afferent popliteal lymphatic vessel (PL) in the lower leg, which feeds into the popliteal node behind the knee (Figure 10). Figure 10A is an image taken from a Prox1-GFP mouse, a mouse line with fluorescent lymphatic endothelial cells, allowing capture of the lymphatic vessels *in vivo* after the overlying skin is retracted (Choi *et al.*, 2011). Of the two vessels, the PLs are more difficult to cannulate and clean because the surrounding connective tissue and fat cells are more tightly attached to the lymphatic wall and the vessel

diameter is smaller. At 3cmH_2O, EDD of PLs averages 86.9±1.5µm, while EDD of IALs averages 106.7±3.2µm. The use of two lymphatic vessels from different regions, which presumably experience different pressures *in vivo* could potentially provide stronger support for my conclusions about a common role of T-type Ca^{2+} channels in lymphatic pacemaking.

The pressure step protocol went from 0.5, 1, 2, 3, 5, and 8cmH_2O for both IALs and PLs. An additional increase to 10cmH_2O was added for PLs, given that it likely experiences higher pressure *in vivo* than the IALs (at least in some body positions). As shown from the traces in Figure 10B and C, popliteal vessels continue to show a measureable contraction amplitude at 10cmH_20, whereas the inguinal-axillary contraction amplitude is close to zero at pressures above 5cmH_2O. The absolute contraction amplitude change is quite similar between the two vessel types at low pressures. The amplitude peaked at either 1 or 2cmH_2O in IALs, and either 2 or 3cmH_2O in PLs. The pressure at which the contraction amplitude peaks reflects the optimal LSM cell length/circumferential stretch prior to generation of force, which is determined by the optimal level of overlap between actin and myosin. Circumferential stretch greater than the optimal pressures caused IAL amplitude to drop dramatically while the PL amplitude was able to withstand higher pressures and maintain a reasonable contraction amplitude over a wider range of pressure. In IALs, amplitude ranged from 5.1 to 34.9µm (3.4 to 22% when normalized to maximal diameter), while in PLs, it ranged from 10.9 to 40.3µm (11.7 to 42.6% when normalized). Absolute frequency ranged from 15.3 to 30.7 contractions/min in IALs and from 4.8 to 12 contractions/min in PLs. In both types of lymphatic vessels, normalizing absolute frequency to peak frequency revealed an overlapping frequency response to

pressure changes in both types of vessels. Frequency increased up to the optimal pressure, reached a plateau over the middle pressure range, and was maintained in PLs or slightly increased in IALs. When diastolic diameter was normalized to the maximal diameter in Ca^{2+}-free solution, PLs had a lower basal tone, around 10%, while IALs had a higher basal tone, around 30%. The level of IAL tone is comparable to tone is some arterioles (Hill *et al.*, 2001). As a volume-index of contraction amplitude, ejection fraction (EF) considers the lymph volume expelled in a lymphatic contraction; EF showed a similar response to pressure as contraction amplitude. Fractional pump flow incorporates both frequency and EF; it peaks at 1-2cmH_20 for IALs and at 2-3cmH_2O for PLs. In summary, both lymphatic vessels contract most efficiently at low pressures, likely reflecting the innate pressure levels in the lymphatic vasculature. Both vessels regulate their function following the Frank-Starling Law analogous to the heart, that is, increasing intraluminal pressure over a certain range can lead to an increase of contractile function and pump output.

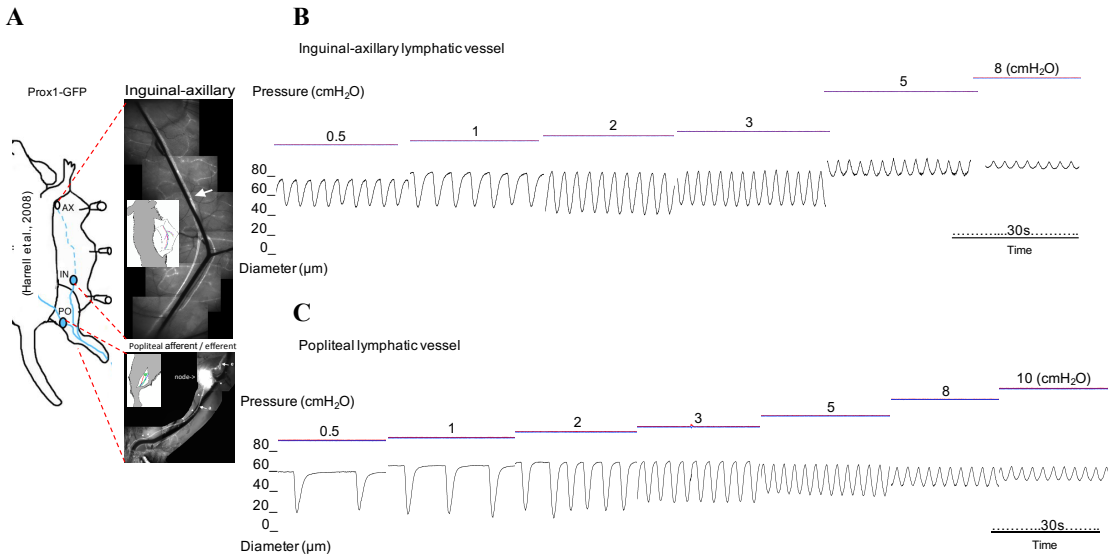

D. Summary of contractile parameters as a function of pressure

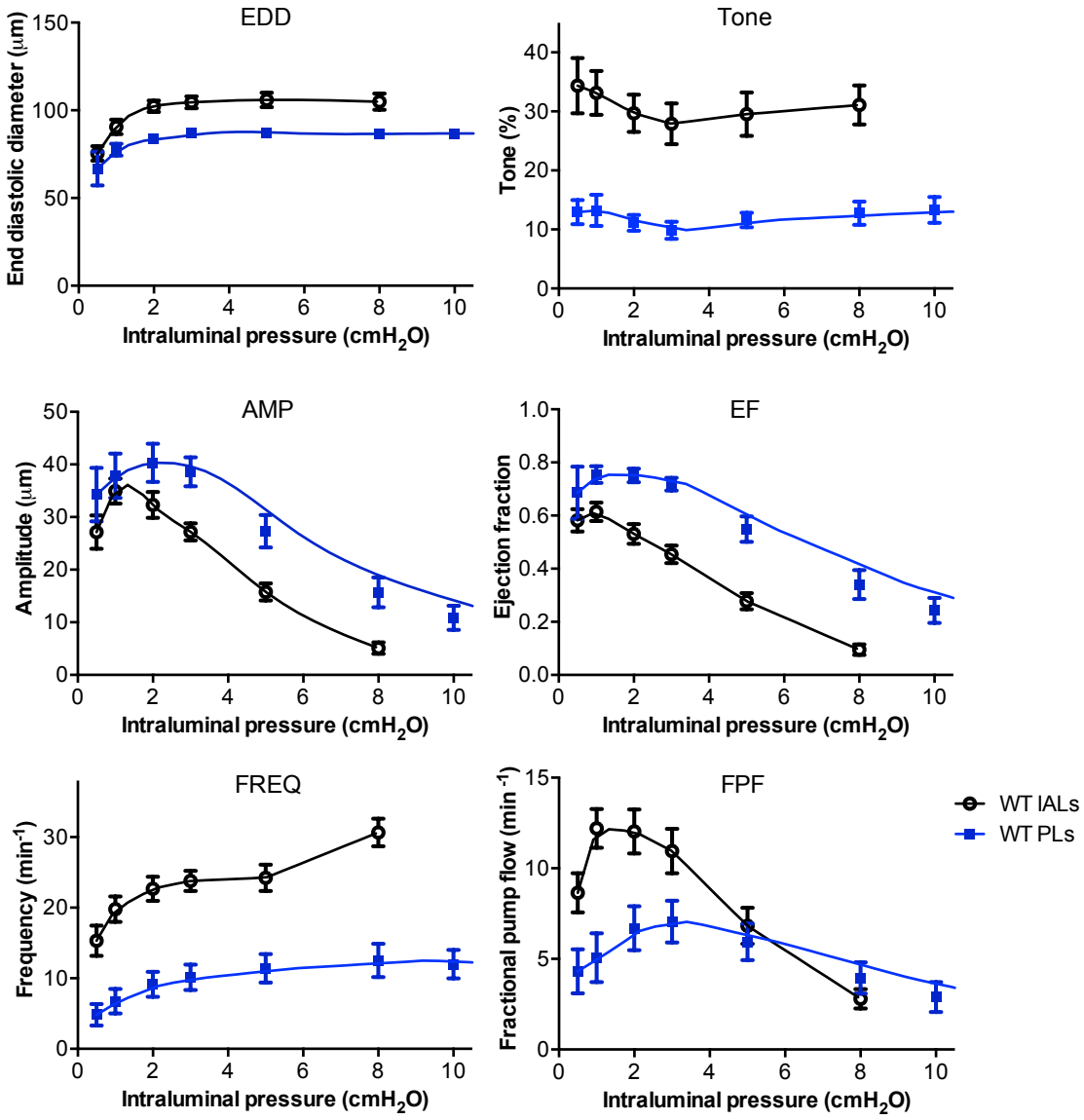

Figure 10. Position of inguinal-axillary and popliteal lymphatics in the mouse body, their patterns of contraction and summary of contractile parameters. A: The anatomical locations of inguinal-axillary and popliteal lymphatics in the mouse. Photomontages were captured in Prox1-GFP mice (by MJD). B & C: Representative pressure myograph recordings throughout the pressure step protocol for the two types of vessels (popliteal traces by MJD). D: Summary data showing the change in contractile patterns for the

pressure step protocol in inguinal-axillary (black lines, open symbols; n=6) and popliteal lymphatics (blue lines, closed symbols; n=8), refers to the number of lymphatic vessels; popliteal data collected by MJD. Timescales indicate intervals of 30s.

3.3 Nomenclature

Scientists studying lymphatic contractile function use the two terms "lymphatic muscle" and "lymphatic smooth muscle" interchangeably to indicate the layer of cells in the tunica media of the collecting lymphatic vessel wall that drive the spontaneous contractions of that vessel. When studying pacemaking properties, the term "lymphatic muscle" is often used to contrast its properties to those of cardiac muscle. However, in the literature LSM has been molecularly characterized by expression of smooth muscle markers, i.e., smooth muscle heavy chain (SMMHC) and smooth muscle α-actin (SMA) (Muthuchamy *et al.*, 2003), therefore the term "lymphatic smooth muscle" is commonly used. To be consistent with the current literature, I will use the term "lymphatic smooth muscle" (LSM) throughout the rest of this dissertation.

3.4 Lymphatic smooth muscle cell isolation

A digestion protocol was optimized for the isolation of rat or mouse LSM cells from the mixture of cell and tissue types present in an isolated lymphatic vessel: including lymphatic endothelial cells, smooth muscle cells, immune cells, neural cells, adipose cells and connective tissue cells (e.g. mast cells, fibroblasts). Morphology, cell size and cell capacitance are features used to differentiate between some of the different cell types, as described in the Methods section.

The membrane capacitance of LSM cells ranged between 9-25pF. After enzymatic isolation, their initial morphology in physiological solution is bean- or spindle shaped. The

cell morphology can change during the voltage clamp process: cells can round up when depolarized, indicating a healthy cell membrane. The cell morphology matches with the fluorescent lymphatic cells digested from αSMA-DsRed^{P} and SMMHCCre-eGFP lymphatic vessels, with smooth muscle indicators constitutively fluorescing at 635nm (Figure 11A) and 488nm (Figure 11B), respectively. Figure 11C shows the LSM cell morphology in brightfield mode. These isolated LSM cells were used in two different ways in my project: 1) to record ion movement through VGCCs and 2) to test for the expression of T-channels in the LSM.

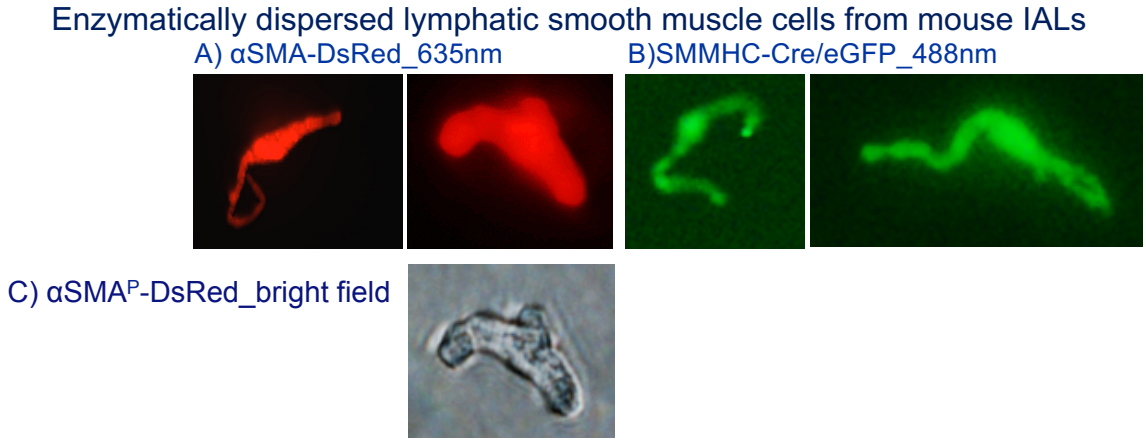

Figure 11. Morphology of lymphatic smooth muscle cells from mouse inguinal-axillary lymphatic vessels. LSM cells from transgenic mice expressing fluorescence in smooth muscle cells using two different promoters: A) αSMA and B) SMMHC: the cells are elongated in Ca^{2+}-free solution); C) image of an αSMA-DsRed LSM cell in PSS in brightfield mode.

3.5 Evidence of T-channels in collecting lymphatics at the mRNA level

3.5.1 mRNA expression of voltage-gated Ca^{2+} channels in rat mesenteric lymphatic vessels

To detail the profile of voltage-gated Ca^{2+} channels in lymphatic vessels, I started by confirming their mRNA expression in rat mesenteric lymphatics, as reported by Lee *et al.*, 2014a. These vessels can be dissected in relatively large quantities because post-prandially they appear visibly off-white and are easy to dissect and clean of fat and connective tissue. End-point PCR was utilized to detect the presence of L and T-type Ca^{2+} channels at the mRNA level in rat brain (as a positive control) and in whole mesenteric lymphatic vessels (LVs). In whole rat mesenteric LVs, I found the expression of two out of three isoforms of T-channels ($Ca_v3.1$ and $Ca_v3.2$). $Ca_v3.3$ was absent, which is not surprising because $Ca_v3.3$ is predominantly expressed in neural tissue (Astori *et al.*, 2011). Also, the L-channel isoform that is predominantly expressed in blood vessels and cardiac muscle, $Ca_v1.2$, was expressed in rat mesenteric lymphatics (Figure 12A).

Before I performed endpoint PCR on lymphatic vessels and LSM cells, preliminary quantitative PCR for all VGCCs (Ca_v1, Ca_v2, $Ca_v3.x$) was performed in Donald Welsh's laboratory (University of Calgary, Canada) to provide an independent, comprehensive quantitative profile of VGCCs in rat mesenteric LVs, and mouse popliteal LVs (vessels dissected by MJD). Similar to the end-point PCR results, qPCR confirmed the expression of the two T-channel isoforms $Ca_v3.1$ and $Ca_v3.2$ and the absence the neuronal T-isoform $Ca_v3.3$ (Figure 12B). $Ca_v3.2$ appeared to show stronger expression in rat mesenteric LVs. Also, three out of four L-channel isoforms $Ca_v1.1$, 1.2, and 1.3 were detected, with strongest expression of $Ca_v1.2$, and the signals were all stronger than that for the T-channel isoform $Ca_v3.1$. The neuronal voltage-gated N-type Ca^{2+} channel isoform $Ca_v2.2$ and the

R-type Ca^{2+} channel isoform $Ca_v2.3$ were also detected, possibly due to the remnants of neural cell processes innervating the lymphatic wall. These findings aligned with those of Lee *et al.*, 2014a who showed convincing evidence for the expression of the T-channel isoform $Ca_v3.2$ at both mRNA and protein levels along with $Ca_v3.1$ (only at the mRNA level) in rat mesenteric lymphatics (Lee *et al.*, 2014a). Consistent with our findings, they also found the expression of three L-channel isoforms $Ca_v1.1$, 1.2, and 1.3. Because their study also reported the expression of $Ca_v3.2$ and $Ca_v1.2$ at the protein level, colocalizing with SMA, I did not repeat immunostaining for Ca^{2+} channels in rat mesenteric lymphatic vessels.

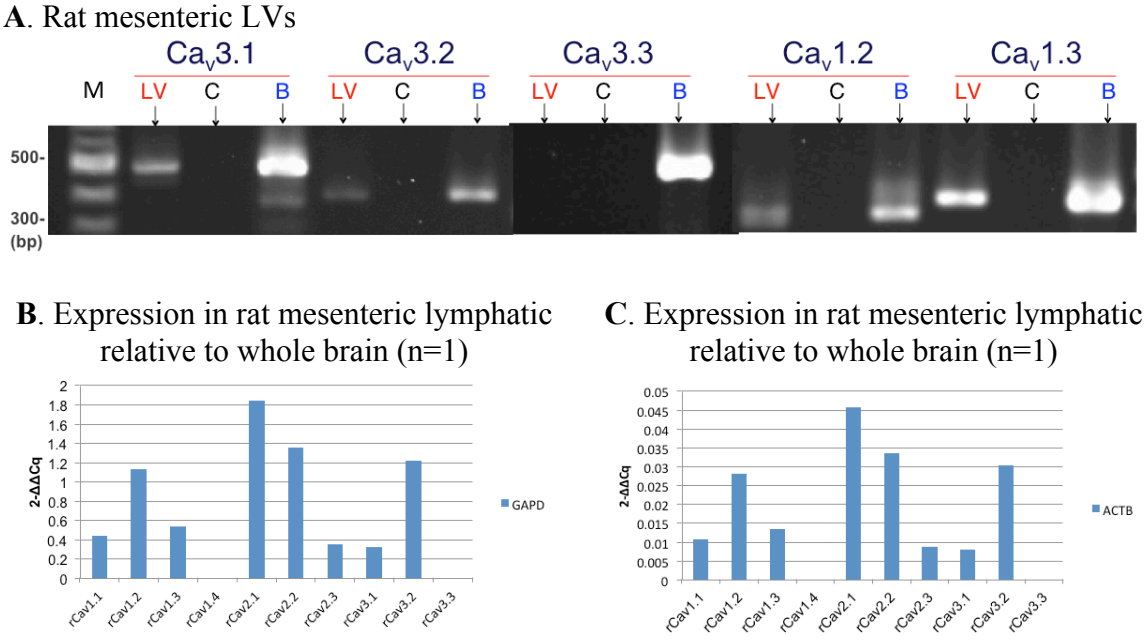

Figure 12. mRNA expression of VGCCs in rat whole mesenteric lymphatic vessels detected by end-point and quantitative PCR. A: Representative end-point PCR gel (n=3) shows the mRNA for Ca^{2+} channels from rat mesenteric lymphatic vessels (LV), negative control: H_2O (C), and positive control: brain (B). Each PCR experiment was performed on at least eight lymphatic vessels dissected from one rat. The "n" is the number of animals

used, as well as the number of PCR experiments performed. The sizes of PCR amplicons coincide with those of the RNA sequences in the targeted genes. B and C: Real-time quantitative PCR of Ca^{2+} channels in rat (e.g., rCav3.1 denotes rat $Ca_v3.1$) mesenteric lymphatic vessels using two different housekeeping genes: glyceraldehyde-3-phosphate dehydrogenase (GAPD) and β-actin (ACTB) performed by Welsh laboratory. The results are shown as relative Ca^{2+} channel mRNA expression to that in the rat whole brain. The ratios between the mRNA expression of different Ca^{2+} channels with two housekeeping genes are nearly identical, strengthening the finding of T-channels detected in rat whole mesenteric lymphatic vessels. M: molecular markers using 100 base pairs (bp) DNA ladder.

3.5.2 RNA expression of voltage-gated Ca^{2+} channels in mouse popliteal lymphatic vessels

To profile the VGCCs expressed in mouse lymphatic vessels, I started with mouse PLs, the lymphatic vessels possessing strong pumping capacity. Using end-point PCR and rat brain as positive control, I found, similar to rat mesenteric LVs, that whole popliteal LVs expressed message for two out of the three isoforms of T-channels, $Ca_v3.1$ and $Ca_v3.2$ ($Ca_v3.3$ was absent), along with the predominant cardiovascular L-channel isoform ($Ca_v1.2$) (Figure 13A). In addition, we sent whole PLs (dissected by MJD) to Donald Welsh's laboratory to quantitatively measure PCR of all VGCC mRNA and found that the material from one mouse is inadequate to be detected by traditional qPCR (n=1). The whole T-channel family was undetectable, partially reflecting the lower density of the T-channels in lymphatic vessels compared to L-channels (Figure 13B and C).

In later assays to detect RNA message, I used end-point PCR, using primers/nested primers, to answer the yes/no question as to the presence of T-channels in pure samples of

freshly digested and dispersed mouse LSM cells. Nested PCR, utilizing an internal set of primers to further amplify the PCR products, was performed in case the first round of PCR products showed no signal or a very faint signal, to detect any potential false negatives due to the low density of T-channels in LSM. The goal was to determine whether T-channels are expressed in mouse LSM.

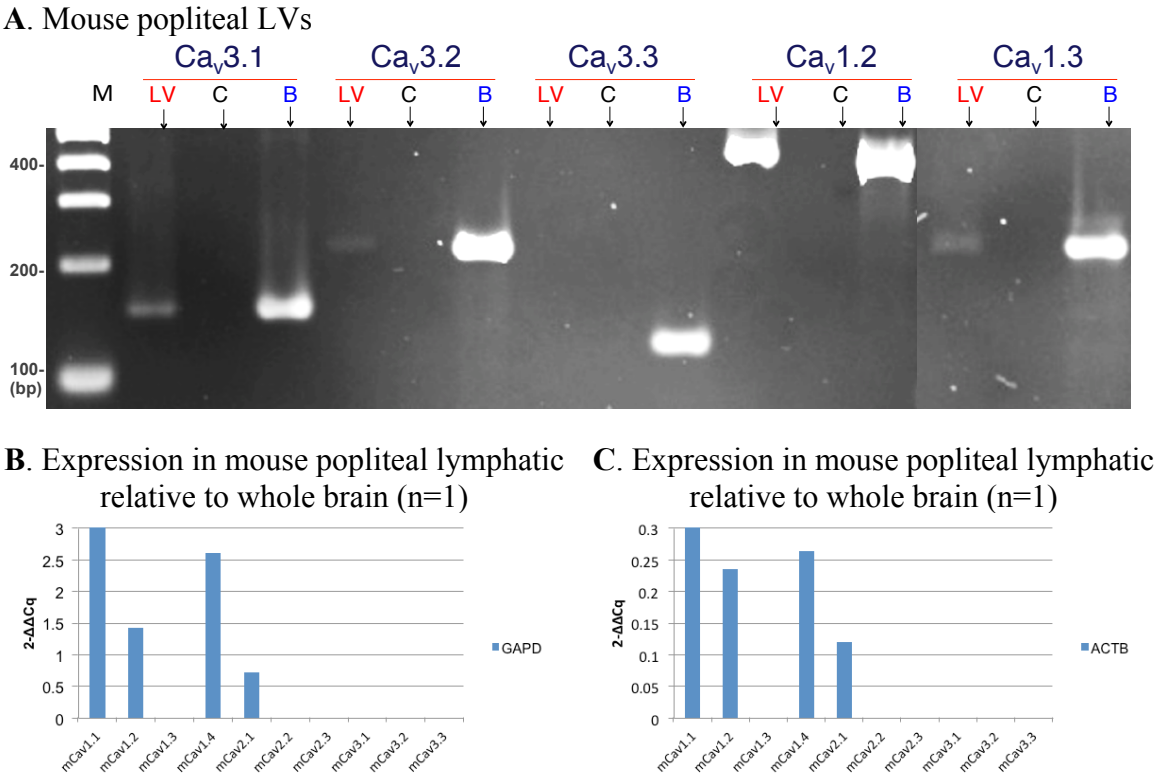

Figure 13. mRNA expression of VGCCs in mouse whole popliteal lymphatic vessels. A: Representative end-point PCR gel (n=3, refers to number of tissue batch, each was harvested from at least 4 mice) shows the mRNA expression for Ca^{2+} channel in mouse whole popliteal lymphatic vessels (LV), negative control: H_2O (C), and positive control: brain (B). Each experiment was performed on at least sixteen lymphatic vessels dissected

from four mice. The sizes of PCR amplicons coincide with those of the RNA sequences in the targeted genes. B and C: Real-time quantitative PCR for Ca^{2+} channels in mouse ($mCa_v3.1$ denotes mouse $Ca_v3.1$) popliteal lymphatic vessels using two different housekeeping genes: glyceraldehyde-3-phosphate dehydrogenase (GAPD) and β-actin (ACTB) performed by Welsh laboratory. The results are shown as Ca^{2+} channel mRNA expression relative to that in the mouse whole brain. M: molecular markers using 100-bp DNA ladder.

3.5.3 RNA expression of voltage-gated Ca^{2+} channels in LSM cells isolated from mouse popliteal lymphatic vessels

I found signal for T-channels by PCR from whole lymphatic vessels both in rat and mouse. However, the whole vessel is a complex structure with many types of cells, as mentioned earlier, in section "3.4 Lymphatic smooth muscle cell isolation". To answer the question as to whether T-channels are expressed specifically by lymphatic smooth muscle cells, I digested PLs and collected single LSM cells using a micropipette, based on their morphology, and performed end-point PCR to ensure that the signal I found previously in whole popliteal vessels was specifically from the muscle cells. Each PCR was performed with ~500 smooth muscle cells digested and isolated from sixteen PLs collected from four mice. Since single LSM cell collection yielded less primary material than that from whole lymphatic vessels, nested PCR was used if the signal was weak. In addition to using primers for VGCCs as described for whole vessels, I also used eNOS primers to detect potential contamination from endothelial cells accidentally collected by the pipette aspiration. α-actin primers were used to confirm the identity of individually collected cells based on that reported molecular marker for LSM (Muthuchamy *et al.*, 2003).

In LSM cells, I consistently detected the expression of the two isoforms $Ca_v3.1$ and $Ca_v3.2$ found in whole vessels. The signal for the L-channel isoform $Ca_v1.2$ was also present abundantly. α-actin was detected, consistent with a molecular identity for LSM; however, eNOS was also found, raising the need for checking for T-channel expression in lymphatic endothelial cells.

I subsequently performed PCR on a lymphatic endothelial tube, digested and divested of lymphatic smooth muscle cells. Lymphatic vessels served as a positive control. eNOS signal confirmed endothelial cell identity. This is the first time eNOS has been shown at the mRNA level from a PL endothelial tube, although eNOS has been found at protein level inside collecting lymphatics by immunostaining in cross-sections of vessels (Hagendoorn *et al.*, 2004). The absence of α-actin signal suggested complete elimination of LSM cells. While $Ca_v3.1$ or $Ca_v3.2$ signals were detected in whole lymphatic vessels, no $Ca_v3.1$ or $Ca_v3.2$ signals were amplified in the endothelial sample (Figure 14C).

A. A lymphatic muscle cell with a collecting pipette tip

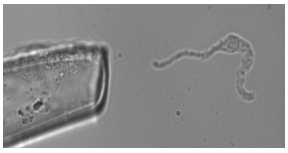

B. Popliteal lymphatic smooth cells

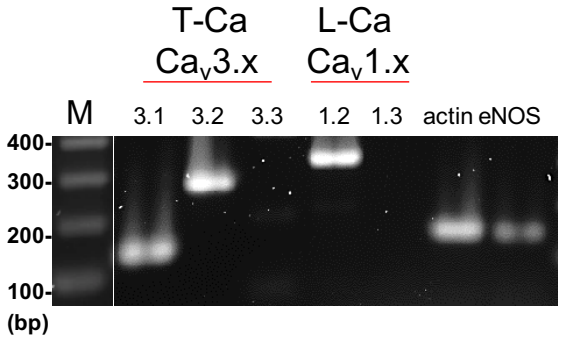

C. Popliteal lymphatic endothelial cells (LEC)

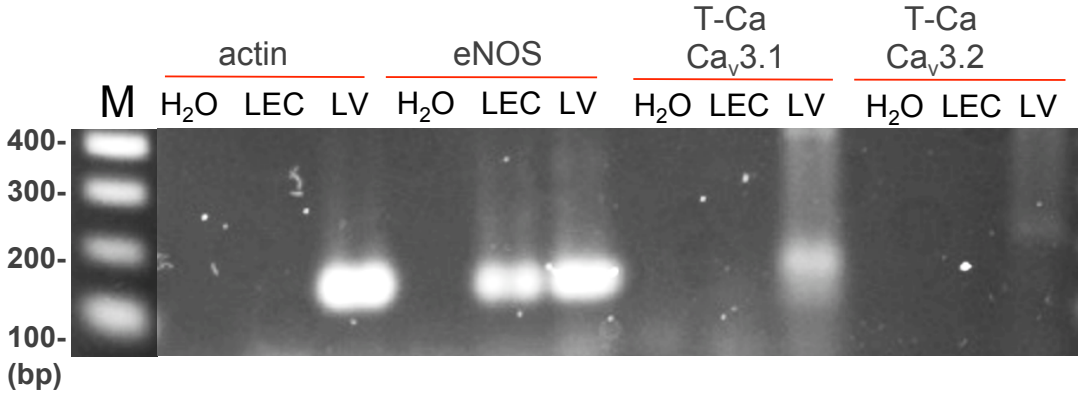

Figure 14. mRNA expression of VGCCs in single LSM cells freshly digested and isolated from mouse popliteal lymphatic vessels. A: A 30μm-pipette tip used to collect LSM cells identified by spindle-shaped morphology. B: Representative end-point PCR gel (n=3) shows mRNA expression for Ca^{2+} channels in popliteal LSM cells, with α-actin and eNOS serving as endothelial cell-specific positive and negative controls, respectively. At least sixteen popliteal lymphatic vessels (LV) dissected from four mice were used for one set of experiments, and I repeated each set of experiments thrice. The "n" refers to the number of tissue harvest repetitions; each required at least four mice. The sizes of PCR amplicons coincide with those of the RNA sequences in the targeted genes. C: End-point PCR gel of a popliteal lymphatic endothelial cell (LEC) tube. Again, α-actin and eNOS were negative and positive controls for cell type, respectively. To test whether T-channels were expressed

in LEC tubes, I used primers for two T-channel isoforms $Ca_v3.1$ and 3.2 that had been detected in whole popliteal lymphatic vessels and collected popliteal LSM cells. M: molecular markers using 100 base-pair (bp) DNA ladder.

3.5.4 RNA expression of voltage-gated Ca^{2+} channels in mouse whole IAL vessels and in LSM cells isolated from mouse IAL vessels

Since I was also interested in testing the functional role of T-channels in IALs with patch-clamp and pressure myography, I repeated the PCR assay in whole IAL vessels and freshly-isolated IAL smooth muscle cells to assess their VGCC profile. I was able to detect all three T-channel isoforms $Ca_v3.1$, 3.2 and 3.3 in whole IAL vessels. I was only able to detect the expression of T-channel isoforms $Ca_v3.1$ and 3.2 in inguinal-axillary LSM cells; therefore, the $Ca_v3.3$ signal in whole IALs may originate from neuronal processes remaining in the vessel wall after dissection. Again, α-actin confirmed that the majority of the sample was LSM cells with very little contamination from lymphatic endothelial cells. This reflects the advantage of using the longer IALs, which requires fewer animals, saves time otherwise committed to harvesting cells, and offers less contamination. Since I could harvest longer vessels from the flank region between inguinal and axillary lymph nodes, each set of PCR required four IAL vessels from only two mice and two days to collect cells in comparison with the minimum requirements of sixteen PL vessels from four mice and four days of cell harvesting.

A

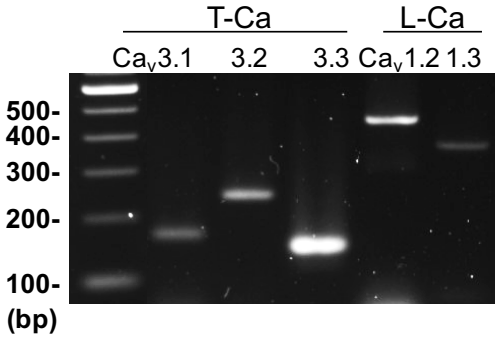

B

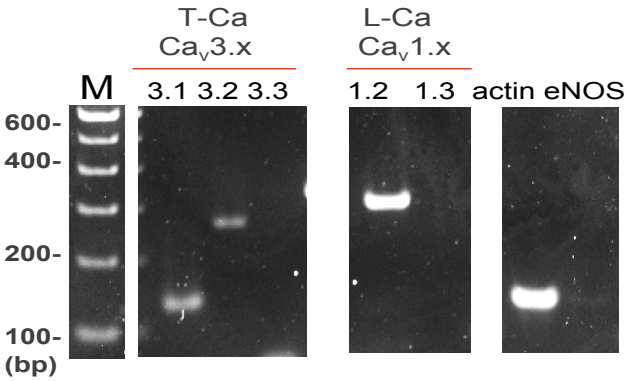

Figure 15. mRNA expression of VGCCs in mouse whole inguinal-axillary lymphatic vessels and their freshly digested and isolated single LSM cells. A: Representative end-point PCR gel (n=3) shows the mRNA expression for Ca^{2+} channel in IAL vessels. B: Representative end-point PCR gel (n=3) shows the mRNA expression for Ca^{2+} channel in inguinal-axillary LSM cells; actin and eNOS served as cell-type positive and negative controls, respectively. At least six lymphatic vessels dissected from at least two mice were used for one set of experiments, and I repeated each set of experiments thrice. The "n" refers to the number of tissue harvesting repetitions. The sizes of PCR amplicons coincide with those of the RNA sequences in the targeted genes. M: molecular markers using 100-bp DNA ladder.

3.6 Evidence for T-channels in collecting lymphatics at the protein level

In rat mesenteric lymphatic vessels, expression of the T-channel isoform $Ca_v3.2$ was confirmed with immunohistochemistry (Lee *et al.*, 2014a). However, no data were shown for the expression of the other T-channel isoforms, $Ca_v3.1$ or $Ca_v3.3$. I performed staining for the T-channel protein expression in mouse IALs utilizing the same antibody from Alomone used by Lee *et al.*, 2014a. For positive controls, I used an antibody for the L-channel isoform $Ca_v1.2$, which was abundantly expressed at the mRNA level and protein level (Lee *et al.*, 2014a), and I tested for T-channel expression in 2^{nd} or 3^{rd} order mesenteric arteries in which $Ca_v3.1$ and $Ca_v3.2$ expressions were previously verified (Harraz *et al.*, 2015) (Figure 16Ad and Bd). For negative controls, the same immunostaining process was performed after antibody pre-absorption with the appropriate antigen provided by Alomone. In WT mouse IALs, I found expression of both T-channel isoforms $Ca_v3.1$ and $Ca_v3.2$, with expression colocalizing substantially with smooth muscle α-actin (Figure 16Aa & Ba). Similarly, mesenteric artery smooth muscle cells also showed expression of both $Ca_v3.1$ and 3.2 (Figure 16Ad & Bd). In contrast, IALs from $Ca_v3.1^{-/-}$ mice showed spotty, non-specific binding rather a staining pattern that aligned with the vessel structure (Figure 16Ac); the negative controls using antibody pre-absorption by antigen also showed a spotty pattern. Surprisingly, IALs from $Ca_v3.2^{-/-}$ mice showed staining that did not align with any previously known vessel structure and seemed to form a layer outside. One can argue that the expression is in the adventitia and that the signal is from compensatory upregulation in cells outside of the muscle layer (Harraz *et al.*, 2015). The neuronal T-isoform $Ca_v3.3$ also showed similar non-specific binding rather than a staining pattern that

aligned with the vessel structure. The L-type Ca^{2+} channel positive control accordingly showed protein expression of $Ca_v1.2$ in the LSM cells (Figure 16Cc).

Table 7. Confocal and image processing settings for Ca^{2+} channel immunostaining

λ (nm)	**Exposure time (ms)**	**Power**	**Step distance (µm)**	**Primary antibodies**	**Brightness & contrast adjustment**
638	75-400	20-40	0.5	Ca^{2+} channel	Min: 9
448	750	100	0.5	SMA	Max: 115

(ImageJ)

A

a/ WT inguinal-axillary lymphatic

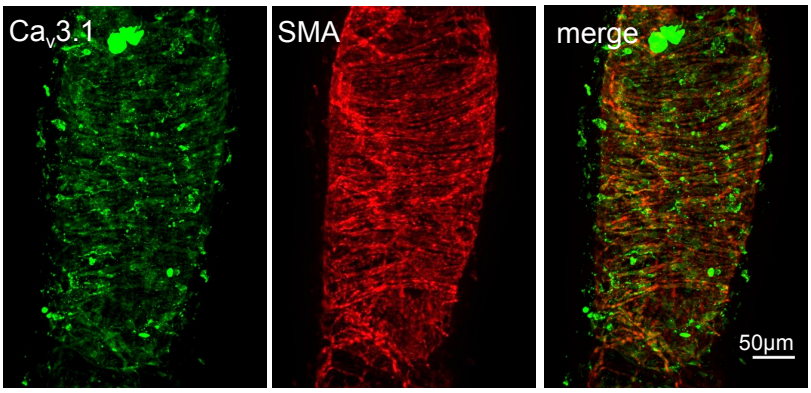

b/ WT inguinal-axillary lymphatic with antibody absorption (-) control

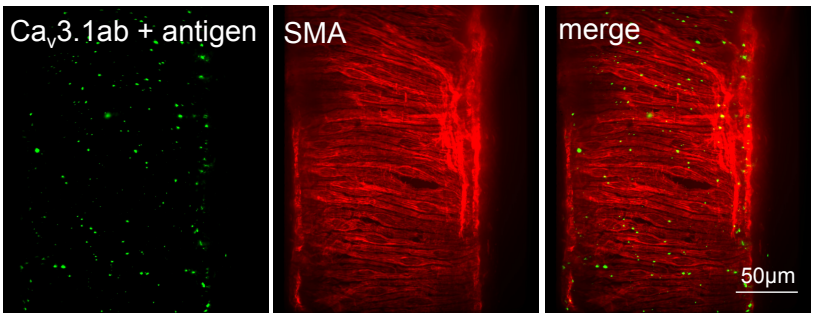

c/ $Ca_v3.1^{-/-}$ inguinal-axillary lymphatic

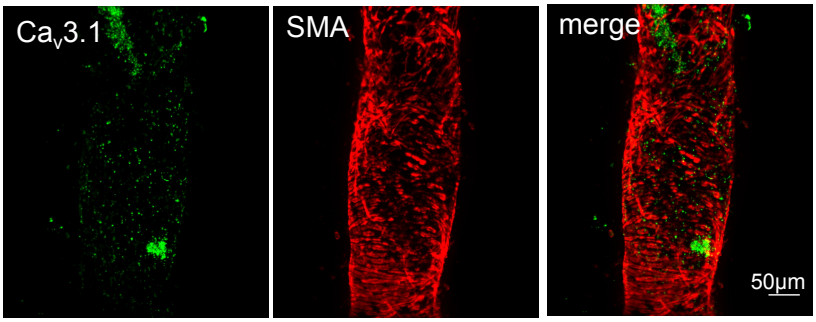

d/ WT mesenteric artery

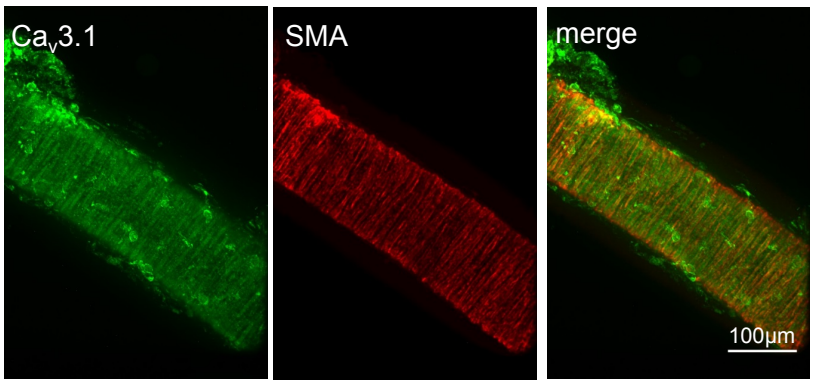

B

a/ WT inguinal-axillary lymphatic

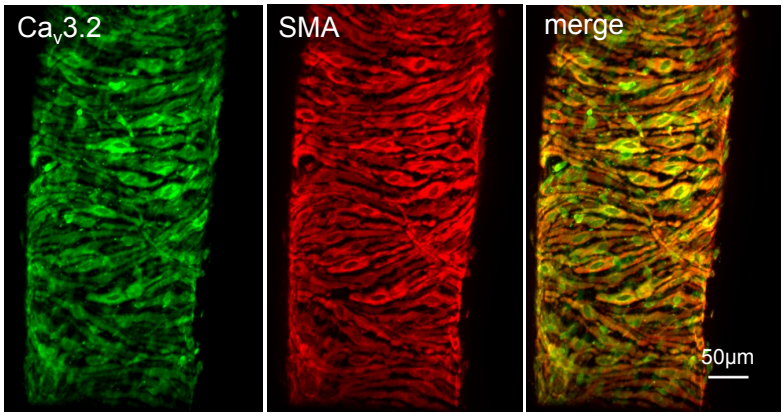

b/ WT inguinal-axillary lymphatic with antibody absorption (-) control

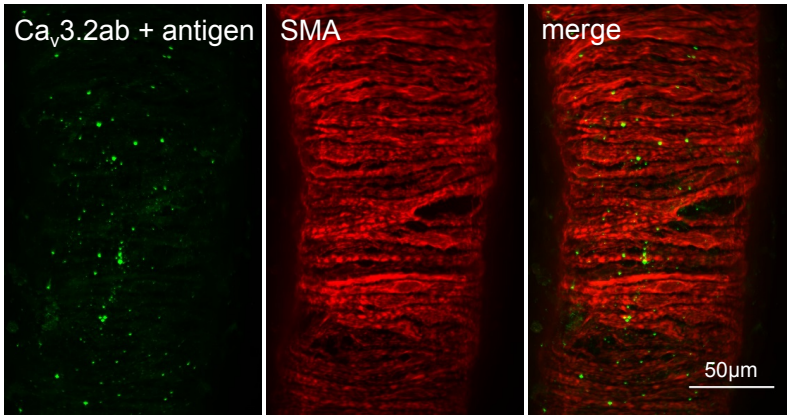

c/ $Ca_v3.2^{-/-}$ inguinal-axillary lymphatic

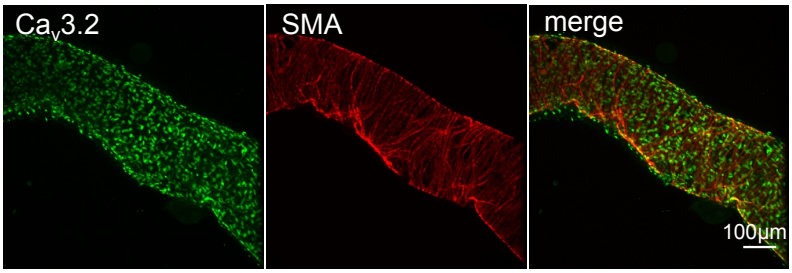

d/ WT mesenteric artery

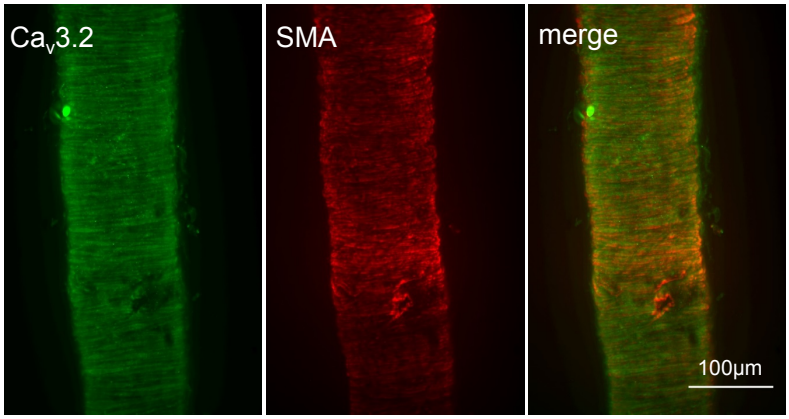

C

a/ WT inguinal-axillary lymphatic

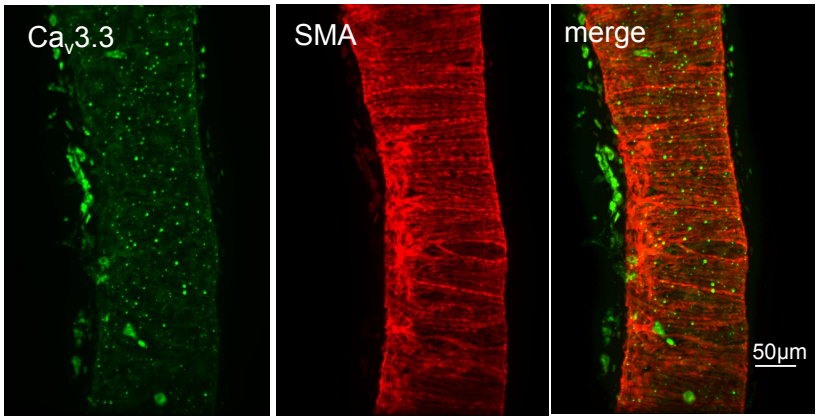

b/ WT inguinal-axillary lymphatic with antibody absorption (-) control

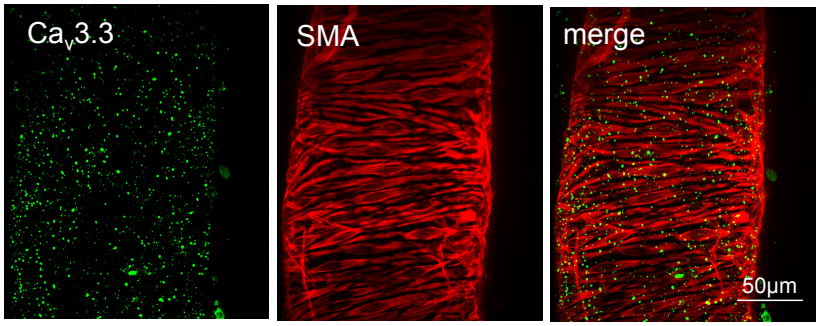

c/ WT inguinal-axillary lymphatic

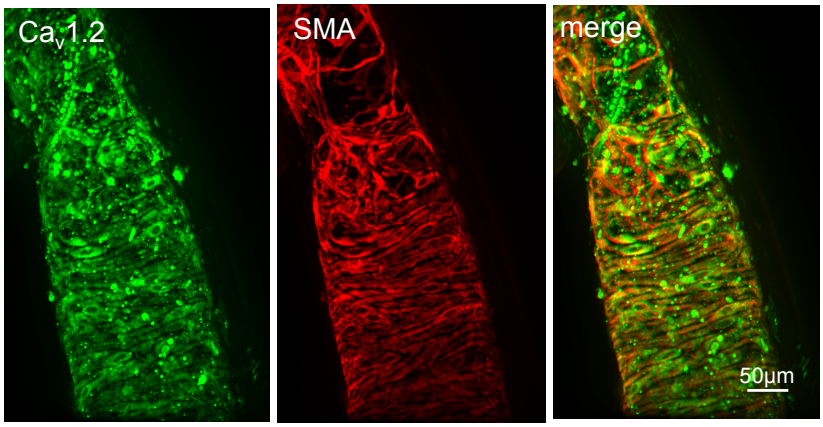

d/ WT inguinal-axillary lymphatic with antibody absorption (-) control

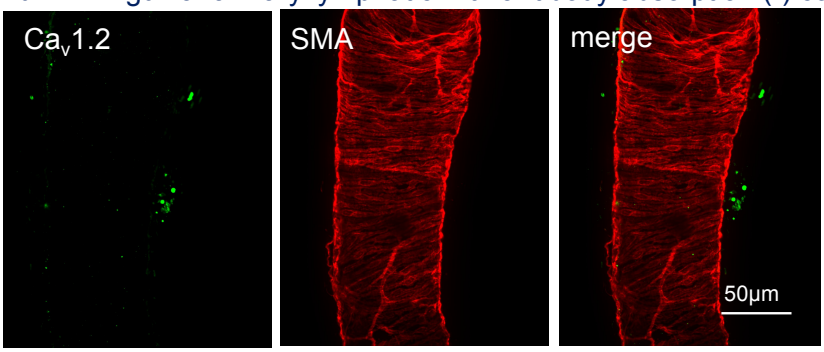

Figure 16. Immunohistaining of inguinal-axillary lymphatics for T and L-channels and their control counterparts. Immunostaining for A) $Ca_v3.1$, B) $Ca_v3.2$, C) $Ca_v3.3$ and $Ca_v1.2$ in inguinal-axillary lymphatics and their negative (i.e., antigen absorption negative control) and positive (WT mesenteric artery) controls. $Ca_v1.2$ staining also served as a positive control for VGCCs. Smooth muscle α-actin (SMA). Immunostaining was repeated at least three times for each Ca^{2+} channel isoform.

3.7 Electrophysiological evidence for T-type Ca^{2+} current in LSM cells

3.7.1 T-channel current in rat mesenteric lymphatic smooth muscle cells

To test for functional VGCCs, I used the patch-clamp technique to measure the current flowing through voltage gated-Ca^{2+} channels in single, isolated LSM cells. After digestion, the cell suspension was placed in a recording chamber perfused with bath solution containing Ca^{2+} 1.8mM at room temperature (see Methods). The cells that gave good gigaseals (>1GΩ) and recordings were healthy-looking and usually rounded up further during Ba^{2+} solution perfusion and repeated voltage manipulations. Unusable cells either had a thin cell membrane with damage spots and granulated intracellular organelles or had intact, shiny, but a less digested cell membrane with remaining undigested extracellular matrix. The Ca^{2+} 1.8mM bath solution contains a physiological Ca^{2+} level to better maintain the LSM cell vitality compared to high concentration of Ba^{2+} such as 10 or 20mM. To determine a usable cell for Ca^{2+} current recordings, the ability of a cell to respond to voltage stimulation was first tested with a voltage ramp protocol (Figure 17B) to see whether the cell was healthy and could give a measurable Ca^{2+} current with a typical U-shape I-V relationship. Whole-cell Ca^{2+} current density was low in 1.8mM Ca^{2+} bath solution, but could be enhanced by increasing the $[Ca^{2+}]$ and/or substitution with Ba^{2+}

(which is more permeable). However, prolonged incubation in 10 or 20mM Ba^{2+} bath solution caused cells to hypercontract or die rather than maintaining a partially relaxed, spindle/bean shape. Therefore, Ba^{2+} solution perfusion was applied only after finding a promising cell with a good seal and detectable Ca^{2+} current in 1.8mM Ca^{2+} (>5pA); after the perfusion had been changed to Ba^{2+}, the leftover cells would be discarded. My strategy to find a decent cell was to scan the whole chamber for several good cells and find the most promising ones to patch. A holding potential of -70mV was used to reset all VGCCs. The membrane potential was then depolarized using a ramp or step protocol. The ramp protocol provides a pseudo-instantaneous record of the I-V relationship, while the step protocol shows the time course of activation in response to depolarization to different levels. Figure 17C shows recordings from a rat mesenteric LSM cell in 10mM Ba^{2+} before and after addition of nifedipine 1μM to inhibit L-channels; subsequent addition of Ni^{2+} (1mM) was used to test for inhibition of the remaining nifedipine-insensitive current. The total current in control Ba^{2+} solution peaked in the range between 10-20mV. The treatment with 1μM nifedipine revealed a residual current, which accounted for approximately 20% of the total Ba^{2+} current, and peaked at a more hyperpolarized voltage than the total current (voltage ramp protocol recording is representative of at least five cells). This T-channel-like current was also inhibited by the classical T-channel blocker Ni^{2+} (1mM), and any residual L-channel current resistant to 1μM nifedipine was also inhibited. One can extrapolate that nifedipine-sensitive current, primarily through L-channels, accounted for 80% of total Ba^{2+} current (Figure 17C).

In the reverse protocol, in a cumulative Ni^{2+} dose-response protocol, when the cell was treated first with increasing doses of Ni^{2+}, the current tracing shifted toward a more

depolarized voltage. At 50μM Ni^{2+}, when $Ca_v3.2$ should be substantially inhibited, the current reduction was less than 10% of the total Ca^{2+} current. At 500μM Ni^{2+}, when $Ca_v3.1$ should be inhibited, the total Ba^{2+} current was reduced by 50%; however, at this concentration, L-channels, should also begin to be affected. At 1mM Ni^{2+}, 25% of the total Ba^{2+} current remained, this Ni^{2+}-insensitive current could be current through L-channels. Since in the test with nifedipine (Figure 17C), L-channels conducted 80% of the total Ca^{2+}-channel current, the Ni^{2+}-insensitive current is additional evidence of the off-target effect of Ni^{2+} on L-channels. Finally, treatment with 1μM nifedipine totally inhibited the remaining Ca^{2+}-channel current, suggesting that the Ni^{2+}-insensitive current passed through L-channels (Figure 17D).

A. Patch-clamp set-up

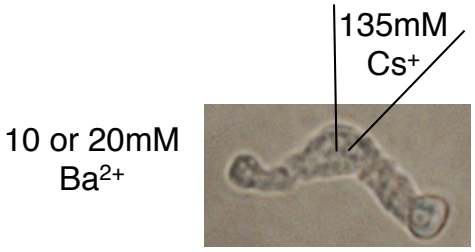

B. Ramp protocol

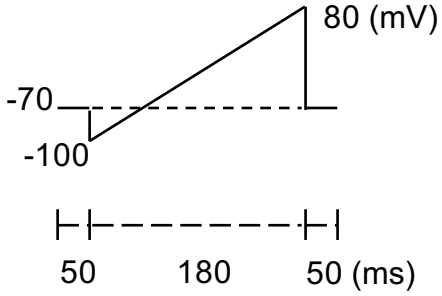

Rat mesenteric lymphatic smooth muscle cells

C. Nifedipine+Ni^{2+} (10mM Ba^{2+})

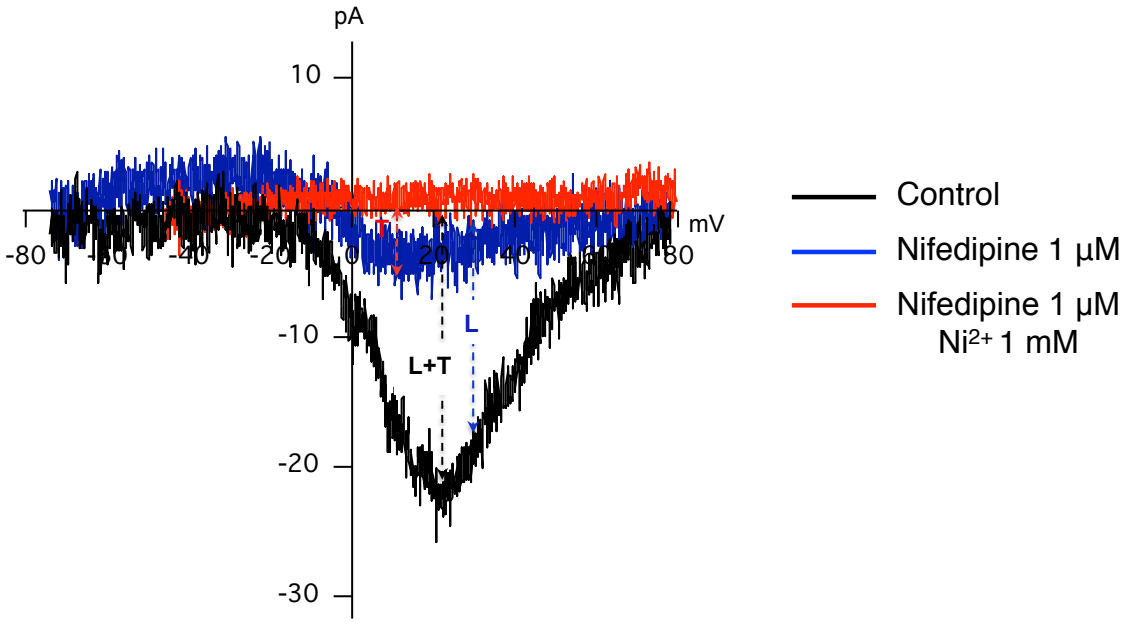

D. Ni^{2+}+nifedipine (10mM Ba^{2+})

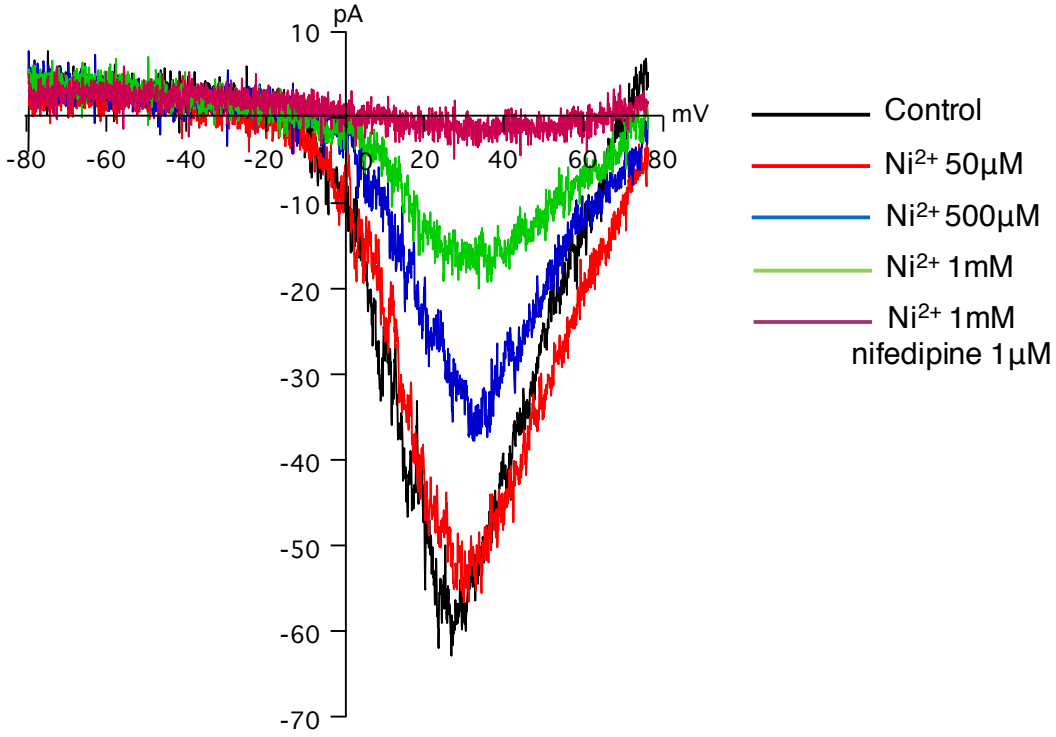

Figure 17. T-channel current in rat mesenteric lymphatic smooth muscle cells. A: Schema describing patch-clamp set-up perfusing freshly digested LSM cells with 10 or 20mM Ba^{2+} perfusing solution and patching cell membrane with pipette containing Cs^{+} to make whole-cell recordings; B: Ramp protocol used to elicit voltage-dependent current by progressively depolarizing from -100 to +80mV from a holding potential of -70mV. C: Representative traces of whole-cell Ba^{2+} currents in 10mM Ba^{2+} perfusing solution (black), after treatment with nifedipine 1µM (blue) and after the combined treatment of nifedipine 1µM and Ni^{2+} 1mM (red). D: Representative traces of whole-cell Ba^{2+} currents in 10mM Ba^{2+} perfusion solution, after treatment with a protocol of Ni^{2+} (50, 500 and 1000µM) and then additional treatment with nifedipine 1µM. The recording traces were filtered at 20kHz.

3.7.2 T-channel current in mouse popliteal lymphatic smooth muscle cells

Compared to rat mesenteric lymphatics, mouse PLs provided more limited material and therefore required a less aggressive and shorter digestion protocol, and yielded more fragile LSM cells. However, I could still find cells that had capacitances as large as rat mesenteric lymphatic cells and allowed as much current to flow through VGCCs. Figure 18 shows representative recordings during a ramp protocol similar to that shown in Figure 17B under nifedipine treatment, and then nifedipine+Ni^{2+} combined treatment. Similar to the observations in rat, Ca^{2+} channel current peaked between +20 and +30mV. The nifedipine-sensitive current peaked at -10 to 0mV, a more hyperpolarized voltage range. The addition of Ni^{+} (1mM) to the bath eliminated all remaining current not inhibited by 1μM nifedipine.

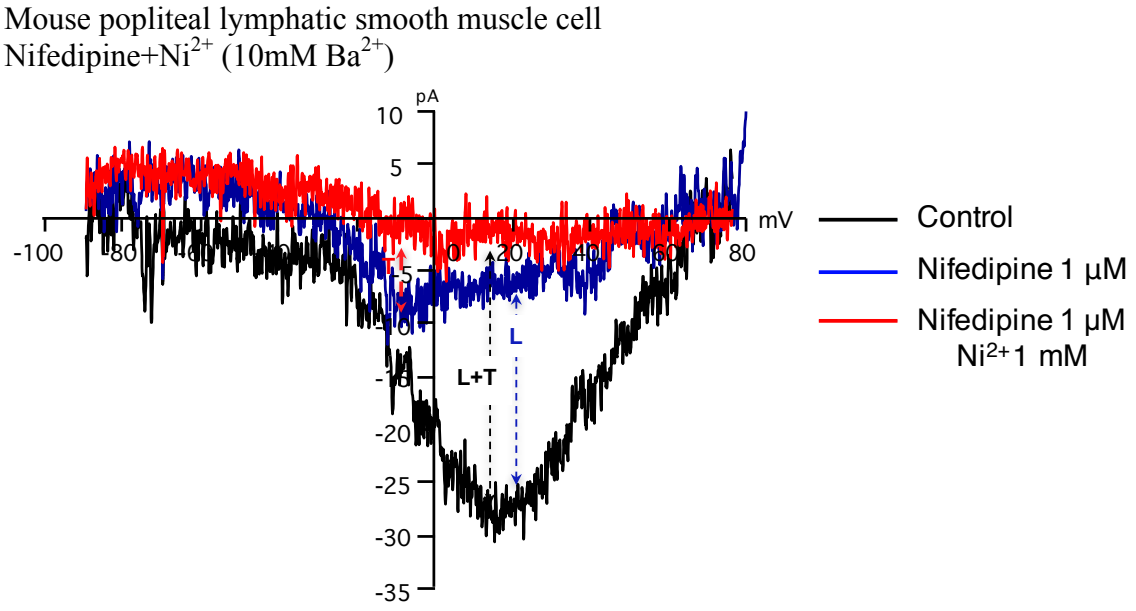

Figure 18. T-channel current recorded from a popliteal lymphatic smooth muscle cell. Representative traces of whole-cell Ba^{2+} currents in 10mM Ba^{2+} bath solution, before (black) and after treatment with 1µM nifedipine (blue) and 1µM nifedipine plus 1mM Ni^{2+} (red). The recording traces were filtered at 5kHz.

3.7.3 T-channel current in mouse inguinal-axillary lymphatic (IAL) smooth muscle cells

Compared to PLs, longer segments of IALs are easier to dissect and yield more LSM cells after disgestion. This is the type of mouse lymphatic vessel with which I had more experience recording Ca^{2+} current. Here, I show Ca^{2+} channel recordings in an IAL smooth muscle cell in 20mM Ba^{2+} bath solution using both ramp and step voltage protocols (Figure 19). In response to a voltage ramp (Figure 19C), the total VGCC current (recorded in 20mM Ba^{2+}) peaked between +20 and +30mV, a slightly more depolarized voltage compared the voltage ramp recordings in rat mesenteric and popliteal LSM cells shown in Figure 17 and Figure 18 (recorded in 10mM Ba^{2+}), which peaked between +10 and +20mV. This is consistent with the observation that an increase in charge carrier concentration shifts

the peak voltage to more depolarized potentials, as reported by Harraz and Welsh (2013). Eventually, the T-channel identitity was confirmed when this nifedipine-insensitive current was inhibited by 1mM Ni^{2+}. In IAL smooth muscle cells, I observed that in inguinal-axillary LSM cells, VGCC current could persist at concentrations as high as 2mM Ni^{2+} and was only completely abolished at 3mM Ni^{2+}, consistent with small vasomotion persisting in pressurized vessels at Ni^{2+} concentrations higher than 1mM (Figure 23). One can speculate that this persistent current could be an indication of a VGCC that is insensitive to both 1μM nifedipine and 1mM Ni^{2+}.

Besides using ramp voltage protocols, I also used a step-voltage protocol to differentiate between L and T-channels by the time course of current activation/inactivation after a depolarizing step ranging from -80 to +40mV. In IAL smooth muscle cells, total VGCC current exhibited both a fast-inactivating component, typical of T-channels, and a long-lasting component, typical of L-channels. In the presence of 1μM nifedipine, the long-lasting component disappeared from control total VGCC current (shown in black), revealing a fast-inactivating component (shown in blue). This fast-inactivating component was sensitive to 1mM Ni^{2+}, which is known to be a T-channel inhibitor (Harraz *et al.*, 2013).

To analyze the activation potential of VGCCs present in LSM cells, I separated recordings at different depolarizing steps: -40 to +40mV (Figure 19F). The steps to voltages from -80 to -40mV evoked no significant Ca^{2+} current. A fast-inactivating current appeared at the step to -10mV, with almost no long-lasting component, although a certain degree of VGCC current with a fast-inactivating component manifested early after at the step to -20mV. At the step to 0mV, the fast-inactivating current was most prominent when

L-channels were not yet activated. This is consistent with findings in the ramp protocol mentioned above, showing that nifedipine-insensitive current peaked at 0mV. Steps to more depolarized voltages from +10 to +40mV elicited both fast-inactivating and long-lasting components. The depolarizing step to +30mV was able to activate the largest total VGCC current, consistent with my observations using the ramp protocol. Since I used Ba^{2+} to record current VGCCs, the absolute activation voltages could be shifted toward a more depolarized value compared with physiological condition (extracellular $[Ca^{2+}]$=1.8mM). Figure 19 summarizes of current densities of 5 IAL smooth muscle cells at different pressure steps under control, under treatment with 1μM nifedipine or 1mM Ni^{2+}. Under nifedipine treatment the current densities peaked at a more hyperpolarized voltage (+10mV) compared to control (+15mV), reflecting the low-voltage activation characteristics of T-channels. When T-channels were subsequently blocked with Ni^{2+} 1mM, the peak shifted back toward more depolarized voltage (+20mV).

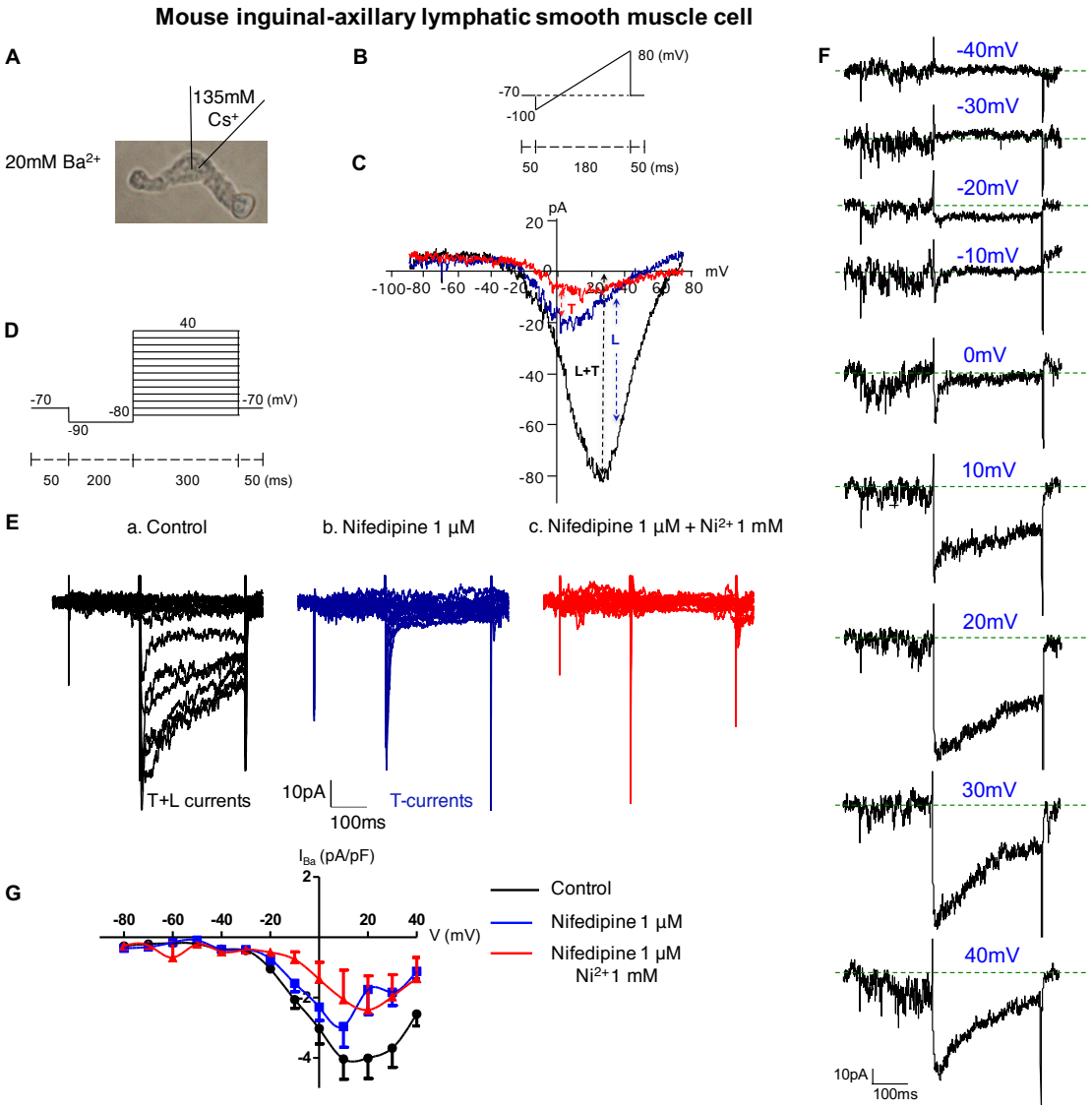

Figure 19. T-channel current recorded from a mouse IAL smooth muscle cell. A: A typical mouse IAL smooth muscle cell patched with a micropipette containing Cs^{+} solution to inhibit K^{+} current, and perfused with 20mM Ba^{2+} solution. B: Ramp protocol starting at a holding potential of -70mV, hyperpolarized to -100mV and gradually depolarized to 80mV, as in Figure 17 and Figure 18. C: Representative traces of whole-cell Ba^{2+} current in 20mM Ba^{2+} solution (control), treated with 1μM nifedipine, and subsequently treated with 1mM Ni^{2+}. The recording traces were filtered at 5kHz. D: Step protocol with an initial

step to a hyperpolarized potential of -90mV followed by series of depolarizing steps to a voltage range from -80 to 40mV in 10mV increments, and a final step back to the original holding potential of -70mV. E: Representative recordings of whole-cell Ba^{2+} currents during a step protocol in the same cell patched in (C): a) control, b) with nifedipine 1μM and c) with subsequent 1mM Ni^{2+}. F: Single raw Ba^{2+} current traces from control/total T+L-current in (E). The green lines indicate 0mV. The voltages above the green lines indicate the level of depolarization. The traces were filtered at 1kHz. G: Summary of current density at voltage steps from -80 to +40mV (n=5 inguinal-axillary LSM cells)

3.8 Effect of mibefradil on lymphatic contractile patterns in rat mesenteric lymphatics

Mibefradil is reported to be a specific T-channel inhibitor at doses in the nanomolar range and only affects L-channels at doses in the micromolar range, based on studies of recombinant channels in HEK cells (Jensen and Holstein-Rathlou, 2009). However, because I am ultimately interested in the potential role of T-channels in determining lymphatic pacemaking frequency and contraction strength in intact vessels, the effective concentrations reported for mibefradil in electrophysiological studies of recombinant channels are only a guideline. The context of the more complicated environment of a native LSM cell, with a low T-channel density, the possible expression of T-channel splice variants, and the possibility of off-target effects on other types of Ca^{2+} channels e.g., $Ca_v1.2$, $Ca_v1.3$, TRPs, NCX in reverse mode that contribute to pacemaker modulation and/or contraction strength, can lead to uncertainties about the specific effects of mibefradil on T-channels. To collect more information and reduce uncertainties, rather than a single dose of mibefradil, as used in many previous studies (e.g., Lee *et al.*, 2014a; Beckett *et al.*,

2007), I applied cumulative mibefradil concentrations to yield a complete dose-response curve. Using pressure myography with rat mesenteric lymphatics, contraction frequency slowed (IC_{50}=66nM) at a lower concentration than that required to affect the contraction amplitude (IC_{50}=423nM); (Figure 20), which is consistent with the findings of Lee *et al.*, 2014a, who treated rat mesenteric lymphatics with 100nM mibefradil and concluded that T-channels regulate only lymphatic contraction frequency. However, mibefradil has been shown not only to inhibit T-channels but to also inhibit voltage-gated Na^+ channels, IC_{50}=0.5μM (Schafer *et al.*, 2016; Strege *et al.*, 2005; McNulty and Hanck, 2004); delayed rectifier K^+ channels, IC_{50}=0.3μM; and L-channels, IC_{50}=1.4μM (Lee *et al.*, 2006; Liu *et al.*, 1999); all of which are known to play functional roles in mesenteric lymphatics: L-channels modulate contraction strength (Lee *et al.*, 2014a), K^+ and Na^+ channels modulate contraction frequency (Gui *et al.*, 2014; Hollywood *et al.*, 1997; Zawieja *et al.*, 1993). Therefore, I cannot rule out the possibility that mibefradil is acting via L-channels, Na^+ and/or K^+ channels to inhibit lymphatic contraction amplitude and frequency.

A

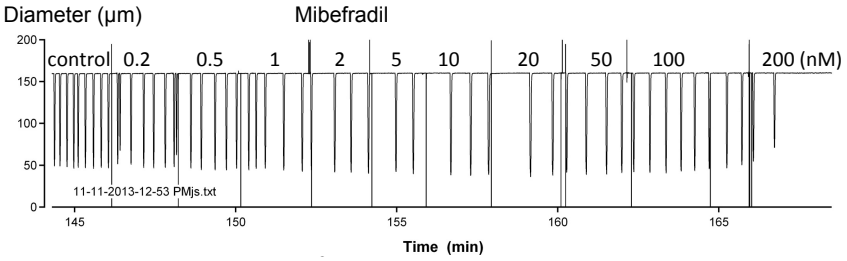
Diameter (µm)
Mibefradil
control
0.2
0.5
1
2
5
10
20
50
100
200 (nM)
200
150
100
50
0
11-11-2013-12-53 PMjs.txt
145
150
155
160
165
Time (min)

B

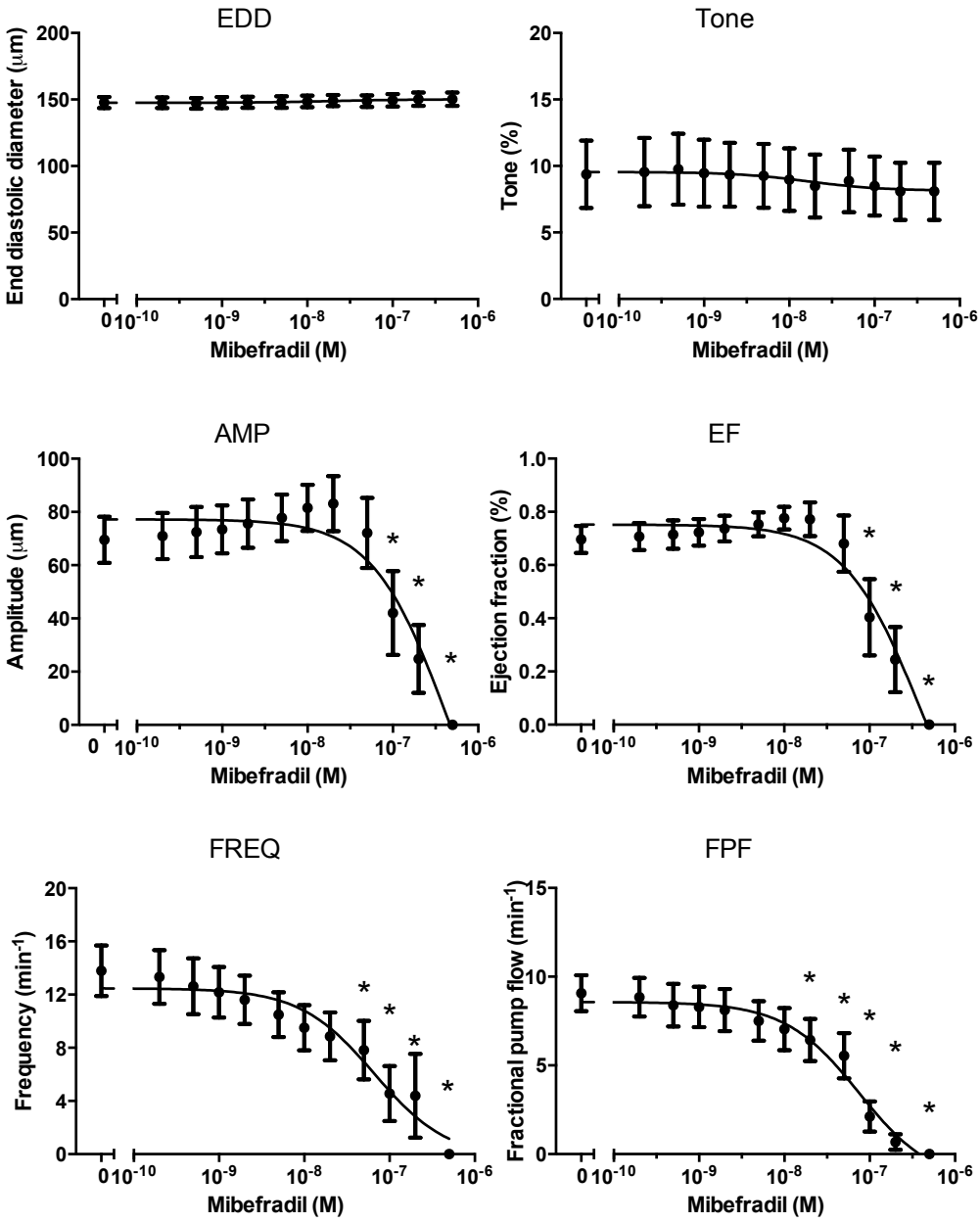

Figure 20. Effect of mibefradil on the contractile patterns of rat mesenteric lymphatics.

A: A representative diameter recording from a rat mesenteric lymphatic during a mibefradil dose-response protocol; B: Summary data showing the effect of cumulative mibefradil dose-response on contractile parameters of rat mesenteric lymphatic vessels (n=8). The IC_{50} was 66μM for contraction frequency, while the IC_{50} was 423μM for contraction

amplitude. *p<0.05 indicates significant difference between marked concentration vs. control. Data are presented as mean±SEM.

3.9 Effect of Ni^{2+} on lymphatic contractile patterns in rat mesenteric lymphatics

Ni^{2+} is a commonly used T-channel inhibitor that is reputedly selective for $Ca_v3.2$ at low concentrations (IC_{50}=12μM for $Ca_v3.2$ expressed in HEK cells; Lee *et al.*, 1999). In vascular smooth muscle cells, 60μM Ni^{2+} has been estimated to inhibit 60% of T-current (Harraz *et al.*, 2013). However, to be able to target $Ca_v3.1$ (IC_{50}=250μM for $Ca_v3.1$ expressed in HEK cells; Lee *et al.*, 1999) the required concentration needed to be higher and overlapped with the concentration range that inhibited L-channels (IC_{50}=324μM; Bradley *et al.*, 2004). Previously, Ni^{2+}, at 100μM, was shown to inhibit AP firing and contraction frequency in sheep and rat mesenteric lymphatics (Lee *et al.*, 2014a; Beckett *et al.*, 2007), a concentration somewhat specific for $Ca_v3.2$ and presumably leaving $Ca_v3.1$ relatively unaffected. I treated rat mesenteric lymphatics with cumulative concentrations of Ni^{2+} to obtain a Ni^{2+} dose-response curve (Figure 21). Surprisingly, the contraction frequency (IC_{50}=279μM) slowed almost simultaneously with contraction amplitude (IC_{50}=248nM), in contrast to the findings of Lee *et al.*, 2014a. Ni^{2+}, at 100μM, can be specific for T-channels, especially the $Ca_v3.2$ isoform (Harraz and Welsh, 2013). However, because rat whole mesenteric lymphatic vessels express $Ca_v3.1$, $Ca_v3.2$ and $Ca_v1.2$ at the mRNA level, a 100μM Ni^{2+} can only be used to extrapolate a role for $Ca_v3.2$ in lymphatic pacemaking. Since Ni^{2+} can also have non-selective effect on other channels, e.g., Na^+ and K^+ channels (Lacinova, 2011; Sheng *et al.*, 2002; Stockland *et al.*, 1993), the observed effects of Ni^{2+} could also be a reflection/consequence of its non-selectivity.

A

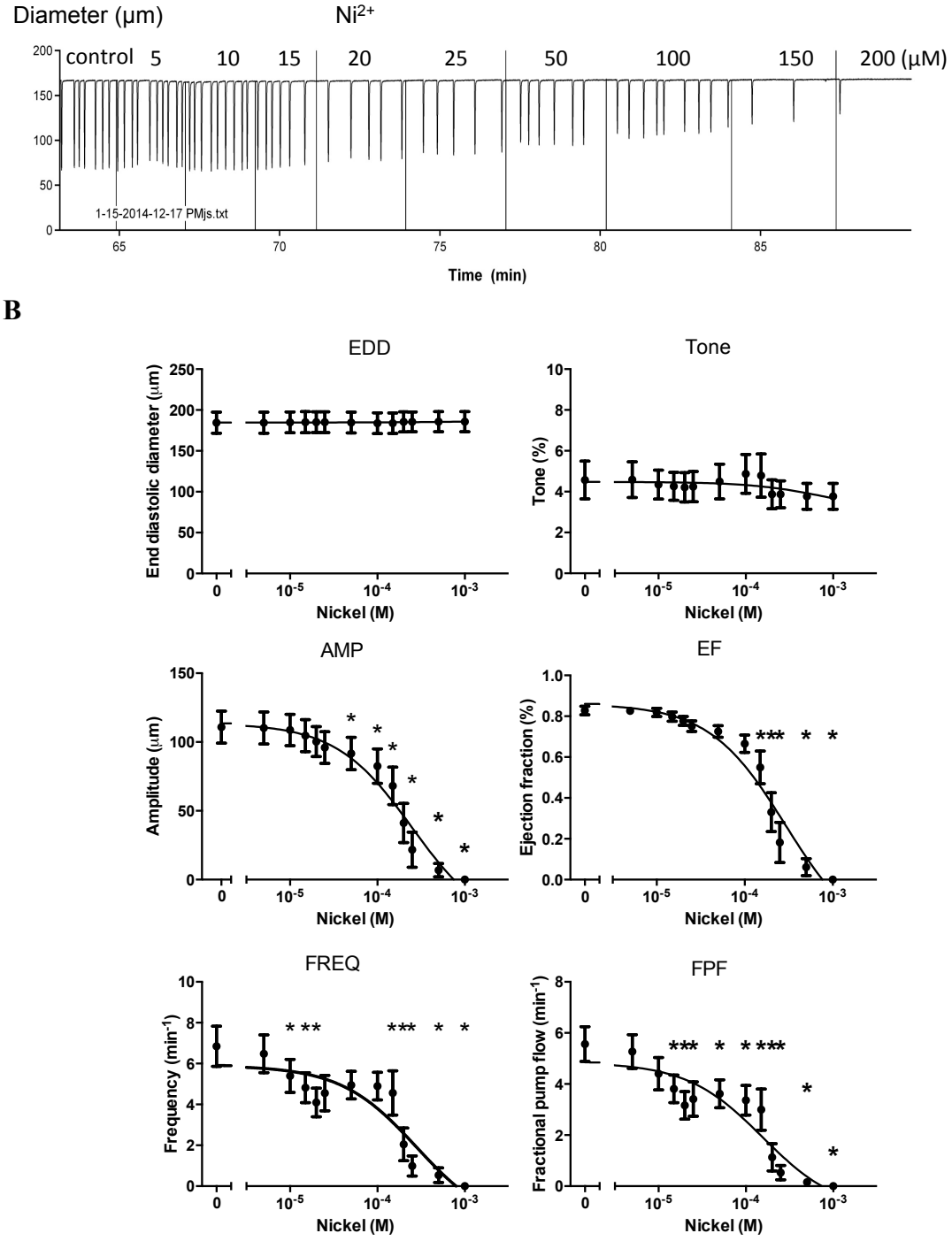

Figure 21. Effect of Ni^{2+} on the contractile patterns of rat mesenteric lymphatics. A: A representative diameter recording from a rat mesenteric lymphatic during a Ni^{2+} dose-response protocol; B: Summary data showing the effect of cumulative Ni^{2+} dose-response on contractile parameters of rat mesenteric lymphatic vessels (n=9). the IC_{50} was 248µM

for contraction amplitude, while the IC_{50} was 279μM for the contraction frequency. *p<0.05 indicates significant difference between marked concentration vs. control. Data are presented as mean±SEM.

3.10 Effect of Ni^{2+} on lymphatic contractile patterns in mouse popliteal lymphatics

Since 1987, Ni^{2+} has been used in studies of T-channels, in contrast to newer inhibitors such as mibefradil (since 1994) and TTA-A2 (since 2009). Ni^{2+} is the only inhibitor that is repeatedly capable of differentiating between $Ca_v3.1$ and $Ca_v3.2$. I consistently used Ni^{2+} in many experiments of my project. I repeated the Ni^{2+} dose-response protocol on mouse vessels to be consistent with the literature of using pharmacological inhibitors in studying lymphatic pacemaking (Lee *et al.*, 2014a; Beckett *et al.*, 2007; Hollywood *et al.*, 1997). Similar to my results found in rat mesenteric lymphatic vessels, Ni^{2+} inhibited mainly lymphatic contraction amplitude (IC_{50}=110μM), while leaving the contraction frequency unchanged (IC_{50}=452M) until very high doses were reached and the amplitude was nearly zero (Figure 22).

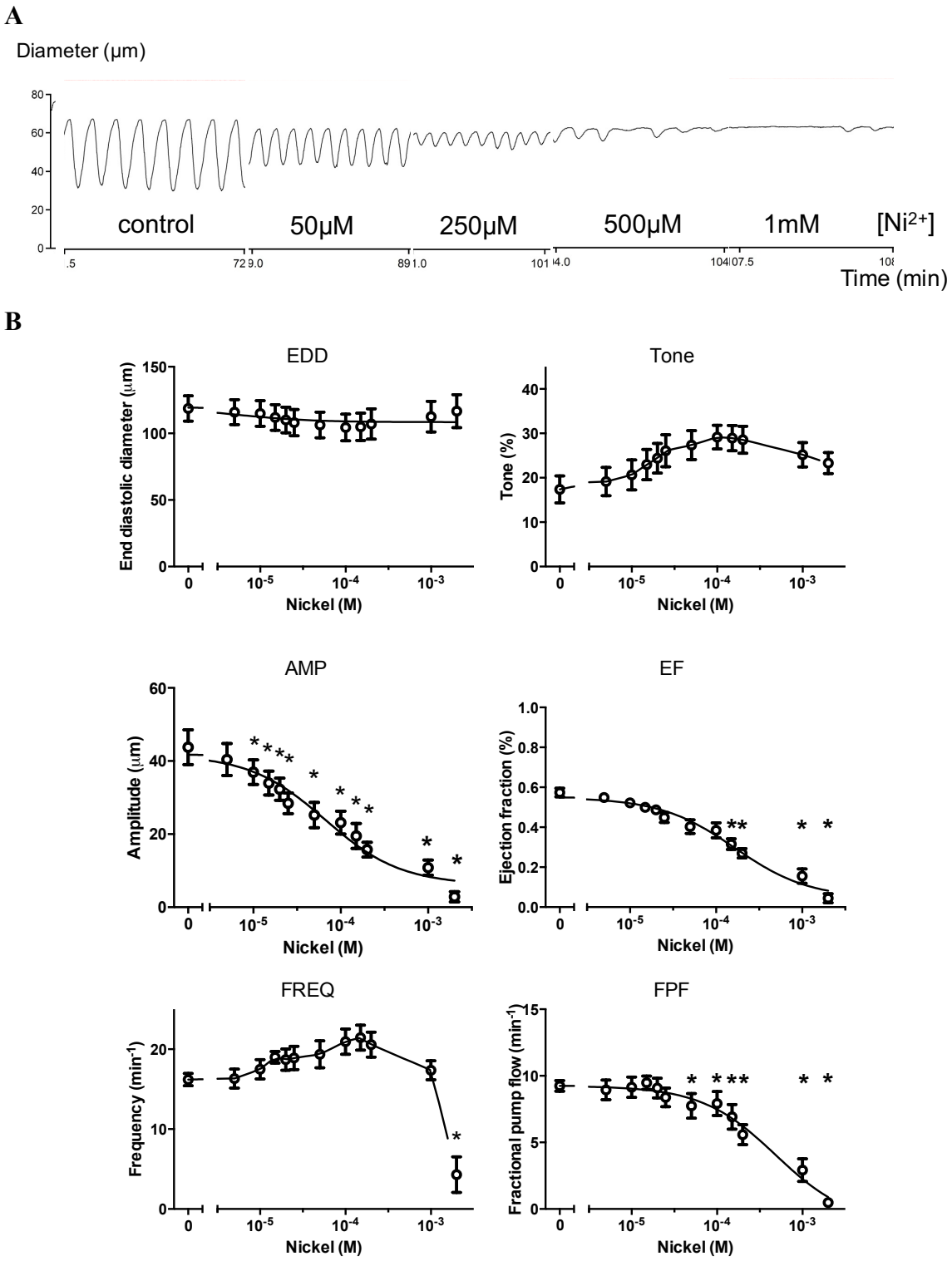

Figure 22. Effect of Ni^{2+} on the contractile patterns of mouse popliteal lymphatics. A: Representative diameter recording from a mouse popliteal lymphatic during a Ni^{2+} dose-

response protocol; B: Summary data showing the effect of cumulative Ni^{2+} doses on contractile parameters of mouse popliteal lymphatics (n=11). The IC_{50} for amplitude was 110μM Ni^{2+}, while frequency remained unaffected (IC_{50}=452M) until the contraction amplitude was severely attenuated. *$p<0.05$ indicates significant difference when the indicated concentration was compared to control before treatment. Data are expressed as mean±SEM.

3.11 Effect of Ni^{2+} on lymphatic contractile patterns in mouse inguinal-axillary lymphatics

I treated mouse IALs with Ni^{2+} to obtain a dose-response curve. IAL vessels have a fairly high contraction frequency, which we initially thought to be beneficial for studying lymphatic pacing, because a decrease in contraction frequency could be more easily detected. I hoped that the addition of experiments on IALs to my project could strengthen my study in a way that can contribute to more understanding of lymphatic-related disorders such as lymphedema.

Consistent with the recordings in mouse PLs, Ni^{2+} mainly altered the lymphatic contraction amplitude (IC_{50}=66μM), while leaving the lymphatic pacing unaffected until a dose of 2mM Ni^{2+} was reached (Figure 22). One can see that the cummulative Ni^{2+} concentration required to inhibit the IAL contractions is twice as high as the concentration required to inhibit the contraction of PLs (1mM). In the representative recording below, even the highest Ni^{2+} concentration could only silence the contraction for less than two minutes, and was accompanied by vasodilation, after which contractions returned with small amplitude <5μm; these were classified as “vasomotion”, similar to what is observed in mouse mesenteric lymphatics (Scallan *et al.*, 2015), and were not the focus of my

analyses, as these small and uncoordinated movements can not move lymph between lymphangions.

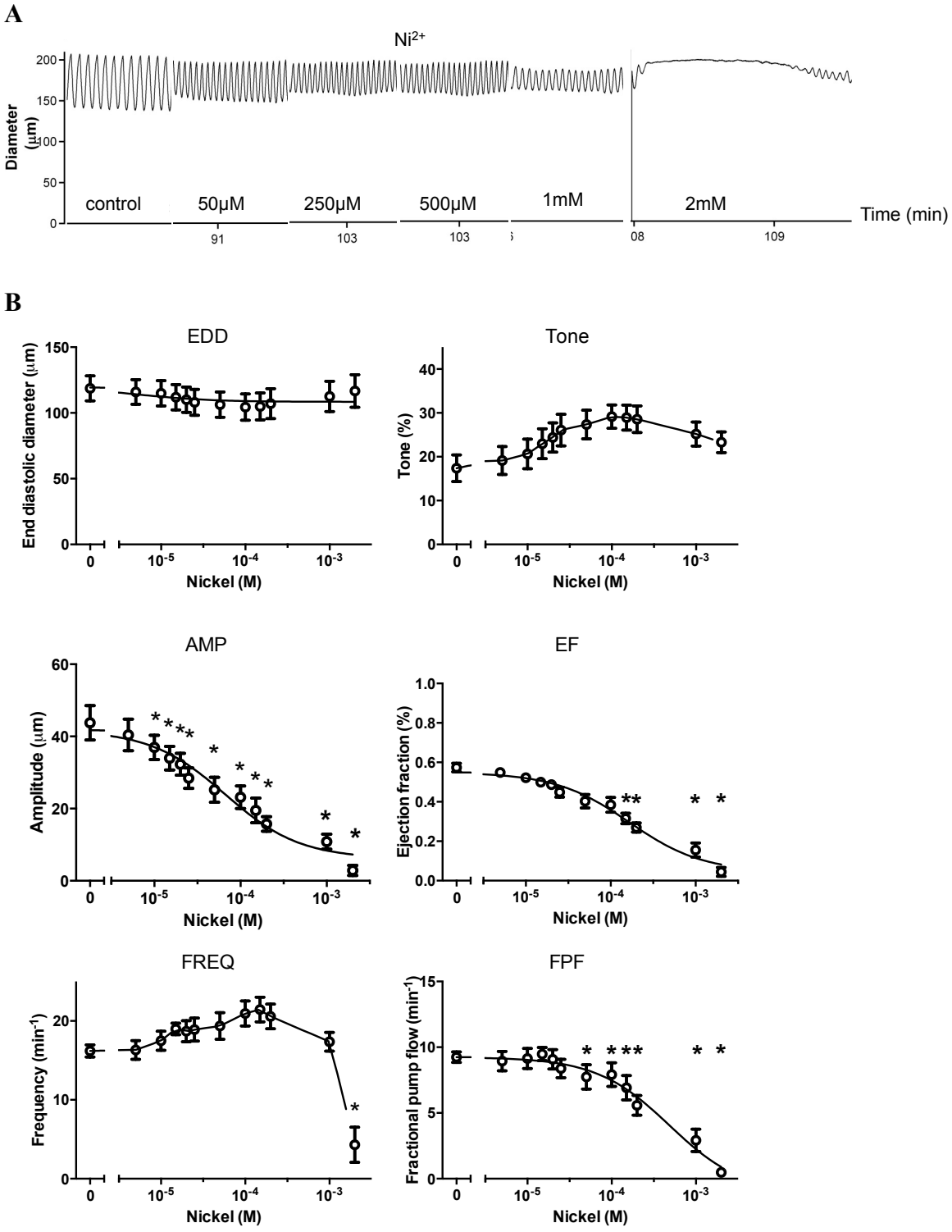

Figure 23. Effect of Ni^{2+} on the contractile patterns of mouse inguinal-axillary lymphatics. A: A representative diameter recording from a mouse inguinal-axillary

lymphatic during a Ni^{2+} dose-response protocol; B: Summary data showing the effect of cumulative Ni^{2+} addition on contractile parameters of mouse inguinal-axillary lymphatics (n=8). The IC_{50} for amplitude was 66μM Ni^{2+}, while frequency remained unaffected until the contraction amplitude approached zero. *$p<0.05$ indicates significant difference when the marked concentration with control before treatment were compared. Data are expressed as mean±SEM.

3.12 Effect of TTA-A2 on lymphatic contractile patterns in mouse popliteal lymphatics

To exhaust all the possibilities of testing the role of T-channels using pharmacological approaches, I decided to use a more recently developed T-channel inhibitor. Based on the number, quality of publications and availability of solid information about effective concentrations, I chose TTA-A2, a novel T-channel inhibitor that is thought to be specific for T-channels (15 publications), among several options such as TTA-P2 (13 publications) and ML 218 (4 publications). It was developed by Uebele *et al.*, 2009 at Merck Research Laboratories, WestPoint, USA (Schaffer and Li, 2014). In response to cumulative doses of TTA-A2, the contraction amplitude was only affected by 20% (IC_{50}=1.3μM), with almost no effect on frequency.

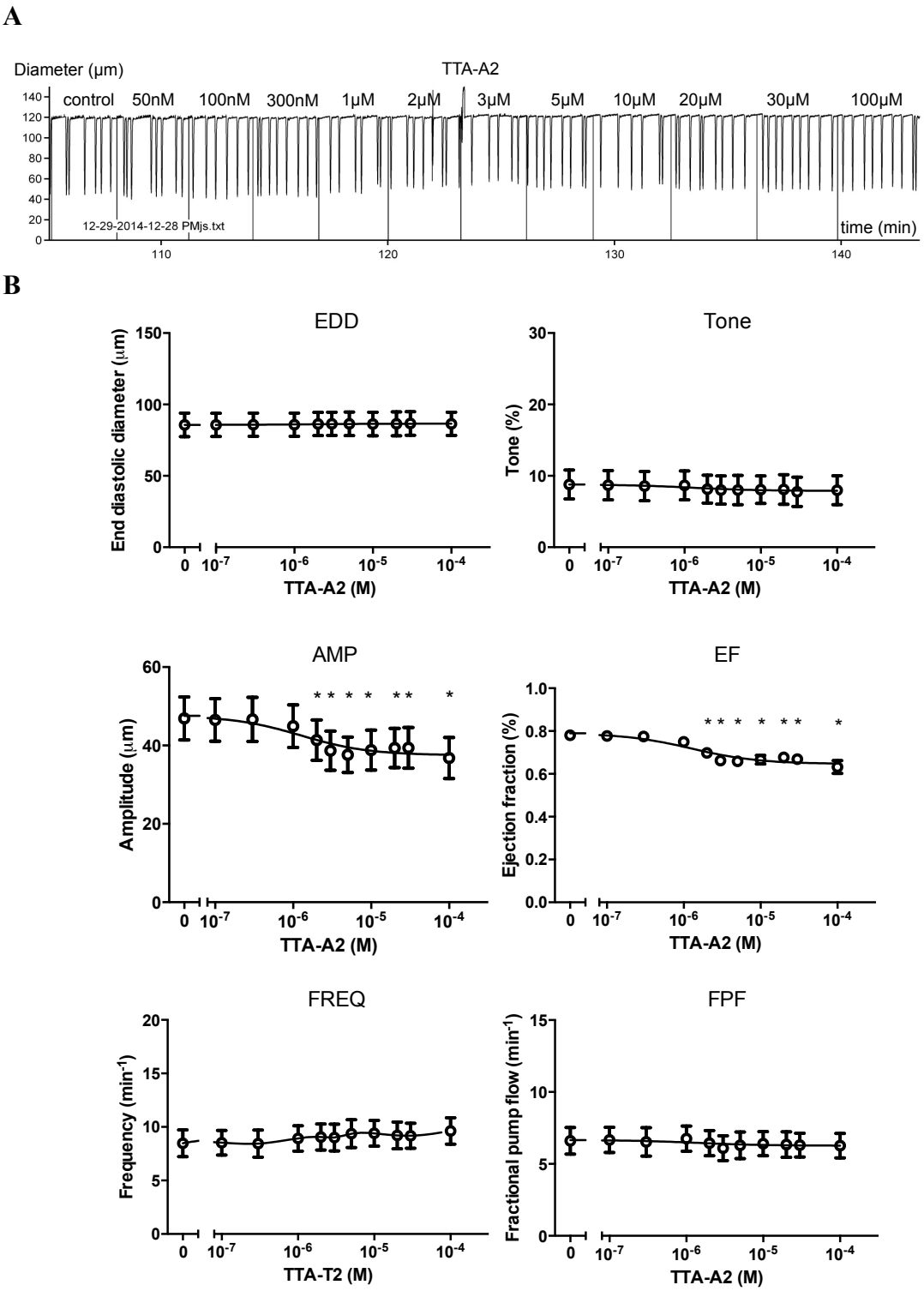

Figure 24. Effect of TTA-A2 on the contractile patterns of mouse popliteal lymphatics.

A: A representative myograph recording from a mouse popliteal lymphatic during a TTA-

A2 dose-response protocol; B: Summary data showing the effect of cumulative doses of TTA-A2 on the contractile parameters of popliteal lymphatics (n=8). The IC_{50}=1.3μM for contraction amplitude TTA-A2. *p<0.05 indicates significant difference between marked concentration vs. control. Data are graphed as mean±SEM (Table 2).

The contraction frequency tended to increase, possibly as a secondary effect consequent to a decrease in amplitude, allowing less refractory time between contractions. TTA-A2 is claimed by Alomone labs to be a specific and state-dependent T-channel blocker that is 40 times more potent at -80mV than at -100mV. They also admit that the chemical cannot differentiate between different T-channel isoforms, although in one study the agent showed 3.3-times more selectivity for $Ca_v3.2$ compared to $Ca_v3.1$ (François *et al.*, 2013). However, there are several problems with using TTA-A2. Alomone Labs found that 1μM TTA-A2 inhibits about 50% of the current through $Ca_v3.1$, while 100μM inhibits about 90% current through $Ca_v3.2$ (http://www.alomone.com/p/tta-a2/t-140/7). Presuming that the potency for the T-channel isoform $Ca_v3.2$ is similar to that of $Ca_v3.1$ mentioned above, an effective concentration of more than 1μM is problematic because of its possible off-target effects. TTA-A2 has only been used in one publication on the microcirculation using a concentration as low as 1μM (Fernández *et al.*, 2015). In summary, since there are many uncertainties of the selectivity of currently available T-channel inhibitors, I turned to transgenic mouse models to genetically delete specific T-channel isoforms and test their specific roles in lymphatic pacemaking.

Table 8. Summary of pharmacological inhibitors used and their IC_{50} on lymphatic contraction amplitude and frequency

Drug	Species	LV location	IC_{50} for amplitude	IC_{50} for frequency
Mibefradil	Rat	Mesenteric	423nM	66nM
Ni^{2+}	Rat	Mesenteric	248μM	279μM
	Mouse	Inguinal-axillary	66μM	1287M
	Mouse	Popliteal	110μM	452M
TTA-A2	Mouse	Popliteal	1.3μM	nd

*nd stands for not-determined.

3.13 Effect of smooth muscle-specific genetic deletion of $Ca_v1.2$ on lymphatic contractions in mouse popliteal lymphatics

According to the current hypothesis regarding the respective roles of L and T-channels in LSM, L-channels only modulate contraction amplitude and T-channels (i.e., $Ca_v3.2$; Lee *et al.*, 2014a) modulate pacemaking frequency (Beckett *et al.*, 2007). First, we attempted to delete $Ca_v1.2$ from LSM to test if T-channels were capable of generating any significant contractile activities on their own. Since the global deletion is embryonically lethal (Seisenberger *et al.*, 2000), we used the SMMHC promoter to specifically delete the $Ca_v1.2$ gene in smooth muscle. From SMMHC-CreERT2 mice and $Ca_v1.2^{fl/fl}$ mice, we generated SMMHC-CreERT2; $Ca_v1.2^{fl/fl}$ mice and induced deletion by tamoxifen i.p. injection. The tamoxifen induction protocol was the same as worked out previously in our laboratory using $ROSA^{mT/mG}$ reporter mice to follow the time course of GFP expression in LSM (SDZ and JAC's unpublished observations). Previously this floxed $Ca_v1.2$ construct was combined with a SM22 promoter to generate SMAKO mice (smooth muscle-specific alpha 1.2 calcium channel knockout) which were induced with tamoxifen for five days and allowed to recover for two weeks (Moosmang *et al.*, 2003). Moosmang *et al.* assessed the

role of $Ca_v1.2$ in vascular smooth muscle, without evaluating the genetic deletion consequences in lymphatic vessels. However, the SM22 alpha promoter has been reported to be expressed not only in smooth muscle cells (Shen *et al.*, 2012), but also in immune cells, including monocytes, neutrophils, and macrophages, each of which is known to influence lymphatic contractile activity (Zawieja *et al.*, 2016; Chakraborty *et al.*, 2015; and Gashev *et al.*, 2013). Alternatively, the SMMHC (*Myh11*) promoter is currently considered to be the most selective promoter for smooth muscle (Long *et al.*, 2014) and its RNA and protein expression are found in lymphatic vessels (Muthuchamy *et al.*, 2008). Therefore, for this dissertation, we used the SMMHC promoter to specifically excise $Ca_v1.2$ sequences in smooth muscle cells. Initially we planned to replicate the conventional tamoxifen injection (Moosmang *et al.*, 2003). However, we experienced lethality of $Ca_v1.2^{-/-}$ as early as ten days after the first tamoxifen injection. Therefore, we started our experiments as early as ten days after Cre induction with i.p. tamoxifen injection. The mice showed excessive grooming, hunched posture, sluggish movement and a dramatic GI phenotype: a bloated, distended and paralyzed GI tract. The current established view is that L-channels only regulate contraction amplitude (Lee *et al.*, 2014a; Beckett *et al.*, 2007). Surprisingly, in smooth muscle-specific $Ca_v1.2^{-/-}$ mice, both PLs and IALs were completely quiescent, showing zero contraction amplitude and zero frequency at all intraluminal pressures, in contrast to the spontaneous contractions normally observed in control vessels, which were $Ca_v1.2^{fl/fl}$ mice (no Cre) subjected to the same tamoxifen injection protocol (Figure 26). One additional observation was that in PLs lacking $Ca_v1.2$, has basal tone that was slightly less than that measured in tamoxifen-injected $Ca_v1.2^{fl/fl}$ mice without Cre expression: 10% vs. 30%, respectively (Figure 26).

A. Inguinal-axillary lymphatic from tamoxifen-induced SMMHC-Cre; $Ca_v1.2^{fl/fl}$ mouse

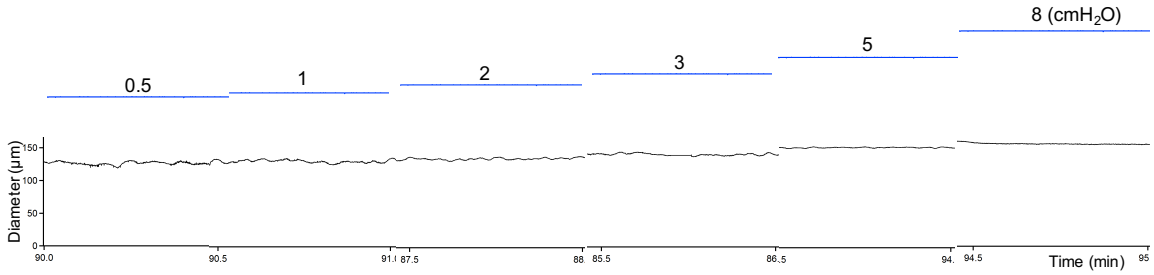

B. Inguinal-axillary lymphatic from tamoxifen-induced $Ca_v1.2^{fl/fl}$ mouse

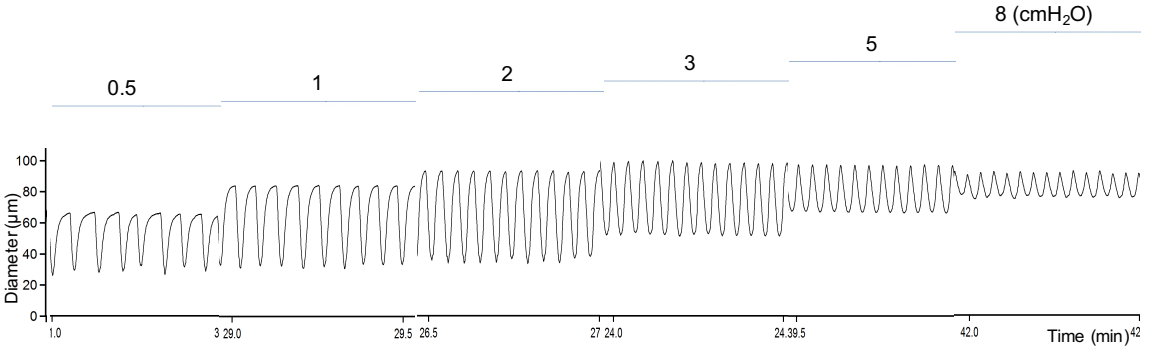

Figure 25. Contractile patterns of inguinal-axillary lymphatics from smooth-muscle specific $Ca_v1.2$KO during a pressure step protocol. Representative pressure myograph recordings from A) a $Ca_v1.2^{-/-}$ inguinal-axillary lymphatic (tamoxifen-injected SMMHC-Cre; $Ca_v1.2^{fl/fl}$) and B) its control counterpart (from a tamoxifen-induced SMMHC-Cre; $Ca_v1.2^{fl/fl}$ mouse).

A. Popliteal lymphatic from tamoxifen-induced $Ca_v1.2^{fl/fl}$ mouse lacking Cre

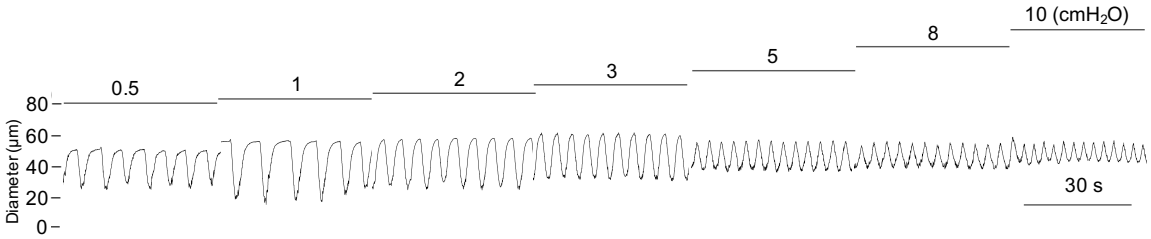

B. Popliteal lymphatic from tamoxifen-induced SMMHC-Cre; $Ca_v1.2^{fl/fl}$ mouse

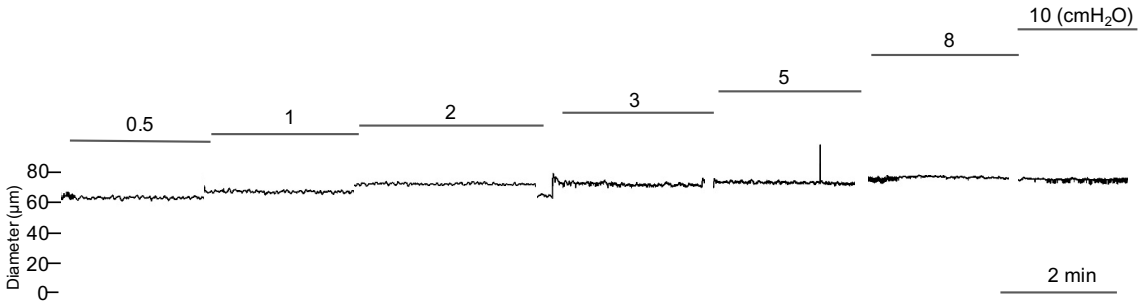

C. Illustration of small amplitude vasomotion in a popliteal lymphatic from a tamoxifen-induced SMMHC-Cre; $Ca_v1.2^{fl/fl}$ mouse, $P_{in}=P_{out}=2cmH_2O$

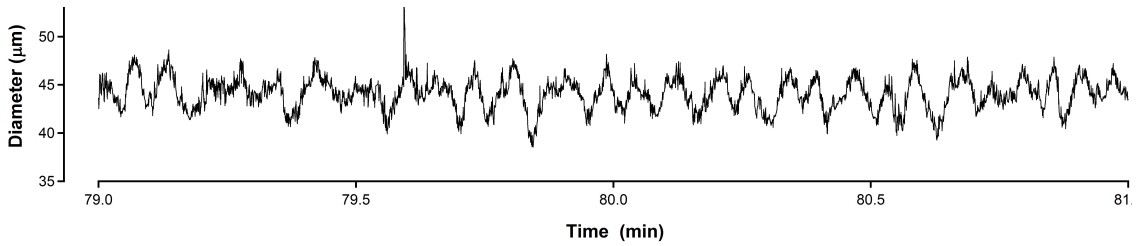

D

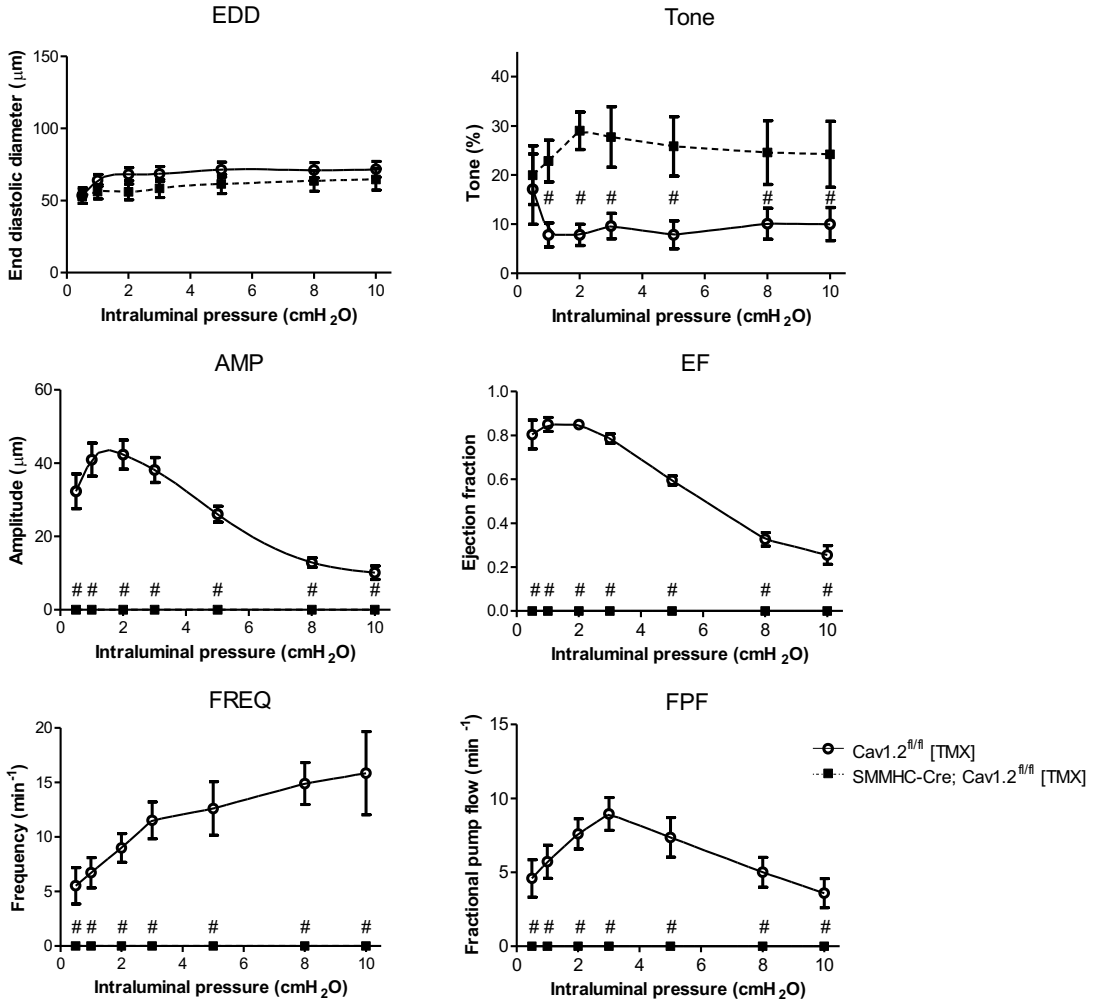

Figure 26. Contractile patterns of popliteal lymphatics from smooth-muscle specific $Ca_v1.2$KO mice during pressure step protocol. Representative pressure myograph recordings from A) a smooth muscle-specific $Ca_v1.2$KO popliteal lymphatic (tamoxifen-injected SMMHC-Cre; $Ca_v1.2^{fl/fl}$) and B) its control counterpart (from a tamoxifen-induced SMMHC-Cre; $Ca_v1.2^{fl/fl}$ mouse). C: Illustration of residual vasomotion in a PL from a tamoxifen-induced SMMHC-Cre; $Ca_v1.2^{fl/fl}$ mouse. D: The contractile parameters calculated from pressure myograph recordings in popliteal lymphatics comparing between smooth muscle-specific $Ca_v1.2$KO and their control counterparts (tamoxifen-induced

SMMHC-Cre; $Ca_v1.2^{fl/fl}$ mice: n=5; tamoxifen-injected $Ca_v1.2^{fl/fl}$ mice, in the absence of Cre: n=7). Experiments were performed by MJD. n refers to the number of lymphatic vessels. Timescales indicate 30s for control LV and 2 min for smooth muscle-specific $Ca_v1.2$KO, note the more expanded timescale for smooth muscle-specific $Ca_v1.2$KO.

I observed small vasomotions in both PLs (Figure 26C) and IALs specifically deleted of $Ca_v1.2$ in smooth muscle. We were uncertain of the ionic origin of these small events. They are also present in lymphatic vessels treated with 1μM nifedipine (personal observations in IALs and PLs), consistent with observations in guinea pig lymphatic vessels, in which they are hypothesized to be driven by STDs (von der Weid *et al.*, 2008). These small events can sometimes be observed in diastole in PLs from control mice, although they are often obscured by large amplitude contractions. They are also observed in mouse mesenteric and iliac lymphatics, which do not exhibit spontaneous, coordinated contractions (for unknown reasons). In contrast, in the fast-pacing IALs from WT mice with higher basal frequency, these small events, if present, are totally masked. To check for any remaining functional $Ca_v1.2$ channels, smooth muscle-specific $Ca_v1.2^{-/-}$ PLs were treated with Bay K8644 (BayK), an L-channel activator. Subsequently, 1μM nifidipine was administered to the bath to test if the vasomotions were driven by Ca^{2+} entry through L-channels. Experiments were performed under isobaric conditions with equal input and output pressure (P_{in}=P_{out}= 2 or 3cmH_2O, whichever produced peak contraction strength). In popliteals from tamoxifen-treated control without Cre construct, BayK increased amplitude from 37.9±4 to 52.1±3.8μm and decreased frequency from 12±2.8 to 9±2.8 contractions/min, while 1μM nifedipine decreased amplitude from 37.9±4 to 5.2±2.3μm and increased frequency from 12±1.9 to 13.2±4.2 contractions/min (Figure 27). However,

PLs from induced SMMHC-Cre; $Ca_v1.2^{fl/fl}$ mice did not respond to either BayK or nifedipine (Table 9).

Table 9. Effects of nifedipine and Bay K8466 on contraction amplitude and frequency in mouse popliteal lymphatics after tamoxifen induction

		$Ca_v1.2^{fl/fl}$, no Cre (n=7)	SMMHCCre; $Ca_v1.2^{fl/fl}$ (n=3)
$P_{in}=P_{out}$=2 or 3cmH_2O		Mean ± SEM	
Amplitude (μm)	Control	37.9±4	0
	Bay K8644 (1μM)	52.1±3.8	0
	Nifedipine (1μM)	5.2±2.3	0
Frequency (contractions/min)	Control	12±1.9	0
	Bay K8644 (1μM)	9±2.8	0
	Nifedipine (1μM)	13.2±4.2	0

* Notes: amplitude and frequency values are expressed as mean±SEM.

A. Popliteal lymphatic from a tamoxifen-induced $Ca_v1.2^{fl/fl}$ control mouse, $P_{in}=P_{out}=2cmH_2O$

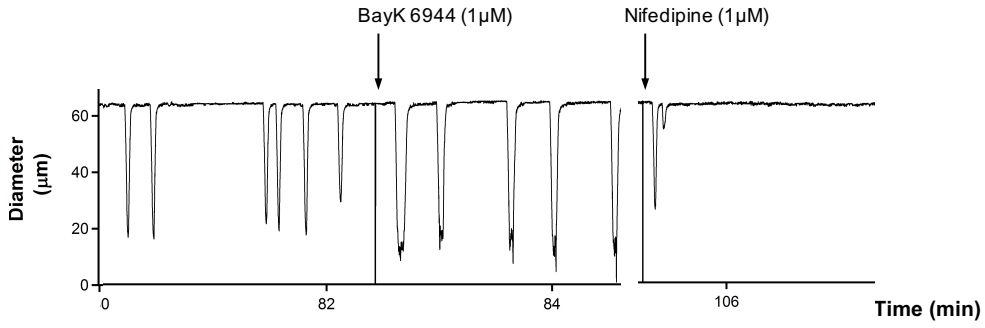

B

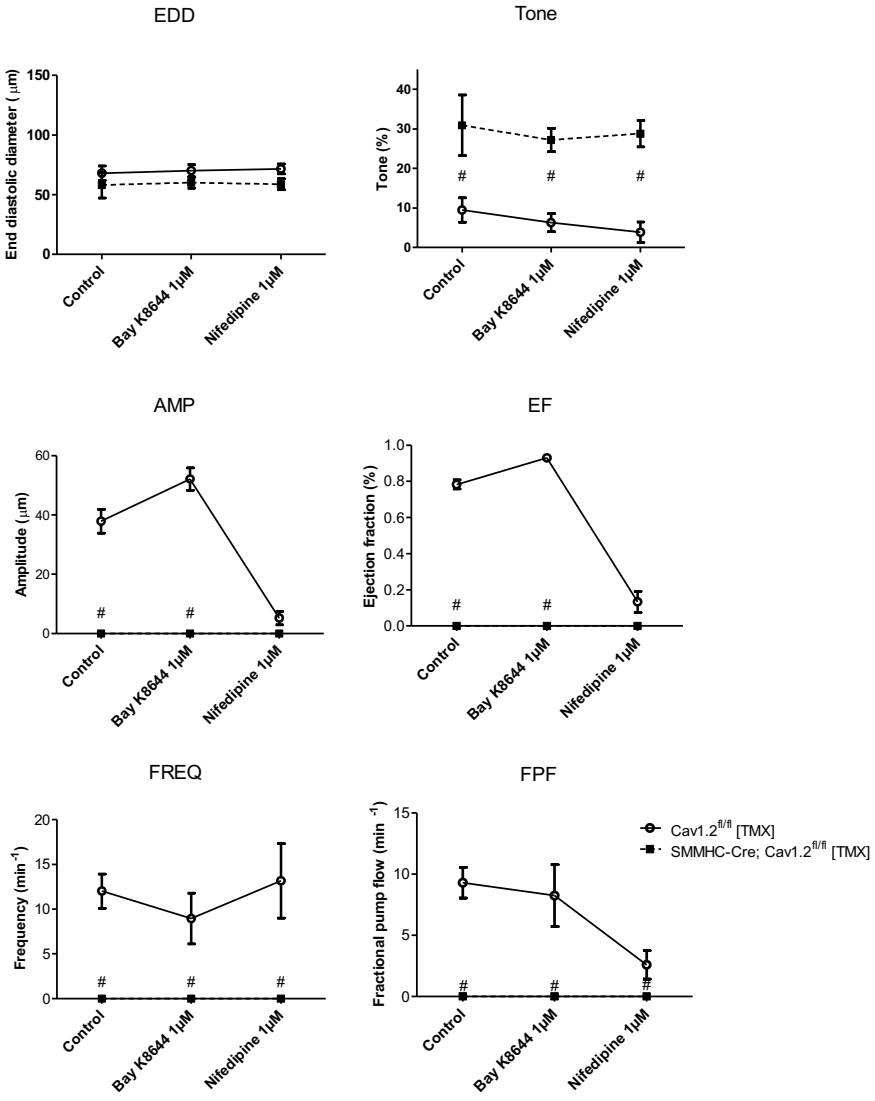

Figure 27. Effect of Bay K8644 and nifedipine on popliteal lymphatic contractile function in smooth muscle-specific $Ca_v1.2$KO mice. A: Representative inner diameter

recording during a series of drug applications 1) activating L-channels by 1μM BayK8644 and 2) inhibiting L-channels with 1μM nifedipine in a popliteal lymphatic vessel from a tamoxifen-induced $Ca_v1.2^{fl/fl}$ (no Cre) mouse, which served as the control for tamoxifen-induced SMMHC-Cre; $Ca_v1.2^{fl/fl}$ mice. B: Comparison of the contractile parameters in response to Bay K8644 and nifedipine between popliteal lymphatics from SMMHC-Cre; $Cav1.2^{fl/fl}$ and their controls both injected with tamoxifen (tamoxifen-induced SMMHC-Cre; $Ca_v1.2^{fl/fl}$ mice: n=5; tamoxifen-injected $Cav1.2^{fl/fl}$, no Cre: n=6). Experiments by MJD.

3.14 Effect of global genetic deletion of $Ca_v3.2$ on lymphatic contractions in mouse inguinal-axillary lymphatics

According to Lee *et al.* 2014a, a role for T-channels in lymphatic pacemaking is supported by the expression of $Ca_v3.2$, as detected by PCR and immunostaining, and by the sensitivity of frequency of spontaneous APs and contractions to 100μM Ni^{2+}. Since I could not replicate their findings either in rat or mouse lymphatics using ranges of gradually increasing concentrations of the T-channel inhibitors Ni^{2+} and TTA-A2, I investigated the lymphatic phenotype of $Ca_v3.2$ global knockout mice as an alternative strategy to selectively eliminate the expression of the T-channel isoform $Ca_v3.2$. Reports of tracheal, neuronal and cardiovascular abnormalities in $Ca_v3.2^{-/-}$ mice (Harraz *et al.*, 2015; Beckett *et al.*, 2008, Chen *et al.*, 2003) confirmed other aspects of a $Ca_v3.2^{-/-}$ phenotype and offered hope for a detectable lymphatic phenotype. We purchased $Ca_v3.2^{-/-}$ mice from Jackson Laboratories, and the mouse model validation is elaborated in "Materials and Methods" section.

Surprisingly, during pressure step protocols to test lymphatic contractile function, I found that the contraction frequencies and amplitudes of IAL vessels from $Ca_v3.2^{-/-}$ mice were essentially identical to those of WT lymphatic vessels. Tones and end diastolic diameters also showed no significant differences between $Ca_v3.2^{-/-}$ and WT vessels (Figure 28). These results urged me to continue testing the role of the other T-channel isoform $Ca_v3.1$ expressed in LSM.

A. Inguinal-axillary lymphatic from a $Ca_v3.2^{-/-}$ mouse

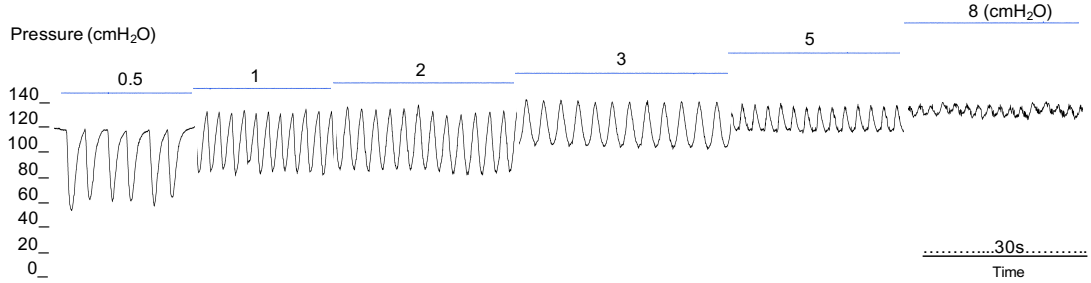

B. Inguinal-axillary lymphatic from a WT mouse

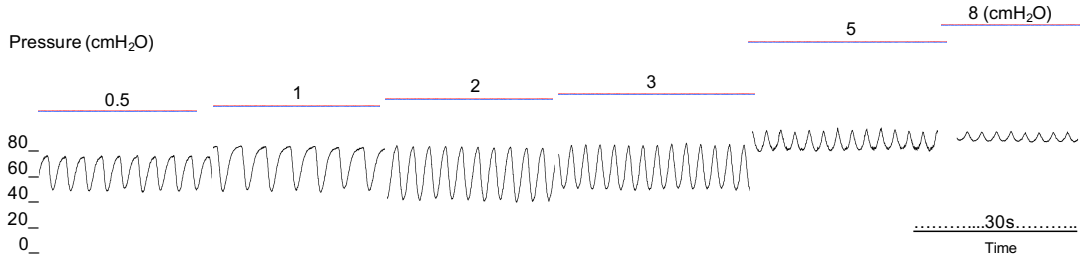

C

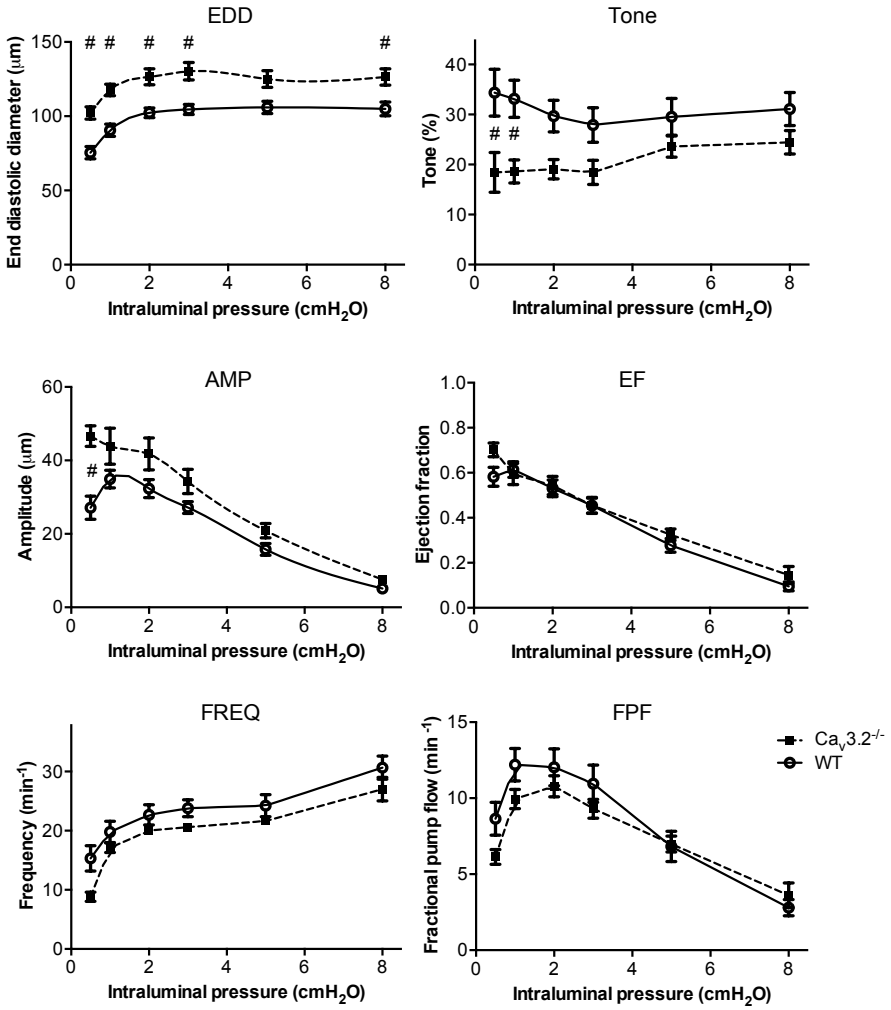

Figure 28. Contractile patterns of IALs from $Ca_v3.2^{-/-}$ mice during pressure step protocol.

A&B: Representative pressure myograph recordings throughout a pressure step protocol for inguinal-axillary lymphatic vessels from $Ca_v3.2^{-/-}$ and WT mice, respectively. C: Summary data comparing contractile characteristics as a function of pressure in inguinal-axillary lymphatic vessels from WT, n=6 (black lines, open symbols) and $Ca_v3.2^{-/-}$ mice, n=10 (dashed lines, closed symbols); "n" refers to the number of lymphatic vessels. WT: C57Bl/6J, which is the background for $Ca_v3.2^{-/-}$. Timescale indicates 30s.

3.15 Effect of global genetic deletion of $Ca_v3.1$ on lymphatic contractions in mouse popliteal lymphatics

Next, I used global $Ca_v3.1^{-/-}$ mice to test the role of this T-channel isoform in lymphatic pacemaking. Similar to IALs from $Ca_v3.2^{-/-}$ mice, IALs from $Ca_v3.1^{-/-}$ mice showed contractile patterns nearly indistinguishable from those of WT mice in response to the pressure step protocol (Figure 29). We also utilized PLs from $Ca_v3.1^{-/-}$ mice and found normal contractile patterns similar to those from WT (experiments by MJD). The current established view posits that the T-channel isoform $Ca_v3.1$ in smooth muscle cells is important in myogenic responses at low pressure from 40-80mmHg (Hansen *et al.*, 2015; Björling *et al.*, 2013). Compared with lymphatic vessels from WT, EDDs inclined to be larger in IALs, but tended to be smaller in PLs from $Ca_v3.1^{-/-}$ mice compared to controls; however, the differences were not statistically significant. Contraction amplitudes in both IALs and PLs tended to be larger in $Ca_v3.1^{-/-}$ than in WT vessels, especially at lower pressures from 0.5 up to 3cmH_2O. However, the differences also were not significant (Figure 29 and Figure 30).

A. Inguinal-axillary lymphatic from $Ca_v3.1^{-/-}$ mouse

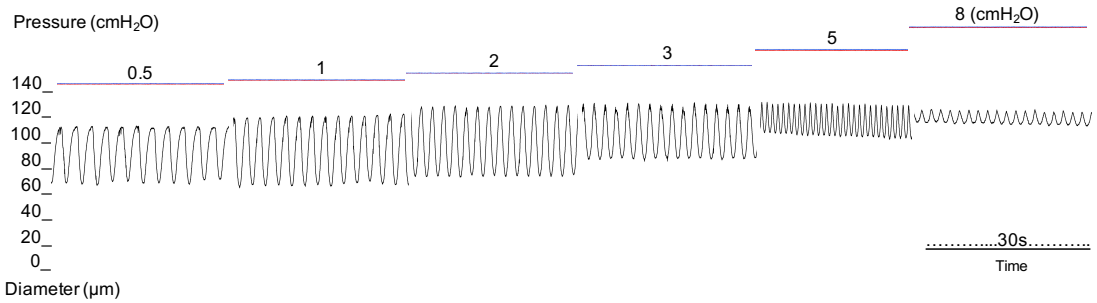

B. Inguinal-axillary lymphatic from WT mouse

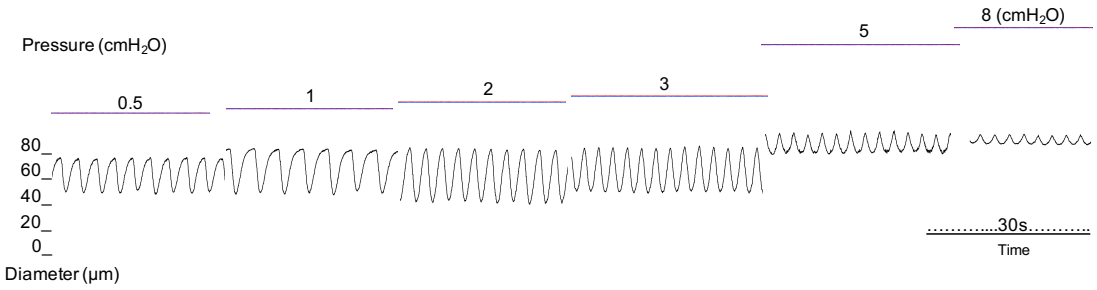

C

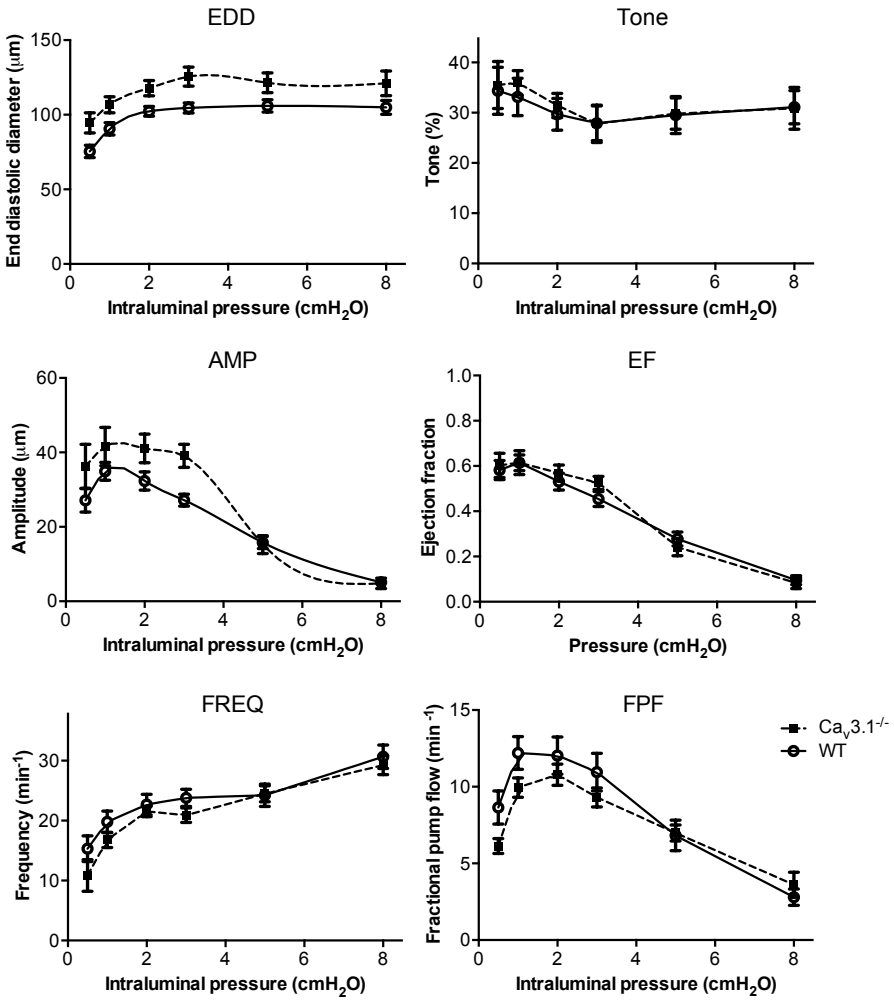

Figure 29. Contractile patterns of IALs from $Ca_v3.1^{-/-}$ mice during pressure step protocol.

A&B: Representative pressure myograph recordings throughout a pressure step protocol in inguinal-axillary lymphatic vessels from $Ca_v3.1^{-/-}$ and WT, respectively. C: Summary data comparing contractile parameters as a function of pressure for inguinal-axillary lymphatic vessels from $Ca_v3.1^{-/-}$, n=8 (dashed lines, closed symbols) and WT, n=6 (black lines, open symbols); n refers to the number of lymphatic vessels. WT: C57Bl/6J, which is the background for $Ca_v3.1^{-/-}$. No significant differences were found.

A. Popliteal lymphatic from a $Ca_v3.1^{-/-}$ mouse

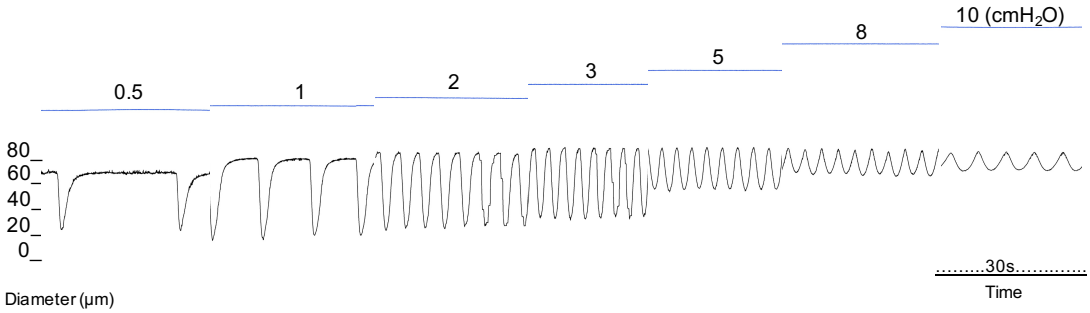

B. Popliteal lymphatics from WT mouse

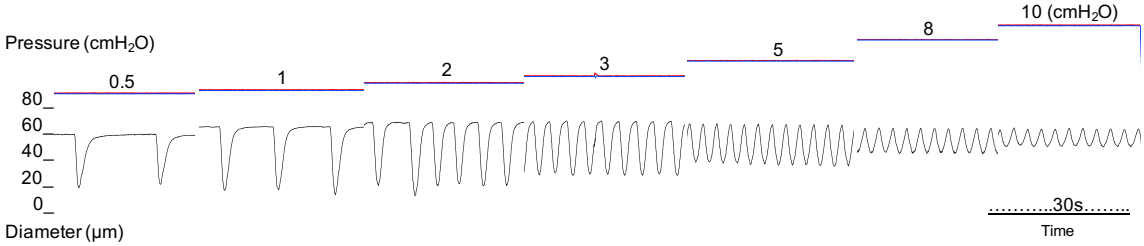

C

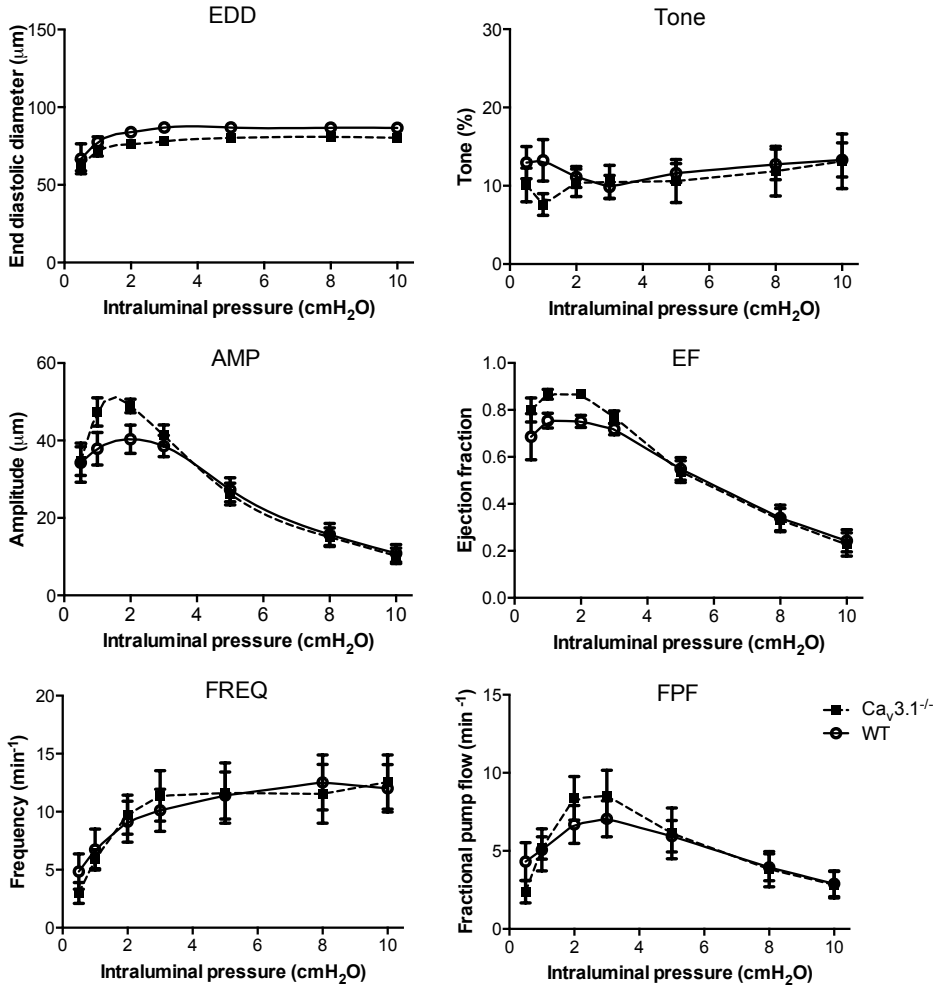

Figure 30. Contractile patterns of PLs from $Ca_v3.1^{-/-}$ mice during pressure step protocol. A&B: Representative pressure myograph recordings throughout a pressure step protocol in popliteal lymphatic vessels from $Ca_v3.1^{-/-}$ and WT, respectively. C: Summary data comparing the contractile patterns for the pressure step protocol in PLs from WT mice (black lines, open symbols, n=8) and $Ca_v3.1^{-/-}$ mice (dashed lines, open symbols, n=6), n refers to the number of lymphatic vessels. Experiments was performed by MJD. No significant differences were found. WT: C57Bl/6J, which is the background for $Ca_v3.1^{-/-}$.

Using transgenic mouse models with deleted or overexpressed $Ca_v3.1$, Nakayama *et al.* suggested a protective role for $Ca_v3.1$ against cardiac hypertrophy via an eNOS-dependent pathway (Nakayama *et al.*, 2009); eNOS was shown to expressed in the cardiac myocytes and interact with $Ca_v3.1$. Likewise, in mesenteric arteries, global deletion of $Ca_v3.1$ interferes with NO-mediated dilation, mediated partially by eNOS activity (Svenningsen *et al.*, 2014). For this reason, we implemented an additional dose-response protocol in which acetylcholine (1-300nM) was used to activate eNOS in WT and $Ca_v3.1^{-/-}$ lymphatic vessels (Scallan *et al.*, 2013a). In comparison with WT mice, PLs from $Ca_v3.1^{-/-}$ mice showed no differences in contractile parameters in response to increasing cumulative concentrations of acetylcholine in the range from 1 to 300nM, which is often sufficient to completely inhibit spontaneous contractions (Figure 31).

A. Popliteal lymphatic from a $Ca_v3.1^{-/-}$ mouse

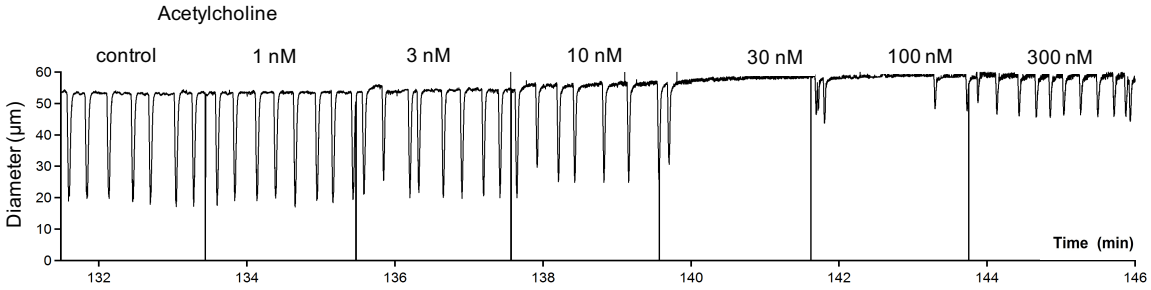

B. Popliteal lymphatic from a WT mouse

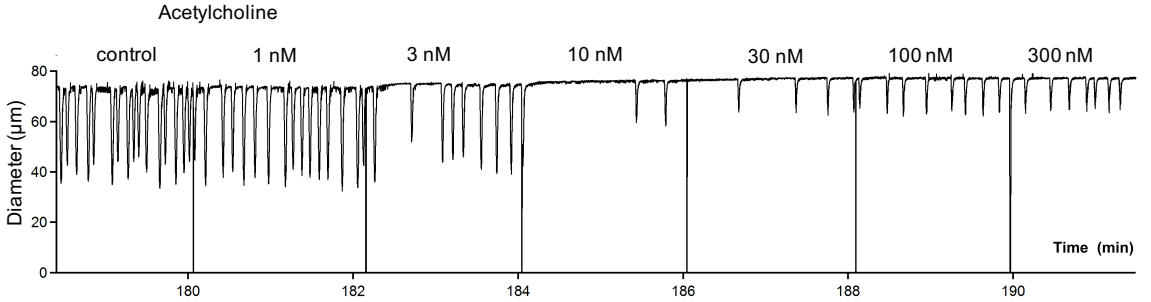

C

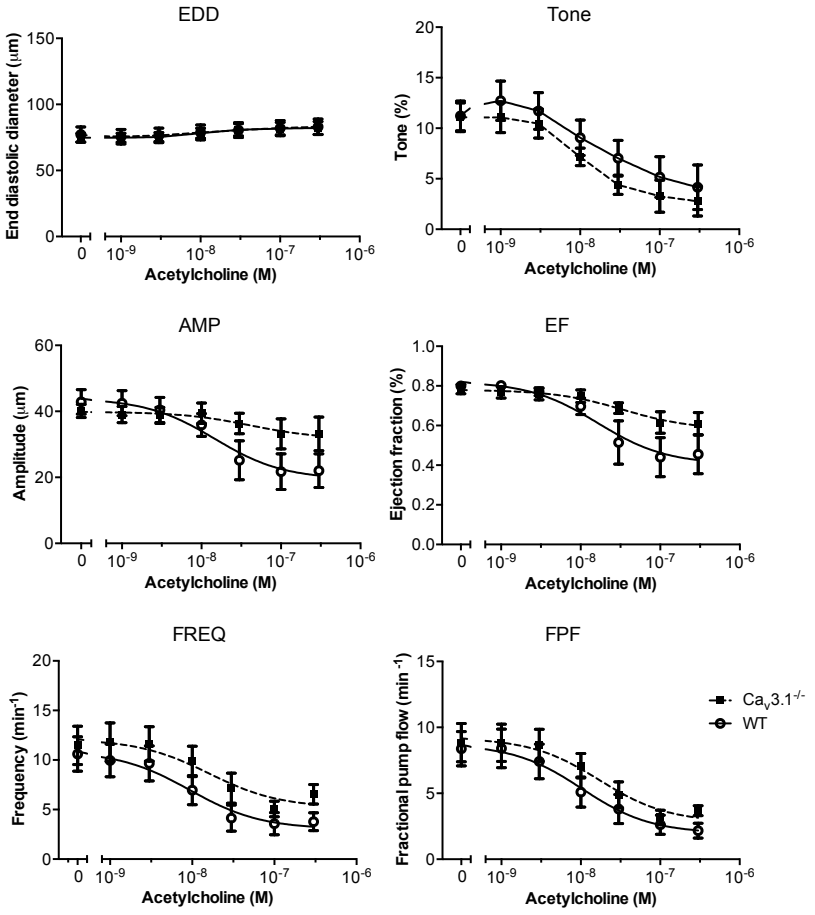

Figure 31. Effect of acetylcholine on the contractile patterns of PLs from $Ca_v3.1^{-/-}$ mice. A&B: Representative pressure myograph recordings during a cumulative acetylcholine dose-response curve in popliteal lymphatic vessels from a $Ca_v3.1^{-/-}$ mouse and a WT mouse, respectively. C: Summary data comparing contractile parameters for the acetylcholine dose-response protocol in PLs from WT mice (black lines, open symbols), n=7, and $Ca_v3.1^{-/-}$ mice (dashed lines, closed symbols), n=9; n refers to the number of lymphatic vessels. Experiments were performed by MJD. No significant differences were found.

Because there were no obvious differences in contractile parameters or Ach responsiveness between $Ca_v3.1^{-/-}$ and WT vessels, we decided to test for more subtle effects. We hypothesized that deletion of $Ca_v3.1$ might cause a shift in the nifedipine dose-response curve if T-channels contributed an additional source of Ca^{2+} entry in LSM cells. However, the nifedipine dose-response curves of $Ca_v3.1^{-/-}$ and WT PLs were nearly identical in regard to all contraction parameters except frequency (Figure 32). Spontaneous contractions in WT vessels persisted at higher nifedipine concentrations compared to $Ca_v3.1^{-/-}$ vessels (IC_{50}=40nM and 45nM, respectively), but this difference was not significant. Also, applying nifedipine on rat mesenteric lymphatics, Souza-Smith *et al.* showed that 100nM nifedipine decreased both contraction amplitude and frequency (Souza-Smith *et al.*, 2015). Unlike this finding in the rat, our experiments on mouse popliteals showed that lower concentrations of nifedipine (1-100nM) slightly increased the contraction frequency while decreasing contraction amplitude. Indeed, this was a common trend for almost all of the pharmacological inhibitors used, and suggests a common effect of those compounds on L-

type channels. In summary, I found no showed significant differences in contractile parameters of lymphatic vessels from WT and $Ca_v3.1^{-/-}$ mice at any nifedipine concentrations.

One explanation for the collective findings is that either one of the two T-channel isoforms is needed to ensure normal lymphatic contractile function. Thus, if $Ca_v3.1$ is deleted, $Ca_v3.2$ may be able to compensate, and vice versa. This possibility led us to generate double knock-outs of both $Ca_v3.1$ and $Ca_v3.2$ to study the lymphatic phenotype. However, those mice were not yet ready to study at the time of my defense and so the results are part of this dissertation.

A. $Ca_v3.1^{-/-}$ popliteal lymphatic

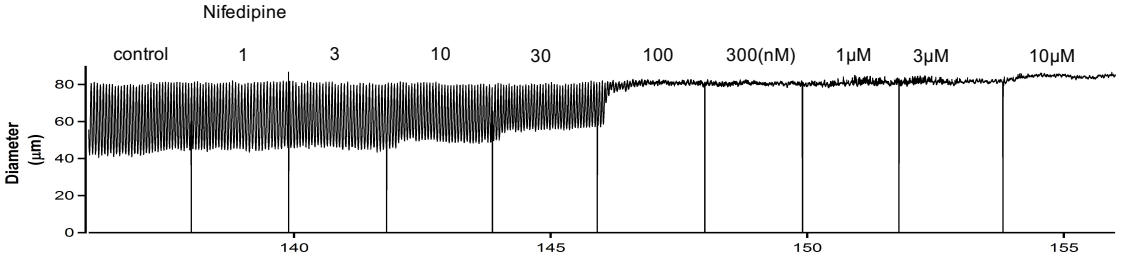

B. WT popliteal lymphatic

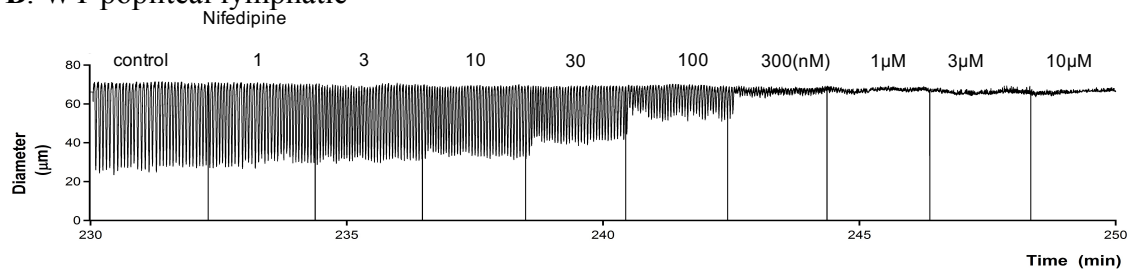

C.

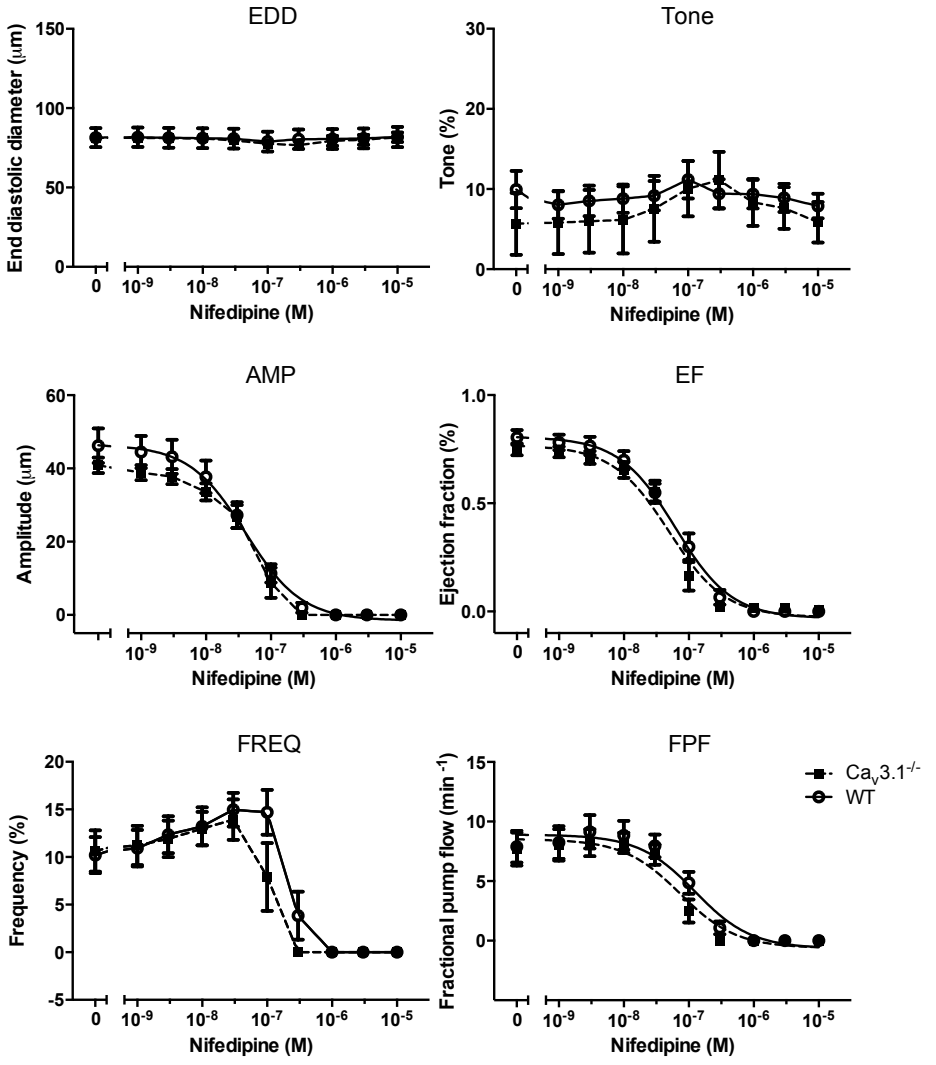

Figure 32. Effect of nifedipine on the contractile patterns of PLs from $Ca_v3.1^{-/-}$ mice. A&B: Representative pressure myograph recordings throughout cumulative nifedipine doses in popliteal lymphatic vessels from $Ca_v3.1^{-/-}$ and WT, respectively. C: Summary data comparing contractile patterns for the nifedipine dose-response protocol in $Ca_v3.1^{-/-}$ PLs from WT PLs (solid lines), n=8, and $Ca_v3.1^{-/-}$ (dashed lines), n=6; n refers to the number of lymphatic vessels. Experiments were performed by MJD.

CHAPTER 4: DISCUSSION

This study investigated role of the T-type voltage-gated Ca^{2+} channels ($Ca_v3.1$ and $Ca_v3.2$ isoforms) in lymphatic pacemaking. For the first time in this field, I combined both conventional pharmacological modulators and mouse models genetically deleted of specific voltage-gated Ca^{2+} channel isoform(s) to find out the contribution of $Ca_v3.1$ and $Ca_v3.2$ in lymphatic pacemaking. Based on the literature, I hypothesized that both pharmacological inhibition and genetic deletion of T-type voltage-gated Ca^{2+} channels would selectively decrease the frequency of lymphatic contractions in mice. I also attempted to reproduce experiments on rat mesenteric lymphatic vessels using pharmacological T-channel inhibitors. In both rat and mouse LSM, I was able to collect evidence for T-channel expression at the mRNA and electrophysiological levels using PCR, and patch-clamp techniques, respectively. Immunostaining was also used to detect expression of T-channels in mouse IALs at the protein level. $Ca_v3.1$ and 3.2 are the two T-channel isoforms predominantly expressed by LSM, along with L-channel isoform $Ca_v1.2$. When lymphatic contractile function was tested using pressure myography in both mouse and rat lymphatic vessels, reputedly-specific T-channel inhibitors Ni^{2+} and TTA-A2, produced effects that were not in accord with the currently established view about the role of T-channels in lymphatic pacemaking reported in rat and sheep lymphatic vessels (Lee *et al.*, 2014a; Beckett *et al.*, 2007).

Genetic deletion of either T-channel isoform $Ca_v3.1$ or $Ca_v3.2$ in mice was utilized as an alternative, but more powerful and specific, way to test the role of T-channels. However, I was unable to find any significant changes in lymphatic pacemaking and/or

contractile patterns in either IALs from $Ca_v3.2$KO mice or in IALs and PLs from $Ca_v3.1$KO mice compared to their control counterparts from WT mice. I will now offer explanations for the discrepancies between my findings and previous studies and propose future experiments that might enhance our understanding of how voltage-gated Ca^{2+} channels contribute to lymphatic vessel contractions and pacemaking.

Discrepancies from the current literature

Previous publications on the role of T-type voltage-gated Ca^{2+} channels in lymphatic pacemaking relied only on pharmacology, even though none of the currently available T-channel inhibitors are specific. T-channel inhibitors can also affect L-type Ca^{2+} channels due to structural similarities between them. For example, Ni^{2+} and mibefradil, the two most commonly used T-channel inhibitors, also inhibit L-channels (Jensen and Holstein-Rathlou, 2009; Moosmang *et al.*, 2006). My data (Figure 20, Figure 21, Figure 22, Figure 23 and Figure 24) are consistent with effects of mibefradil, Ni^{2+} and TTA-A2 on both types of channels because both contraction frequency and amplitude were inhibited to approximately the same extent as the inhibitor concentration increased. Therefore, I conclude that it is impossible to differentiate the role of T- and L-channels in lymphatic pacemaking/contraction using currently available T-channel inhibitors.

Moreover, the proposed role of T-channels in lymphatic pacemaking based on the current literature was established by using single concentrations of inhibitors on lymphatic vessels from two different species i.e., sheep (Beckett *et al.*, 2007) and rat (Lee *et al.*, 2014a). Both Lee *et al.* and Beckett *et al.* utilized 100μM Ni^{2+} to inhibit T-channels and 100nM nifedipine to inhibit L-channels. In the presence of 100μM Ni^{2+} and 100nM nifedipine, rat mesenteric lymphatics kept firing APs (Lee *et al.*, 2014a). In the presence

of the same doses of Ni^{2+} and nifedipine, sheep mesenteric lymphatic vessels ceased firing APs (Beckett *et al.*, 2007). Therefore, lymphatic vessels from different species can have different responses to the same drug concentration. I encountered a similar phenomenon when rat mesenteric lymphatic vessels usually stopped contracting at lower Ni^{2+} concentrations than mouse lymphatic vessels (Figure 21, Figure 22 and Figure 23). And even among mouse lymphatics from different body regions, mouse IALs required two to three times the Ni^{2+} concentration than PLs to stop contractions (Figure 22 and Figure 23). To my knowledge, this is the only study using full dose-response protocols for both Ni^{2+} and nifedipine.

The discrepancies between my results and previous results might also stem from different ways of administering inhibitors. Lee *et al.* 2014a seemingly exchanged the whole tissue bath gradually with drug solution at its final concentrations in the majority of their experiments. Although, it is not specifically stated in their study, that is the method used in many previous studies from the same laboratory. This gradual exchange method results in a slow increase in drug concentration until the bath is completely exchanged. We found that rapid exchange of the bath was not possible in our lab without inducing a substantial temperature change (that could have influenced pacemaking frequency which is very temperature sensitive). Beckett *et al.* 2007 seemingly applied a stock solution of inhibitors, and mixed it to dilute to the final concentration directly in the bath. Similar to Beckett *et al.* 2007, I added an aliquot of inhibitors to one end of the chamber and mixed it rapidly with the whole bath to rapidly obtain the final concentration. This method may transitionally expose the vessels to a higher concentration of inhibitors. Therefore, ways of

administering pharmacological inhibitors can greatly distort conclusions from different laboratories about the same physiological questions.

Additionally, the previous two studies assessed the effect of T-channel inhibitors on the frequency and amplitude of lymphatic pacemaking at different times after exposure to those inhibitors. Beckett *et al.* 2007 made observations immediately after drug application (see Figure 5). Lee *et al.* 2014 made observations after exchange of the whole tissue bath, which can take 10-15min in based on my experience. In my studies, I averaged contraction parameters over a period of two to three minutes after drug application and mixing, allowing for the lymphatic contraction patterns to stabilize.

Based on my collective results, I was not able to confirm the current view that T-channels regulate the frequency of lymphatic contractions while L-channels regulate amplitude. Comparing my results using pharmacological inhibition and genetic deletion on the same type of mouse lymphatic vessels, I found that each of the T-channel inhibitors produced a major effect on lymphatic contraction amplitude, while genetic deletion of either T-channel isoform, $Ca_v3.1$ or 3.2, resulted in no defect in lymphatic pacemaking or contraction amplitude. In contrast, I found that inhibiting or deleting L-channels had a great impact on both lymphatic contraction amplitude and frequency. Therefore, T-channels play no detectable role in regulating phasic lymphatic contraction frequency or amplitude and the inhibitory effects on pacemaking observed when treating lymphatic vessels with T-channel inhibitors are likely to be a non-specific effect of those inhibitors on L-channels.

Future directions

The lack of a lymphatic pacemaking phenotype in $Ca_v3.1^{-/-}$ and $Ca_v3.2^{-/-}$ mice could be explained by the functional redundancy of these two T-channel isoforms. The breeding of double knockout mice lacking both $Ca_v3.1^{-/-}$ and $Ca_v3.2^{-/-}$ takes about nine months to complete and results will be included in a future publication. The expression of one isoform could be increased to compensate for deletion of the other isoform. Although double knock-out mice of T-channels ($Ca_v3.3^{-/-}$ and $Ca_v3.2^{-/-}$) have been generated by Shin's group for neuronal function studies (Lee *et al.*, 2014b), this will be the first time that any physiological studies will be investigated using mice lacking both $Ca_v3.1$ and $Ca_v3.2$.

With respect to the possibility of compensation of other channels in Ca_v3 knockout mice, it was previously reported that in both $Ca_v3.1^{-/-}$ and $Ca_v3.2^{-/-}$ mice, the mRNA expression of other channels such as L-type Ca^{2+} channels, TRP channels and K^+ channels are unchanged (Mikkelsen *et al.*, 2016; Björling *et al.*, 2013). However, possible functional compensation of other channels in KO mice were not investigated (e.g., membrane trafficking, phosphorylation state, accessory subunits or activation by second messengers). Furthermore, $Ca_v3.2^{-/-}$ mice with mixed background (C57Bl/6x129) were reported to produce more nitric oxide in response to depolarization by 70mM KCl compared to WT and $Ca_v3.2^{-/-}$ mice with C57Bl/6 background. In this study, I purchased $Ca_v3.2^{-/-}$ mice from the Jackson laboratory, backcrossed into C57Bl/6, therefore their NO production should not be altered. In addition, in human arterial smooth muscle cells, $Ca_v3.3$ was found to substitute functionally for $Ca_v3.1$, which is the isoform expressed in arterial smooth muscle cells from mouse. $Ca_v3.3$ is suggested to play a role in the constriction of human cerebral arteries, similar to the role of $Ca_v3.1$ in rodent arteries (Harraz *et al.*, 2015). Therefore, it

is possible that there could be functional compensation of $Ca_v3.3$ in knockout mice lacking $Ca_v3.1$ or/and $Ca_v3.2$. This could be tested using PCR and immunostaining for $Ca_v3.3$ in the double KO. Functional compensation, if it exists, could be prevented using conditional knockout mice (e.g. conditional $Ca_v3.1$KO + global $Ca_v3.2$KO) in which the timing of genetic deletion is controlled with studies conducted before compensation can occur.

Specifically deleting $Ca_v1.2$ from smooth muscle cells rendered lymphatic vessels quiescent (Figure 26). Since inhibiting L-channels with nifedipine depolarizes LSM by 5-10mV (preliminary data by MJD; von der Weid *et al.*, 2014; Telinius *et al.*, 2013), LSM cells lacking $Ca_v1.2$ could have a depolarized V_m that is unfavorable for T-channel activation. One hypothesis that I would like to test using vessels from $Ca_v1.2$KO mice is whether spontaneous contractions can be restored if I activate T-channels. The first step would be resetting V_m of LSM cells lacking $Ca_v1.2$ to around -45 to -35mV, the normal resting membrane potential recorded in LSM cells. Ideally, a series of gradually increasing depolarizing currents would be injected to find a voltage that is able to recruit a maximal number of T-channels. However, this is not possible experimentally in a vessel with a LSM cell syncytium, but an alternative approach could be using low K^+ solution to hyperpolarize all the LSM cells in the vessel. I would be testing whether T-channels alone can take over the spontaneous lymphatic activity in LSM lacking $Ca_v1.2$. Perhaps T-channels are normally only important when LSM is hyperpolarized by mediators such as NO, VIP, cyclic nucleotides (von der Weid *et al.*, 2012 and 1998). Another remaining question is: what are the T-channel splice variants predominantly expressed in lymphatic muscle cells? This raises the issue of whether there are splice variants of T-channels expressed in LSM that have more positive window currents. In a T-channel mRNA construct, splicing could

occur between exon 25-26 to either transcribe for vascular-specific (25bc) or brain-specific (25a) splice variants distinguishable by their window currents (Emeric *et al.*, 2006; Zhong *et al.*, 2006). Splice variant 25bc was shown to have a more depolarized window current from -35 to -45mV (Kuo *et al.*, 2014). From my patch-clamp data T-channel current (recorded after 1μM nifedipine) is likely to be activated more in the depolarized range than V_m of LSM, and I would predict that a certain population of T-channels in lymphatic muscle cells is activated at a more depolarized potential, similar to the vascular-specific splice variants (25bc).

Smooth muscle-specific deletion of $Ca_v1.2$ offers a mouse model that possesses lymphatic vessels lacking spontaneous pacemaking. An interesting question is: what is the impact of lack of $Ca_v1.2$ on LSM *in vivo*? Do the mice eventually develop lymphedema? The major obstacle to testing this idea is that SMMHC-Cre, $Ca_v1.2^{fl/fl}$ mice have a low survival rate after systemic tamoxifen induction, beginning to die as early as ten days after tamoxifen injection due to gastrointestinal problems. I imagine that limited Cre induction in a localized body region might prolong survival time of tamoxifen-induced SMMHC-Cre; $Ca_v1.2^{fl/fl}$ mice and reveal pathological consequences of lacking lymphatic pacemaking. Cre recombination has been successfully induced using topical tamoxifen (Boneva *et al.*, 2016; Vasioukihin *et al.*, 1999). Therefore, it may be feasible to silence lymphatic pacemaking in collecting lymphatic vessels from one limb and use the other limb as control to investigate the lymphatic consequences of localized, chronic $Ca_v1.2$ deletion in smooth muscle.

There is a possibility that T-channels indeed do not play any role in lymphatic pacemaking. The question then becomes whether T-channels play roles in other aspects of

lymphatic physiology. One possible role for T-channels is in endothelial-dependent lymphatic responses. In my immunostaining protocols, I occasionally found a $Ca_v3.2$ signal in parallel with the orientation of LECs. It could suggest the expression of $Ca_v3.2$ in the LEC layer. In blood vessels, $Ca_v3.2$ channels were suggested to play a role in vasodilatory feedback by endothelial cells, although no data were provided to support that idea (Figueroa *et al.*, 2007). Their role would rely on electrical communication between blood endothelial layer and smooth muscle layer via myoendothelial gap junctions (Kuo *et al.*, 2011). However, such communication is not likely to be present in lymphatic vessels because LSM cells and LECs are electrically uncoupled. In experiments from our laboratory, V_m of the mouse LEC layer is -70mV and quiescent, while V_m in the mouse LSM cells is more depolarized from -40 to -35mV and repetitively fires APs (MJD and SDZ unpublished observations).

In LSM, Ca_v3 channels could contribute to Ca^{2+} signaling that regulates lymphatic remodeling in response to a sustained high lymph load (Dongaonkar *et al.*, 2013 and 2015). In the heart, $Ca_v3.1$ has been shown to play a role in cardiac pacemaking (Mangoni *et al.*, 2006) and in hypertrophic process via calcineurin-NFAT hypertrophic pathways (Nakayama *et al.*, 2009). Likewise, $Ca_v3.2$ also has been shown to induce calcineurin-NFAT pathways in overload-induced cardiac hypertrophy. Could $Ca_v3.x$ expression and function therefore be altered in lymphatic pathological conditions such as increased lymph load in lymphedema?

Ultimately, by studying the ionic mechanisms regulating lymphatic pacemaking, I am aiming to find a way to improve lymphatic function in humans, especially in pathological conditions such as lymphedema where the lymphatic pacemaker may be

compromised. Targeting the pacemaker of lymphatic vessels may be a novel way to directly treat lymphedema. Although it is unclear whether T-channels are expressed in human lymphatic vessels and have a functional role in lymphatic contractions, we are in the process of analyzing the molecular expression of T-channels in human mesenteric lymphatic vessels harvested as a by-product of bariatric surgery. Since transgenic approaches cannot be used, the development of specific inhibitors for T-type Ca^{2+} channels will be necessary to fully understand the functional role of T-channels in human lymphatic pacemaking.

REFERENCES

1. Abd El-Rahman, R.R., Harraz, O.F., Brett, S.E., Anfinogenova, Y., Mufti, R.E., Goldman, D., and Welsh, D.G. (2013). Identification of L- and T-type Ca2+ channels in rat cerebral arteries: role in myogenic tone development. Am. J. Physiol. Heart Circ. Physiol. *304*, H58-71.

2. Akl, T.J., Nagai, T., Coté, G.L., and Gashev, A.A. (2011). Mesenteric lymph flow in adult and aged rats. Am. J. Physiol. Heart Circ. Physiol. *301*, H1828-1840.

3. Aldrich, M.B., Davies-Venn, C., Angermiller, B., Robinson, H., Chan, W., Kwon, S., and Sevick-Muraca, E.M. (2012). Concentration of Indocyanine Green Does Not Significantly Influence Lymphatic Function as Assessed by Near-Infrared Imaging. Lymphat Res Biol *10*, 20–24.

4. Allen, J.M., Iggulden, H.L., and McHale, N.G. (1986). Beta-adrenergic inhibition of bovine mesenteric lymphatics. J Physiol *374*, 401–411.

5. Amerini, S., Ziche, M., Greiner, S.T., and Zawieja, D.C. (2004). Effects of substance P on mesenteric lymphatic contractility in the rat. Lymphat Res Biol *2*, 2–10.

6. Ando, K., Kurihara, M., Kataoka, H., Ueyama, M., Togo, S., Sato, T., Doi, T., Iwakami, S., Takahashi, K., Seyama, K., et al. (2013). Efficacy and safety of low-dose sirolimus for treatment of lymphangioleiomyomatosis. Respir Investig *51*, 175–183.

7. Aspelund, A., Robciuc, M.R., Karaman, S., Makinen, T., and Alitalo, K. (2016). Lymphatic System in Cardiovascular Medicine. Circ. Res. *118*, 515–530.

8. Astori, S., Wimmer, R.D., Prosser, H.M., Corti, C., Corsi, M., Liaudet, N., Volterra, A., Franken, P., Adelman, J.P., and Lüthi, A. (2011). The Ca(V)3.3 calcium channel is the major sleep spindle pacemaker in thalamus. Proc. Natl. Acad. Sci. U.S.A. *108*, 13823–13828.

9. Atchison, D.J., and Johnston, M.G. (1997). Role of extra- and intracellular Ca2+ in the lymphatic myogenic response. Am. J. Physiol. *272*, R326-333.

10. Atchison, D.J., Rodela, H., and Johnston, M.G. (1998). Intracellular calcium stores modulation in lymph vessels depends on wall stretch. Can. J. Physiol. Pharmacol. *76*, 367–372.

11. Aukland, K., and Reed, R.K. (1993). Interstitial-lymphatic mechanisms in the control of extracellular fluid volume. Physiol. Rev. *73*, 1–78.

12. Badger, C., Preston, N., Seers, K., and Mortimer, P. (2004). Benzo-pyrones for reducing and controlling lymphoedema of the limbs. Cochrane Database Syst Rev CD003140.

13. Ball, C.J., Wilson, D.P., Turner, S.P., Saint, D.A., and Beltrame, J.F. (2009). Heterogeneity of L- and T-channels in the vasculature: rationale for the efficacy of combined L- and T-blockade. Hypertension *53*, 654–660.

14. Baluk, P., Fuxe, J., Hashizume, H., Romano, T., Lashnits, E., Butz, S., Vestweber, D., Corada, M., Molendini, C., Dejana, E., et al. (2007a). Functionally specialized junctions between endothelial cells of lymphatic vessels. J. Exp. Med. *204*, 2349–2362.

15. Bazigou, E., and Makinen, T. (2013). Flow control in our vessels: vascular valves make sure there is no way back. Cell. Mol. Life Sci. *70*, 1055–1066.

16. Bean, B.P. (1985). Two kinds of calcium channels in canine atrial cells. Differences in kinetics, selectivity, and pharmacology. J Gen Physiol *86*, 1–30.

17. Becker, A.J., Pitsch, J., Sochivko, D., Opitz, T., Staniek, M., Chen, C.-C., Campbell, K.P., Schoch, S., Yaari, Y., and Beck, H. (2008). Transcriptional upregulation of Cav3.2 mediates epileptogenesis in the pilocarpine model of epilepsy. J. Neurosci. *28*, 13341–13353.

18. Beckett, E. A. H., Hollywood, M.A., Thornbury, K.D., and McHale, N.G. (2007). Spontaneous electrical activity in sheep mesenteric lymphatics. Lymphat Res Biol *5*, 29–43.

19. Berridge, M.J. (2006). Calcium microdomains: Organization and function. Cell Calcium *40*, 405–412.

20. Bilancini, S., Lucchi, M., Tucci, S., and Eleuteri, P. (1995). Functional lymphatic alterations in patients suffering from lipedema. Angiology *46*, 333–339.

21. Bkaily, G. (1994). Ionic Channels in Vascular Smooth Muscle (R.G. Landes Company).

22. Blum, K.S., Karaman, S., Proulx, S.T., Ochsenbein, A.M., Luciani, P., Leroux, J.-C., Wolfrum, C., and Detmar, M. (2014). Chronic high-fat diet impairs collecting lymphatic vessel function in mice. PLoS ONE *9*, e94713.

23. Bodi, I., Mikala, G., Koch, S.E., Akhter, S.A., and Schwartz, A. (2005). The L-type calcium channel in the heart: the beat goes on. J Clin Invest *115*, 3306–3317.

24. Boneva, S.K., Groß, T.R., Schlecht, A., Schmitt, S.I., Sippl, C., Jägle, H., Volz, C., Neueder, A., Tamm, E.R., and Braunger, B.M. (2016). Cre recombinase expression or topical tamoxifen treatment do not affect retinal structure and function, neuronal vulnerability or glial reactivity in the mouse eye. Neuroscience *325*, 188–201.

25. Bose, T., Cieślar-Pobuda, A., and Wiechec, E. (2015). Role of ion channels in regulating Ca2+ homeostasis during the interplay between immune and cancer cells. Cell Death Dis *6*, e1648.

26. Bouta, E.M., Li, J., Ju, Y., Brown, E.B., Ritchlin, C.T., Xing, L., and Schwarz, E.M. (2015). The Role of the Lymphatic System in Inflammatory-Erosive Arthritis. Semin Cell Dev Biol *38*, 90–97.

27. Brennan, M.J., and Weitz, J.O. (1992). LYMPHEDEMA 30 YEARS AFTER RADICAL MASTECTOMY. Journal of Physical Medicine *71*, 12–14.

28. Brice, G., Mansour, S., Bell, R., Collin, J.R.O., Child, A.H., Brady, A.F., Sarfarazi, M., Burnand, K.G., Jeffery, S., Mortimer, P., et al. (2002). Analysis of the phenotypic abnormalities in lymphoedema-distichiasis syndrome in 74 patients with FOXC2 mutations or linkage to 16q24. J. Med. Genet. *39*, 478–483.

29. Brice, G.W., Mansour, S., Ostergaard, P., Connell, F., Jeffery, S., and Mortimer, P. (1993). Milroy Disease. In GeneReviews(®), R.A. Pagon, M.P. Adam, H.H. Ardinger, S.E. Wallace, A.

Amemiya, L.J. Bean, T.D. Bird, C.-T. Fong, H.C. Mefford, R.J. Smith, et al., eds. (Seattle (WA): University of Washington, Seattle)

30. Bridenbaugh, E.A., Nizamutdinova, I.T., Jupiter, D., Nagai, T., Thangaswamy, S., Chatterjee, V., and Gashev, A.A. (2013). Lymphatic muscle cells in rat mesenteric lymphatic vessels of various ages. Lymphat Res Biol *11*, 35–42.

31. Briggs Boedtkjer, D., Rumessen, J., Baandrup, U., Skov Mikkelsen, M., Telinius, N., Pilegaard, H., Aalkjaer, C., and Hjortdal, V. (2013). Identification of interstitial Cajal-like cells in the human thoracic duct. Cells Tissues Organs (Print) *197*, 145–158.

32. Brorson, H. (2012). From lymph to fat: liposuction as a treatment for complete reduction of lymphedema. Int J Low Extrem Wounds *11*, 10–19.

33. Brown, P. (2005). Lymphatic system: Unlocking the drains. Nature *436*, 456–458.

34. Bundred, N.J., Stockton, C., Keeley, V., Riches, K., Ashcroft, L., Evans, A., Skene, A., Purushotham, A., Bramley, M., Hodgkiss, T., et al. (2015). Comparison of multi-frequency bioimpedance with perometry for the early detection and intervention of lymphoedema after axillary node clearance for breast cancer. Breast Cancer Res. Treat. *151*, 121–129.

35. Cambria, R.A., Gloviczki, P., Naessens, J.M., and Wahner, H.W. (1993). Noninvasive evaluation of the lymphatic system with lymphoscintigraphy: a prospective, semiquantitative analysis in 386 extremities. J. Vasc. Surg. *18*, 773–782.

36. Capel, R.A., and Terrar, D.A. (2015). The importance of Ca(2+)-dependent mechanisms for the initiation of the heartbeat. Front Physiol *6*, 80.

37. Card, C.M., Yu, S.S., and Swartz, M.A. (2014). Emerging roles of lymphatic endothelium in regulating adaptive immunity. J. Clin. Invest. *124*, 943–952.

38. CasleySmith, J.R. (1967). Electron microscopical observations on the dilated lymphatics in oedmatous regions and their collapse following hyaluronidase administration. Br J Exp Pathol *48*, 680–686.

39. Casley-Smith, J.R. (1972). The role of the endothelial intercellular junctions in the functioning of the initial lymphatics. Angiologica *9*, 106–131.

40. Casley-Smith, J.R. (1980). Are the initial lymphatics normally pulled open by the anchoring filaments? Lymphology *13*, 120–129.

41. Casley-Smith, J.R. (1983). Varying total tissue pressures and the concentration of initial lymphatic lymph. Microvasc. Res. *25*, 369–379.

42. Catterall, W.A. (2000). Structure and Regulation of Voltage-Gated Ca2+ Channels. Annual Review of Cell and Developmental Biology *16*, 521–555.

43. Catterall, W.A. (2011). Voltage-gated calcium channels. Cold Spring Harb Perspect Biol *3*, a003947.

44. Cha, B., Geng, X., Mahamud, M.R., Fu, J., Mukherjee, A., Kim, Y., Jho, E.-H., Kim, T.H., Kahn, M.L., Xia, L., et al. (2016). Mechanotransduction activates canonical Wnt/β-catenin signaling to promote lymphatic vascular patterning and the development of lymphatic and lymphovenous valves. Genes Dev. *30*, 1454–1469.

45. Chakraborty, S., Zawieja, S., Wang, W., Zawieja, D.C., and Muthuchamy, M. (2010). Lymphatic system: a vital link between metabolic syndrome and inflammation. Ann. N. Y. Acad. Sci. *1207 Suppl 1*, E94-102.

46. Chakraborty, S., Nepiyushchikh, Z., Davis, M.J., Zawieja, D.C., and Muthuchamy, M. (2011). Substance P activates both contractile and inflammatory pathways in lymphatics through the neurokinin receptors NK1R and NK3R. Microcirculation *18*, 24–35.

47. Chakraborty, S., Zawieja, S.D., Wang, W., Lee, Y., Wang, Y.J., von der Weid, P.-Y., Zawieja, D.C., and Muthuchamy, M. (2015). Lipopolysaccharide modulates neutrophil recruitment and macrophage polarization on lymphatic vessels and impairs lymphatic function in rat mesentery. Am. J. Physiol. Heart Circ. Physiol. *309*, H2042-2057.

48. Chemin, J., Monteil, A., Bourinet, E., Nargeot, J., and Lory, P. (2001). Alternatively spliced alpha(1G) (Ca(V)3.1) intracellular loops promote specific T-type Ca(2+) channel gating properties. Biophys J *80*, 1238–1250.

49. Chen, C.-C., Lamping, K.G., Nuno, D.W., Barresi, R., Prouty, S.J., Lavoie, J.L., Cribbs, L.L., England, S.K., Sigmund, C.D., Weiss, R.M., et al. (2003). Abnormal coronary function in mice deficient in alpha1H T-type Ca2+ channels. Science *302*, 1416–1418.

50. Chen, Y.-C., Chen, S.-A., Chen, Y.-J., Tai, C.-T., Chan, P., and Lin, C.-I. (2004). T-type calcium current in electrical activity of cardiomyocytes isolated from rabbit pulmonary vein. J. Cardiovasc. Electrophysiol. *15*, 567–571.

51. Cheng, X., Pachuau, J., Blaskova, E., Asuncion-Chin, M., Liu, J., Dopico, A.M., and Jaggar, J.H. (2009). Alternative splicing of Cav1.2 channel exons in smooth muscle cells of resistance-size arteries generates currents with unique electrophysiological properties. American Journal of Physiology - Heart and Circulatory Physiology *297*, H680–H688.

52. Chevalier, M., Gilbert, G., Roux, E., Lory, P., Marthan, R., Savineau, J.-P., and Quignard, J.-F. (2014). T-type calcium channels are involved in hypoxic pulmonary hypertension. Cardiovascular Research *103*, 597–606.

53. Chiang, C.-S., Huang, C.-H., Chieng, H., Chang, Y.-T., Chang, D., Chen, J.-J., Chen, Y.-C., Chen, Y.-H., Shin, H.-S., Campbell, K.P., et al. (2009). The CaV3.2 T-Type Ca2+ Channel Is Required for Pressure Overload–Induced Cardiac Hypertrophy in Mice. Circulation Research *104*, 522–530.

54. Chiplunkar, A.R., Curtis, B.C., Eades, G.L., Kane, M.S., Fox, S.J., Haar, J.L., and Lloyd, J.A. (2013). The Krüppel-like factor 2 and Krüppel-like factor 4 genes interact to maintain endothelial integrity in mouse embryonic vasculogenesis. BMC Dev. Biol. *13*, 40.

55. Choe, K., Jang, J.Y., Park, I., Kim, Y., Ahn, S., Park, D.-Y., Hong, Y.-K., Alitalo, K., Koh, G.Y., and Kim, P. (2015). Intravital imaging of intestinal lacteals unveils lipid drainage through contractility. J. Clin. Invest. *125*, 4042–4052.

56. Choi, I., Chung, H.K., Ramu, S., Lee, H.N., Kim, K.E., Lee, S., Yoo, J., Choi, D., Lee, Y.S., Aguilar, B., et al. (2011). Visualization of lymphatic vessels by Prox1-promoter directed GFP reporter in a bacterial artificial chromosome-based transgenic mouse. Blood *117*, 362–365.

57. Chong, C., Scholkmann, F., Bachmann, S.B., Luciani, P., Leroux, J.-C., Detmar, M., and Proulx, S.T. (2016). In vivo visualization and quantification of collecting lymphatic vessel contractility using near-infrared imaging. Sci Rep *6*, 22930.

58. Church, P.J., and Stanley, E.F. (1996). Single L-type calcium channel conductance with physiological levels of calcium in chick ciliary ganglion neurons. J Physiol *496*, 59–68.

59. Cohen, J.N., Guidi, C.J., Tewalt, E.F., Qiao, H., Rouhani, S.J., Ruddell, A., Farr, A.G., Tung, K.S., and Engelhard, V.H. (2010). Lymph node-resident lymphatic endothelial cells mediate peripheral tolerance via Aire-independent direct antigen presentation. J. Exp. Med. *207*, 681–688.

60. Collier, D.M., Hill-Eubanks, D.C., and Nelson, M.T. (2015). Orchestrating Ca2+ influx through CaV1.2 and CaV3.x channels in human cerebral arteries. J Gen Physiol *145*, 481–483.

61. Collin, C., Minami, M., Parvez, H., Saito, H., Parvez, S., Qureshi, and Reiss, C. (2005). Advances in Neuroregulation and Neuroprotection (CRC Press).

62. Cotton, K.D., Hollywood, M.A., McHale, N.G., and Thornbury, K.D. (1997). Outward currents in smooth muscle cells isolated from sheep mesenteric lymphatics. J. Physiol. (Lond.) *503 (Pt 1)*, 1–11.

63. Cribbs, L.L. (2006). T-type Ca2+ channels in vascular smooth muscle: multiple functions. Cell Calcium *40*, 221–230.

64. Cromer, W.E., Zawieja, S.D., Tharakan, B., Childs, E.W., Newell, M.K., and Zawieja, D.C. (2013). The effects of inflammatory cytokines on lymphatic endothelial barrier function. Angiogenesis *17*, 395–406.

65. Cuzzone, D.A., Weitman, E.S., Albano, N.J., Ghanta, S., Savetsky, I.L., Gardenier, J.C., Joseph, W.J., Torrisi, J.S., Bromberg, J.F., Olszewski, W.L., et al. (2014). IL-6 regulates adipose deposition and homeostasis in lymphedema. Am J Physiol Heart Circ Physiol *306*, H1426–H1434.

66. D'Andrea, V., Bianchi, E., Taurone, S., Mignini, F., Cavallotti, C., and Artico, M. (2013). Cholinergic innervation of human mesenteric lymphatic vessels. Folia Morphol. (Warsz) *72*, 322–327.

67. Danussi, C., Spessotto, P., Petrucco, A., Wassermann, B., Sabatelli, P., Montesi, M., Doliana, R., Bressan, G.M., and Colombatti, A. (2008). Emilin1 Deficiency Causes Structural and Functional Defects of Lymphatic Vasculature. Mol Cell Biol *28*, 4026–4039.

68. Danussi, C., Del Bel Belluz, L., Pivetta, E., Modica, T.M.E., Muro, A., Wassermann, B., Doliana, R., Sabatelli, P., Colombatti, A., and Spessotto, P. (2013). EMILIN1/α9β1 Integrin Interaction Is Crucial in Lymphatic Valve Formation and Maintenance. Mol Cell Biol *33*, 4381–4394.

69. Davis, M.J., Lane, M.M., Davis, A.M., Durtschi, D., Zawieja, D.C., Muthuchamy, M., and Gashev, A.A. (2008). Modulation of lymphatic muscle contractility by the neuropeptide substance P. Am. J. Physiol. Heart Circ. Physiol. *295*, H587-597.

70. Davis, M.J., Davis, A.M., Ku, C.W., and Gashev, A.A. (2009). Myogenic constriction and dilation of isolated lymphatic vessels. Am. J. Physiol. Heart Circ. Physiol. *296*, H293-302.

71. Davis, M.J., Rahbar, E., Gashev, A.A., Zawieja, D.C., and Moore, J.E. (2011). Determinants of valve gating in collecting lymphatic vessels from rat mesentery. Am. J. Physiol. Heart Circ. Physiol. *301*, H48-60.

72. Deitch, E.A. (2010). Gut lymph and lymphatics: a source of factors leading to organ injury and dysfunction. Ann. N. Y. Acad. Sci. *1207 Suppl 1*, E103-111.

73. Deng, J., He, P., Zhong, X., Wang, Q., Li, L., and Song, B. (2012). Identification of T-type calcium channels in the interstitial cells of Cajal in rat bladder. Urology *80*, 1389.e1-7.

74. Dhein, S., Salameh, A., Berkels, R., and Klaus, W. (1999). Dual mode of action of dihydropyridine calcium antagonists: a role for nitric oxide. Drugs *58*, 397–404.

75. DiFrancesco, D. (2010). The Role of the Funny Current in Pacemaker Activity. Circulation Research *106*, 434–446.

76. Dolphin, A.C. (2006). A short history of voltage-gated calcium channels. Br. J. Pharmacol. *147 Suppl 1*, S56-62.

77. Dongaonkar, R.M., Nguyen, T.L., Quick, C.M., Heaps, C.L., Hardy, J., Laine, G.A., Wilson, E., and Stewart, R.H. (2015). Mesenteric lymphatic vessels adapt to mesenteric venous hypertension by becoming weaker pumps. Am. J. Physiol. Regul. Integr. Comp. Physiol. *308*, R391-399.

78. Dougherty, P.J., Nepiyushchikh, Z.V., Chakraborty, S., Wang, W., Davis, M.J., Zawieja, D.C., and Muthuchamy, M. (2014). PKC activation increases Ca^{2+} sensitivity of permeabilized lymphatic muscle via myosin light chain 20 phosphorylation-dependent and -independent mechanisms. Am. J. Physiol. Heart Circ. Physiol. *306*, H674-683.

79. Emerick, M.C., Stein, R., Kunze, R., McNulty, M.M., Regan, M.R., Hanck, D.A., and Agnew, W.S. (2006). Profiling the array of Ca(v)3.1 variants from the human T-type calcium channel gene CACNA1G: alternative structures, developmental expression, and biophysical variations. Proteins *64*, 320–342.

80. Engeset, A., Olszewski, W., Jaeger, P.M., Sokolowski, J., and Theodorsen, L. (1977). Twenty-four hour variation in flow and composition of leg lymph in normal men. Acta Physiol. Scand. *99*, 140–148.

81. Escobedo, N., Proulx, S.T., Karaman, S., Dillard, M.E., Johnson, N., Detmar, M., and Oliver, G. (2016). Restoration of lymphatic function rescues obesity in Prox1-haploinsufficient mice. JCI Insight *1*.

82. Essin, K., Welling, A., Hofmann, F., Luft, F.C., Gollasch, M., and Moosmang, S. (2007). Indirect coupling between Cav1.2 channels and ryanodine receptors to generate Ca2+ sparks in murine arterial smooth muscle cells. J. Physiol. (Lond.) *584*, 205–219.

83. Fedulova, S.A., Kostyuk, P.G., and Veselovsky, N.S. (1985). Two types of calcium channels in the somatic membrane of new-born rat dorsal root ganglion neurones. J. Physiol. (Lond.) *359*, 431–446.

84. Fernández, J.A., McGahon, M.K., McGeown, J.G., and Curtis, T.M. (2015). CaV3.1 T-Type Ca2+ Channels Contribute to Myogenic Signaling in Rat Retinal Arterioles. Invest. Ophthalmol. Vis. Sci. *56*, 5125–5132.

85. Figueroa, X.F., Chen, C.-C., Campbell, K.P., Damon, D.N., Day, K.H., Ramos, S., and Duling, B.R. (2007). Are voltage-dependent ion channels involved in the endothelial cell control of vasomotor tone? Am. J. Physiol. Heart Circ. Physiol. *293*, H1371-1383.

86. François, A., Schüetter, N., Laffray, S., Sanguesa, J., Pizzoccaro, A., Dubel, S., Mantilleri, A., Nargeot, J., Noël, J., Wood, J.N., et al. (2015). The Low-Threshold Calcium Channel Cav3.2 Determines Low-Threshold Mechanoreceptor Function. Cell Reports *10*, 370–382.

87. François, M., Caprini, A., Hosking, B., Orsenigo, F., Wilhelm, D., Browne, C., Paavonen, K., Karnezis, T., Shayan, R., Downes, M., et al. (2008). Sox18 induces development of the lymphatic vasculature in mice. Nature *456*, 643–647.

88. Fuentes, I.M., and Christianson, J.A. (2016). Ion channels, ion channel receptors, and visceral hypersensitivity in irritable bowel syndrome. Neurogastroenterol Motil *28*, 1613–1618.

89. Gardenier, J.C., Torrisi, J.S., Savetsky, I.L., Nores, G.D.G., Jowhar, D.K., Hespe, G.E., Nitti, M.D., Kataru, R.P., and Mehrara, B.J. (2015). Topical Tacrolimus for the Treatment of Lymphedema. Journal of the American College of Surgeons *221*, S120.

90. Gashev, A.A., Davis, M.J., and Zawieja, D.C. (2002). Inhibition of the active lymph pump by flow in rat mesenteric lymphatics and thoracic duct. J. Physiol. (Lond.) *540*, 1023–1037.

91. Gashev, A.A., Davis, M.J., Delp, M.D., and Zawieja, D.C. (2004). Regional variations of contractile activity in isolated rat lymphatics. Microcirculation *11*, 477–492.

92. Gashev, A.A., Davis, M.J., Gasheva, O.Y., Nepiushchikh, Z.V., Wang, W., Dougherty, P., Kelly, K.A., Cai, S., Von Der Weid, P.-Y., Muthuchamy, M., et al. (2009). Methods for lymphatic vessel culture and gene transfection. Microcirculation *16*, 615–628.

93. Gashev, A.A., Nagai, T., and Bridenbaugh, E.A. (2010). Indocyanine Green and Lymphatic Imaging: Current Problems. Lymphat Res Biol *8*, 127–130.

94. Gasheva, O.Y., Gashev, A.A., and Zawieja, D.C. (2013). Cyclic guanosine monophosphate and the dependent protein kinase regulate lymphatic contractility in rat thoracic duct. J. Physiol. (Lond.) *591*, 4549–4565.

95. Gaw, R., Box, R., and Cornish, B. (2011). Bioimpedance in the assessment of unilateral lymphedema of a limb: the optimal frequency. Lymphat Res Biol *9*, 93–99.

96. Gibbons, S.J., Strege, P.R., Lei, S., Roeder, J.L., Mazzone, A., Ou, Y., Rich, A., and Farrugia, G. (2009). The alpha1H Ca2+ channel subunit is expressed in mouse jejunal interstitial cells of Cajal and myocytes. J. Cell. Mol. Med. *13*, 4422–4431.

97. Goonasekera, S.A., Hammer, K., Auger-Messier, M., Bodi, I., Chen, X., Zhang, H., Reiken, S., Elrod, J.W., Correll, R.N., York, A.J., et al. (2012). Decreased cardiac L-type Ca^{2+} channel activity induces hypertrophy and heart failure in mice. J. Clin. Invest. *122*, 280–290.

98. Grange, D.K., Nichols, C.G., and Singh, G.K. (2014). Cantú Syndrome and Related Disorders (University of Washington, Seattle).

99. Grillet, B., and Dequeker, J. (1987). Rheumatoid lymphedema. J. Rheumatol. *14*, 1095–1097.

100. Guermazi, A., Brice, P., Hennequin, C., and Sarfati, E. (2003a). Lymphography: An Old Technique Retains Its Usefulness. RadioGraphics *23*, 1541–1558.

101. Gui, P., Li, M., Hill, M., and Davis, M. (2014). KCNQ and ERG channels control the rate of diastolic depolarization and electrical pacemaking frequency in lymphatic muscle (666.3). FASEB J *28*, 666.3.

102. Gui, P., Scallan, J.P., Zawieja, S., Rock, J., and Davis, M.J. (2015). Electrical pacemaking in lymphatics.

103. Gutterman, D.D., Chabowski, D.S., Kadlec, A.O., Durand, M.J., Freed, J.K., Ait-Aissa, K., and Beyer, A.M. (2016). The Human Microcirculation Regulation of Flow and Beyond. Circ Res *118*, 157–172.

104. Haddock, R.E., and Hill, C.E. (2005). Rhythmicity in arterial smooth muscle. The Journal of Physiology *566*, 645–656.

105. Hagendoorn, J., Padera, T.P., Kashiwagi, S., Isaka, N., Noda, F., Lin, M.I., Huang, P.L., Sessa, W.C., Fukumura, D., and Jain, R.K. (2004). Endothelial nitric oxide synthase regulates microlymphatic flow via collecting lymphatics. Circ. Res. *95*, 204–209.

106. Hagiwara, N., Irisawa, H., and Kameyama, M. (1988). Contribution of two types of calcium currents to the pacemaker potentials of rabbit sino-atrial node cells. J. Physiol. (Lond.) *395*, 233–253.

107. Hall, J.E., and Guyton, A.C. (2015). Guyton and Hall Textbook of Medical Physiology (Elsevier Health Sciences).

108. Hansen, P.B.L. (2013). Functional and pharmacological consequences of the distribution of voltage-gated calcium channels in the renal blood vessels. Acta Physiol (Oxf) *207*, 690–699.

109. Harland, M.M., Fedele, C., and Berens v Rautenfeld, D. (2004). The presence of myofibroblasts, smooth muscle cells and elastic fibers in the lymphatic collectors of horses. Lymphology *37*, 190–198.

110. Harraz, O.F., and Welsh, D.G. (2013). Protein kinase A regulation of T-type Ca2+ channels in rat cerebral arterial smooth muscle. J Cell Sci *126*, 2944–2954.

111. Harraz, O.F., Visser, F., Brett, S.E., Goldman, D., Zechariah, A., Hashad, A.M., Menon, B.K., Watson, T., Starreveld, Y., and Welsh, D.G. (2015a). CaV1.2/CaV3.x channels mediate divergent vasomotor responses in human cerebral arteries. J. Gen. Physiol. *145*, 405–418.

112. Harraz, O.F., Brett, S.E., Zechariah, A., Romero, M., Puglisi, J.L., Wilson, S.M., and Welsh, D.G. (2015b). Genetic ablation of CaV3.2 channels enhances the arterial myogenic response by modulating the RyR-BKCa axis. Arterioscler. Thromb. Vasc. Biol. *35*, 1843–1851.

113. Harrell, M.I., Iritani, B.M., and Ruddell, A. (2008). Lymph Node Mapping in the Mouse. J Immunol Methods *332*, 170–174.

114. Heck, M.M., Souvatzoglou, M., Retz, M., Nawroth, R., Kübler, H., Maurer, T., Thalgott, M., Gramer, B.M., Weirich, G., Rondak, I.-C., et al. (2014). Prospective comparison of computed tomography, diffusion-weighted magnetic resonance imaging and [11C] choline positron emission tomography/computed tomography for preoperative lymph node staging in prostate cancer patients. European Journal of Nuclear Medicine and Molecular Imaging *41*, 694–701.

115. Hespe, G.E., Kataru, R.P., Savetsky, I.L., García Nores, G.D., Torrisi, J.S., Nitti, M.D., Gardenier, J.C., Zhou, J., Yu, J.Z., Jones, L.W., et al. (2016). Exercise training improves obesity-related lymphatic dysfunction. J. Physiol. (Lond.) *594*, 4267–4282.

116. Hill, M.A., Zou, H., Potocnik, S.J., Meininger, G.A., and Davis, M.J. (2001). Invited Review: Arteriolar smooth muscle mechanotransduction: Ca2+ signaling pathways underlying myogenic reactivity. Journal of Applied Physiology *91*, 973–983.

117. Hill-Eubanks, D.C., Werner, M.E., Heppner, T.J., and Nelson, M.T. (2011). Calcium Signaling in Smooth Muscle. Cold Spring Harb Perspect Biol *3*, a004549.

118. Hirano, Y., Fozzard, H.A., and January, C.T. (1989). Characteristics of L- and T-type Ca2+ currents in canine cardiac Purkinje cells. Am. J. Physiol. *256*, H1478-1492.

119. Hofmann, F., Flockerzi, V., Kahl, S., and Wegener, J.W. (2014). L-Type CaV1.2 Calcium Channels: From In Vitro Findings to In Vivo Function. Physiological Reviews *94*, 303–326.

120. Hogan, R.D., and Unthank, J.L. (1986). Mechanical control of initial lymphatic contractile behavior in bat's wing. Am. J. Physiol. *251*, H357-363.

121. Hollywood, M.A., Cotton, K.D., Thornbury, K.D., and McHale, N.G. (1997a). Isolated sheep mesenteric lymphatic smooth muscle cells possess both T- and L-type calcium currents. Journal of Physiology *501P*, 109–110.

122. Hollywood, M.A., Cotton, K.D., Thornbury, K.D., and McHale, N.G. (1997b). Tetrodotoxin-Sensitive Sodium Current in Sheep Lymphatic Smooth Muscle. The Journal of Physiology *503*, 13–20.

123. Imtiaz, M.S. (2012). Calcium oscillations and pacemaking. Adv. Exp. Med. Biol. *740*, 511–520.

124. Imtiaz, M.S., Zhao, J., Hosaka, K., von der Weid, P.-Y., Crowe, M., and van Helden, D.F. (2007). Pacemaking through Ca2+ stores interacting as coupled oscillators via membrane depolarization. Biophys. J. *92*, 3843–3861.

125. Imtiaz, M.S., von der Weid, P.-Y., and van Helden, D.F. (2010). Synchronization of Ca2+ oscillations: a coupled oscillator-based mechanism in smooth muscle. FEBS J. *277*, 278–285.

126. Jaggar, J.H., Wellman, G.C., Heppner, T.J., Porter, V.A., Perez, G.J., Gollasch, M., Kleppisch, T., Rubart, M., Stevenson, A.S., Lederer, W.J., et al. (1998). Ca2+ channels, ryanodine receptors and Ca(2+)-activated K+ channels: a functional unit for regulating arterial tone. Acta Physiol. Scand. *164*, 577–587.

127. Jensen, L.J., and Holstein-Rathlou, N.-H. (2009). Is there a role for T-type Ca2+ channels in regulation of vasomotor tone in mesenteric arterioles? Can. J. Physiol. Pharmacol. *87*, 8–20.

128. Jin, D.P., An, A., Liu, J., Nakamura, K., and Rockson, S.G. (2009). Therapeutic responses to exogenous VEGF-C administration in experimental lymphedema: immunohistochemical and molecular characterization. Lymphat Res Biol *7*, 47–57.

129. Johnston, M.G., and Gordon, J.L. (1981). Regulation of lymphatic contractility by arachidonate metabolites. Nature *293*, 294–297.

130. Jung, S., Jeong, Y., and Jeon, D. (2015). Epileptic activity during early postnatal life in the AY-9944 model of atypical absence epilepsy. Cell Calcium *57*, 376–384.

131. Jurkat-Rott, K., and Lehmann-Horn, F. (2004). The impact of splice isoforms on voltage-gated calcium channel α1 subunits. J Physiol *554*, 609–619.

132. Kakei, Y., Akashi, M., Shigeta, T., Hasegawa, T., and Komori, T. (2014). Alteration of Cell–Cell Junctions in Cultured Human Lymphatic Endothelial Cells with Inflammatory Cytokine Stimulation. Lymphat Res Biol *12*, 136–143.

133. Kang, H.-W., Park, J.-Y., Jeong, S.-W., Kim, J.-A., Moon, H.-J., Perez-Reyes, E., and Lee, J.-H. (2006). A Molecular Determinant of Nickel Inhibition in Cav3.2 T-type Calcium Channels. J. Biol. Chem. *281*, 4823–4830.

134. Karkkainen, M.J., Ferrell, R.E., Lawrence, E.C., Kimak, M.A., Levinson, K.L., McTigue, M.A., Alitalo, K., and Finegold, D.N. (2000). Missense mutations interfere with VEGFR-3 signalling in primary lymphoedema. Nat. Genet. *25*, 153–159.

135. Karkkainen, M.J., Haiko, P., Sainio, K., Partanen, J., Taipale, J., Petrova, T.V., Jeltsch, M., Jackson, D.G., Talikka, M., Rauvala, H., et al. (2004). Vascular endothelial growth factor C is required for sprouting of the first lymphatic vessels from embryonic veins. Nat. Immunol. *5*, 74–80.

136. Kasuya, A., Sakabe, J., and Tokura, Y. (2014). Potential application of in vivo imaging of impaired lymphatic duct to evaluate the severity of pressure ulcer in mouse model. Scientific Reports *4*.

137. Kepplinger, K.J.F., and Romanin, C. (2005). The Run-Down Phenomenon of Ca2+ Channels. In Voltage-Gated Calcium Channels, (Boston, MA: Springer US), pp. 219–230.

138. Kim, D., Song, I., Keum, S., Lee, T., Jeong, M.-J., Kim, S.-S., McEnery, M.W., and Shin, H.-S. (2001). Lack of the Burst Firing of Thalamocortical Relay Neurons and Resistance to Absence Seizures in Mice Lacking α1G T-Type Ca2+ Channels. Neuron *31*, 35–45.

139. Kito, Y., Sanders, K.M., Ward, S.M., and Suzuki, H. (2009). Interstitial cells of Cajal generate spontaneous transient depolarizations in the rat gastric fundus. Am J Physiol Gastrointest Liver Physiol *297*, G814–G824.

140. Kriederman, B.M., Myloyde, T.L., Witte, M.H., Dagenais, S.L., Witte, C.L., Rennels, M., Bernas, M.J., Lynch, M.T., Erickson, R.P., Caulder, M.S., et al. (2003). FOXC2 haploinsufficient mice are a model for human autosomal dominant lymphedema-distichiasis syndrome. Hum. Mol. Genet. *12*, 1179–1185.

141. Kuan, E.L., Ivanov, S., Bridenbaugh, E.A., Victora, G., Wang, W., Childs, E.W., Platt, A.M., Jakubzick, C.V., Mason, R.J., Gashev, A.A., et al. (2015). Collecting lymphatic vessel permeability facilitates adipose tissue inflammation and distribution of antigen to lymph node-homing adipose tissue DCs. J Immunol *194*, 5200–5210.

142. Kuo, I.Y.-T., Wölfle, S.E., and Hill, C.E. (2011). T-type calcium channels and vascular function: the new kid on the block? J Physiol *589*, 783–795.

143. Kuo, I.Y.-T., Howitt, L., Sandow, S.L., McFarlane, A., Hansen, P.B., and Hill, C.E. (2014). Role of T-type channels in vasomotor function: team player or chameleon? Pflugers Arch. *466*, 767–779.

144. Kuo, L., Davis, M.J., and Chilian, W.M. (1990). Endothelium-dependent, flow-induced dilation of isolated coronary arterioles. Am. J. Physiol. *259*, H1063-1070.

145. Kurtz, K.H., Souza-Smith, F.M., Moor, A.N., and Breslin, J.W. (2014). Rho kinase enhances contractions of rat mesenteric collecting lymphatics. PLoS ONE *9*, e94082.

146. Lacinová, L'ubica (2011). T-type calcium channel blockers - new and notable. Gen. Physiol. Biophys. *30*, 403–409.

147. Lakatta, E.G., and DiFrancesco, D. (2009). JMCC Point-Counterpoint. J Mol Cell Cardiol *47*, 157–170.

148. Lapinski, P.E., Kwon, S., Lubeck, B.A., Wilkinson, J.E., Srinivasan, R.S., Sevick-Muraca, E., and King, P.D. (2012). RASA1 maintains the lymphatic vasculature in a quiescent functional state in mice. J Clin Invest *122*, 733–747.

149. Larralde, M., Abad, M.E., Luna, P.C., and Hoffner, M.V. (2014). Capillary malformation-arteriovenous malformation: a clinical review of 45 patients. Int. J. Dermatol. *53*, 458–461.

150. Leak, L.V., and Burke, J.F. (1968). Ultrastructural studies on the lymphatic anchoring filaments. J. Cell Biol. *36*, 129–149.

151. Lee, B.-B., Bergan, J., and Rockson, S.G. (2011). Lymphedema: A Concise Compendium of Theory and Practice (Springer Science & Business Media).

152. Lee, J., Kim, D., and Shin, H.-S. (2004). Lack of delta waves and sleep disturbances during non-rapid eye movement sleep in mice lacking α1G-subunit of T-type calcium channels. Proc Natl Acad Sci U S A *101*, 18195–18199.

153. Lee, J.H., Gomora, J.C., Cribbs, L.L., and Perez-Reyes, E. (1999). Nickel block of three cloned T-type calcium channels: low concentrations selectively block alpha1H. Biophys. J. *77*, 3034–3042.

154. Lee, S., Roizes, S., and von der Weid, P.-Y. (2014a). Distinct roles of L- and T-type voltage-dependent Ca2+ channels in regulation of lymphatic vessel contractile activity. J Physiol *592*, 5409–5427.

155. Lee, S.E., Lee, J., Latchoumane, C., Lee, B., Oh, S.-J., Saud, Z.A., Park, C., Sun, N., Cheong, E., Chen, C.-C., et al. (2014b). Rebound burst firing in the reticular thalamus is not essential for pharmacological absence seizures in mice. Proc. Natl. Acad. Sci. U.S.A. *111*, 11828–11833.

156. Lee, T.-S., Kaku, T., Takebayashi, S., Uchino, T., Miyamoto, S., Hadama, T., Perez-Reyes, E., and Ono, K. (2006). Actions of mibefradil, efonidipine and nifedipine block of recombinant T- and L-type Ca channels with distinct inhibitory mechanisms. Pharmacology *78*, 11–20.

157. Levick, J.R., and Michel, C.C. (2010). Microvascular fluid exchange and the revised Starling principle. Cardiovascular Research *87*, 198–210.

158. Li, Y., Wang, F., Zhang, X., Qi, Z., Tang, M., Szeto, C., Li, Y., Zhang, H., and Chen, X. (2012). β-Adrenergic Stimulation Increases Cav3.1 Activity in Cardiac Myocytes through Protein Kinase A. PLOS ONE *7*, e39965.

159. Liang, Q., Ju, Y., Chen, Y., Wang, W., Li, J., Zhang, L., Xu, H., Wood, R.W., Schwarz, E.M., Boyce, B.F., et al. (2016). Lymphatic endothelial cells efferent to inflamed joints produce iNOS and inhibit lymphatic vessel contraction and drainage in TNF-induced arthritis in mice. Arthritis Research & Therapy *18*, 62.

160. Liao, P., and Soong, T.W. (2010). Understanding alternative splicing of Cav1.2 calcium channels for a new approach towards individualized medicine. J Biomed Res *24*, 181–186.

161. Liao, P., Yong, T.F., Liang, M.C., Yue, D.T., and Soong, T.W. (2005). Splicing for alternative structures of Cav1.2 Ca2+ channels in cardiac and smooth muscles. Cardiovascular Research *68*, 197–203.

162. Lim, H.Y., Rutkowski, J.M., Helft, J., Reddy, S.T., Swartz, M.A., Randolph, G.J., and Angeli, V. (2009). Hypercholesterolemic mice exhibit lymphatic vessel dysfunction and degeneration. Am. J. Pathol. *175*, 1328–1337.

163. Lim, H.Y., Thiam, C.H., Yeo, K.P., Bisoendial, R., Hii, C.S., McGrath, K.C.Y., Tan, K.W., Heather, A., Alexander, J.S.J., and Angeli, V. (2013). Lymphatic vessels are essential for the removal of cholesterol from peripheral tissues by SR-BI-mediated transport of HDL. Cell Metab. *17*, 671–684.

164. Lin, S., Kim, J., Lee, M.-J., Roche, L., Yang, N.L., Tsao, P.S., and Rockson, S.G. (2012). Prospective transcriptomic pathway analysis of human lymphatic vascular insufficiency: identification and validation of a circulating biomarker panel. PLoS ONE *7*, e52021.

165. Lin, S.-S., Tzeng, B.-H., Lee, K.-R., Smith, R.J.H., Campbell, K.P., and Chen, C.-C. (2014). Cav3.2 T-type calcium channel is required for the NFAT-dependent Sox9 expression in tracheal cartilage. Proc. Natl. Acad. Sci. U.S.A. *111*, E1990-1998.

166. Liu, J.-H., Bijlenga, P., Occhiodoro, T., Fischer-Lougheed, J., Bader, C.R., and Bernheim, L. (1999). Mibefradil (Ro 40-5967) inhibits several Ca2+ and K+ currents in human fusion-competent myoblasts. British Journal of Pharmacology *126*, 245–250.

167. Liu, Q.-H., Zheng, Y.-M., Korde, A.S., Yadav, V.R., Rathore, R., Wess, J., and Wang, Y.-X. (2009). Membrane depolarization causes a direct activation of G protein-coupled receptors leading to local Ca2+ release in smooth muscle. Proc Natl Acad Sci U S A *106*, 11418–11423.

168. Loirand, G., Mironneau, C., Mironneau, J., and Pacaud, P. (1989). Two types of calcium currents in single smooth muscle cells from rat portal vein. J. Physiol. (Lond.) *412*, 333–349.

169. Longden, T.A., Hill-Eubanks, D.C., and Nelson, M.T. (2015). Ion channel networks in the control of cerebral blood flow. J Cereb Blood Flow Metab 0271678X15616138.

170. Louveau, A., Smirnov, I., Keyes, T.J., Eccles, J.D., Rouhani, S.J., Peske, J.D., Derecki, N.C., Castle, D., Mandell, J.W., Lee, K.S., et al. (2015). Structural and functional features of central nervous system lymphatic vessels. Nature *523*, 337–341.

171. Machnik, A., Neuhofer, W., Jantsch, J., Dahlmann, A., Tammela, T., Machura, K., Park, J.-K., Beck, F.-X., Müller, D.N., Derer, W., et al. (2009). Macrophages regulate salt-dependent volume and blood pressure by a vascular endothelial growth factor-C-dependent buffering mechanism. Nat. Med. *15*, 545–552.

172. Maddala, R., Nagendran, T., de Ridder, G.G., Schey, K.L., and Rao, P.V. (2013). L-Type Calcium Channels Play a Critical Role in Maintaining Lens Transparency by Regulating Phosphorylation of Aquaporin-0 and Myosin Light Chain and Expression of Connexins. PLoS One *8*.

173. Mäkinen, T., Jussila, L., Veikkola, T., Karpanen, T., Kettunen, M.I., Pulkkanen, K.J., Kauppinen, R., Jackson, D.G., Kubo, H., Nishikawa, S.-I., et al. (2001). Inhibition of lymphangiogenesis with resulting lymphedema in transgenic mice expressing soluble VEGF receptor-3. Nat Med *7*, 199–205.

174. Maltsev, V.A., and Lakatta, E.G. (2008). Dynamic interactions of an intracellular Ca2+ clock and membrane ion channel clock underlie robust initiation and regulation of cardiac pacemaker function. Cardiovasc. Res. *77*, 274–284.

175. Mangoni, M.E., and Nargeot, J. (2008). Genesis and regulation of the heart automaticity. Physiol. Rev. *88*, 919–982.

176. Mangoni, M.E., Traboulsie, A., Leoni, A.-L., Couette, B., Marger, L., Le Quang, K., Kupfer, E., Cohen-Solal, A., Vilar, J., Shin, H.-S., et al. (2006). Bradycardia and slowing of the atrioventricular conduction in mice lacking CaV3.1/alpha1G T-type calcium channels. Circ. Res. *98*, 1422–1430.

177. McCloskey, K.D., Toland, H.M., Hollywood, M.A., Thornbury, K.D., and McHale, N.G. (1999). Hyperpolarisation-activated inward current in isolated sheep mesenteric lymphatic smooth muscle. J. Physiol. (Lond.) *521 Pt 1*, 201–211.

178. McCloskey, K.D., Hollywood, M.A., Thornbury, K.D., Ward, S.M., and McHale, N.G. (2002). Kit-like immunopositive cells in sheep mesenteric lymphatic vessels. Cell Tissue Res. *310*, 77–84.

179. McDonald, D.M., Yao, L.-C., and Baluk, P. (2011). Dynamics of Airway Blood Vessels and Lymphatics. Proc Am Thorac Soc *8*, 504–507.

180. McHale, N.G. (1990). Lymphatic innervation. Blood Vessels *27*, 127–136.

181. McHale, N., Hollywood, M., Sergeant, G., and Thornbury, K. (2006). Origin of spontaneous rhythmicity in smooth muscle. J Physiol *570*, 23–28.

182. McNulty, M.M., and Hanck, D.A. (2004). State-Dependent Mibefradil Block of Na+ Channels. Mol Pharmacol *66*, 1652–1661.

183. Meinertz, T. (2001). Mibefradil — a drug which may enhance the propensity for the development of abnormal QT prolongation. European Heart Journal Supplements *3*, K89–K92.

184. Meininger, G.A., and Davis, M.J. (1992). Cellular mechanisms involved in the vascular myogenic response. American Journal of Physiology - Heart and Circulatory Physiology *263*, H647–H659.

185. Mesirca, P., Torrente, A.G., and Mangoni, M.E. (2014). T-type channels in the sino-atrial and atrioventricular pacemaker mechanism. Pflugers Arch. *466*, 791–799.

186. Mesirca, P., Torrente, A.G., and Mangoni, M.E. (2015). Functional role of voltage gated Ca(2+) channels in heart automaticity. Front Physiol *6*, 19.

187. Mikkelsen, M.F., Björling, K., and Jensen, L.J. (2016). Age-dependent impact of CaV 3.2 T-type calcium channel deletion on myogenic tone and flow-mediated vasodilatation in small arteries. J. Physiol. (Lond.) *594*, 5881–5898.

188. Miyamoto, S., Izumi, M., Hori, M., Kobayashi, M., Ozaki, H., and Karaki, H. (2000). Xestospongin C, a selective and membrane-permeable inhibitor of IP3 receptor, attenuates the positive inotropic effect of α-adrenergic stimulation in guinea-pig papillary muscle. Br J Pharmacol *130*, 650–654.

189. Mizuno, R., Ono, N., and Ohhashi, T. (1999). Involvement of ATP-sensitive K+ channels in spontaneous activity of isolated lymph microvessels in rats. American Journal of Physiology - Heart and Circulatory Physiology *277*, H1453–H1456.

190. Modi, S., Stanton, A.W.B., Svensson, W.E., Peters, A.M., Mortimer, P.S., and Levick, J.R. (2007). Human lymphatic pumping measured in healthy and lymphoedematous arms by lymphatic congestion lymphoscintigraphy. J Physiol *583*, 271–285.

191. Monk, B.E., and Mortimer, P.S. (1999). Lymphoedema and Crohn's disease. J R Soc Med *92*, 136–137.

192. Monteil, A., Chemin, J., Bourinet, E., Mennessier, G., Lory, P., and Nargeot, J. (2000). Molecular and functional properties of the human alpha(1G) subunit that forms T-type calcium channels. J. Biol. Chem. *275*, 6090–6100.

193. Moosmang, S., Schulla, V., Welling, A., Feil, R., Feil, S., Wegener, J.W., Hofmann, F., and Klugbauer, N. (2003). Dominant role of smooth muscle L-type calcium channel Cav1.2 for blood pressure regulation. EMBO J *22*, 6027–6034.

194. Moosmang, S., Haider, N., Brüderl, B., Welling, A., and Hofmann, F. (2006). Antihypertensive effects of the putative T-type calcium channel antagonist mibefradil are mediated by the L-type calcium channel Cav1.2. Circ. Res. *98*, 105–110.

195. Morel, N., Buryi, V., Feron, O., Gomez, J.-P., Christen, M.-O., and Godfraind, T. (1998). The action of calcium channel blockers on recombinant L-type calcium channel α1-subunits. Br J Pharmacol *125*, 1005–1012.

196. Morrell, R.M., Halyard, M.Y., Schild, S.E., Ali, M.S., Gunderson, L.L., and Pockaj, B.A. (2005). Breast cancer-related lymphedema. Mayo Clin. Proc. *80*, 1480–1484.

197. Mortimer, P.S., and Rockson, S.G. (2014). New developments in clinical aspects of lymphatic disease. J. Clin. Invest. *124*, 915–921.

198. Munn, L.L., and Padera, T.P. (2014). Imaging the lymphatic system. Microvascular Research *96*, 55–63.

199. Muth, J.N., Varadi, G., and Schwartz, A. (2001). Use of transgenic mice to study voltage-dependent Ca2+ channels. Trends Pharmacol. Sci. *22*, 526–532.

200. Muthuchamy, M., and Zawieja, D. (2008). Molecular regulation of lymphatic contractility. Ann. N. Y. Acad. Sci. *1131*, 89–99.

201. Muthuchamy, M., Gashev, A., Boswell, N., Dawson, N., and Zawieja, D. (2003). Molecular and functional analyses of the contractile apparatus in lymphatic muscle. FASEB J. *17*, 920–922.

202. Nakayama, H., Bodi, I., Correll, R.N., Chen, X., Lorenz, J., Houser, S.R., Robbins, J., Schwartz, A., and Molkentin, J.D. (2009). α1G-dependent T-type Ca2+ current antagonizes cardiac hypertrophy through a NOS3-dependent mechanism in mice. J Clin Invest *119*, 3787–3796.

203. Negrini, D., Marcozzi, C., Solari, E., Bossi, E., Cinquetti, R., Reguzzoni, M., and Moriondo, A. (2016). Hyperpolarization-Activated Cyclic Nucleotide-Gated (hcn) Channels in Peripheral Diaphragmatic Lymphatics. American Journal of Physiology - Heart and Circulatory Physiology ajpheart.00193.2016.

204. Nepiyushchikh, Z.V., Chakraborty, S., Wang, W., Davis, M.J., Zawieja, D.C., and Muthuchamy, M. (2011). Differential effects of myosin light chain kinase inhibition on contractility, force development and myosin light chain 20 phosphorylation of rat cervical and thoracic duct lymphatics. J. Physiol. (Lond.) *589*, 5415–5429.

205. Nichols, C.G., Singh, G.K., and Grange, D.K. (2013). KATP channels and cardiovascular disease: Suddenly a syndrome. Circ Res *112*, 1059–1072.

206. Nowycky, M.C., Fox, A.P., and Tsien, R.W. (1985). Three types of neuronal calcium channel with different calcium agonist sensitivity. Nature *316*, 440–443.

207. Obejero-Paz, C.A., Gray, I.P., and Jones, S.W. (2008). Ni2+ Block of CaV3.1 (α1G) T-type Calcium Channels. J Gen Physiol *132*, 239–250.

208. Ohhashi, T., Azuma, T., and Sakaguchi, M. (1980). Active and passive mechanical characteristics of bovine mesenteric lymphatics. Am. J. Physiol. *239*, H88-95.

209. Olszewski, W.L. (2002). Contractility patterns of normal and pathologically changed human lymphatics. Ann. N. Y. Acad. Sci. *979*, 52-63-79.

210. Olszewski, W.L. (2003). The lymphatic system in body homeostasis: physiological conditions. Lymphat Res Biol *1*, 11-21-24.

211. Olszewski, W.L. (2011). Physiological Principles of Physiotherapy. In Lymphedema, B.-B. Lee, J. Bergan, and S.G. Rockson, eds. (Springer London), pp. 219–227.

212. Olszewski, W.L. (2012). The "Third" circulation in human limbs-tissue fluid, lymph and lymphatics. ResearchGate *41*, 297–303.

213. Paskett, E.D., Naughton, M.J., McCoy, T.P., Case, L.D., and Abbott, J.M. (2007). The epidemiology of arm and hand swelling in premenopausal breast cancer survivors. Cancer Epidemiol. Biomarkers Prev. *16*, 775–782.

214. Pendse, A.A., Arbones-Mainar, J.M., Johnson, L.A., Altenburg, M.K., and Maeda, N. (2009). Apolipoprotein E knock-out and knock-in mice: atherosclerosis, metabolic syndrome, and beyond. J Lipid Res *50*, S178–S182.

215. Perchenet, L., and Clément-Chomienne, O. (2001). External nickel blocks human Kv1.5 channels stably expressed in CHO cells. J. Membr. Biol. *183*, 51–60.

216. Pereira de Godoy, J.M., Azoubel, L.M.O., and de Fátima Guerreiro de Godoy, M. (2010). INTENSIVE TREATMENT OF LEG LYMPHEDEMA. Indian J Dermatol *55*, 144–147.

217. Perez-Reyes, E. (2003). Molecular physiology of low-voltage-activated t-type calcium channels. Physiol. Rev. *83*, 117–161.

218. Petrova, T.V., Karpanen, T., Norrmén, C., Mellor, R., Tamakoshi, T., Finegold, D., Ferrell, R., Kerjaschki, D., Mortimer, P., Ylä-Herttuala, S., et al. (2004). Defective valves and abnormal mural cell recruitment underlie lymphatic vascular failure in lymphedema distichiasis. Nat. Med. *10*, 974–981.

219. Piriz, J., Siri, M.D.R., Pagani, R., and Uchitel, O.D. (2003). Nifedipine-Mediated Mobilization of Intracellular Calcium Stores Increases Spontaneous Neurotransmitter Release at Neonatal Rat Motor Nerve Terminals. J Pharmacol Exp Ther *306*, 658–663.

220. Plumley, C., Gorman, E.M., Munson, E.J., and Berkland, C. (2009). Nifedipine Nanoparticle Agglomeration as a Dry Powder Aerosol Formulation Strategy. Int J Pharm *369*, 136–143.

221. Pluteanu, F., and Cribbs, L.L. (2009). T-type calcium channels are regulated by hypoxia/reoxygenation in ventricular myocytes. Am. J. Physiol. Heart Circ. Physiol. *297*, H1304-1313.

222. Podesser, B.K., and Chambers, D.J. (2010). New Solutions for the Heart: An Update in Advanced Perioperative Protection (Springer Science & Business Media).

223. Porter, C.J.H., Trevaskis, N.L., and Charman, W.N. (2007). Lipids and lipid-based formulations: optimizing the oral delivery of lipophilic drugs. Nat Rev Drug Discov *6*, 231–248.

224. Quirke, M., Ayoub, F., McCabe, A., Boland, F., Smith, B., O'Sullivan, R., and Wakai, A. (2016). Risk factors for non-purulent leg cellulitis: a systematic review and meta-analysis. Br. J. Dermatol.

225. Randolph, G.J., and Miller, N.E. (2014). Lymphatic transport of high-density lipoproteins and chylomicrons. J Clin Invest *124*, 929–935.

226. Rasmussen, J.C., Aldrich, M.B., Tan, I.-C., Darne, C., Zhu, B., O'Donnell, T.F., Fife, C.E., and Sevick-Muraca, E.M. (2016). Lymphatic transport in patients with chronic venous insufficiency and venous leg ulcers following sequential pneumatic compression. J Vasc Surg Venous Lymphat Disord *4*, 9–17.

227. Renkin, E.M. (1986). Some consequences of capillary permeability to macromolecules: Starling's hypothesis reconsidered. American Journal of Physiology - Heart and Circulatory Physiology *250*, H706–H710.

228. Rijke, A., Croft, B., Johnson, R.A., de Jongste, A.B., and Camps, J.A.J. (1990). Lymphoscintigraphy and lymphedema of the lower extremities. *31*, 990–998.

229. Rockson, S.G. (2008). Diagnosis and management of lymphatic vascular disease. J. Am. Coll. Cardiol. *52*, 799–806.

230. Rockson, S.G. (2013). The Lymphatics and the Inflammatory Response: Lessons Learned from Human Lymphedema. Lymphat Res Biol *11*, 117–120.

231. Rossi, A., Weber, E., Sacchi, G., Maestrini, D., Di Cintio, F., and Gerli, R. (2007). Mechanotransduction in lymphatic endothelial cells. Lymphology *40*, 102–113.

232. Rouhani, S.J., Eccles, J.D., Riccardi, P., Peske, J.D., Tewalt, E.F., Cohen, J.N., Liblau, R., Mäkinen, T., and Engelhard, V.H. (2015). Roles of lymphatic endothelial cells expressing peripheral tissue antigens in CD4 T-cell tolerance induction. Nat Commun *6*, 6771.

233. Ruddle, N.H. (2014). Lymphatic vessels and tertiary lymphoid organs. J Clin Invest *124*, 953–959.

234. Russo, E., Teijeira, A., Vaahtomeri, K., Willrodt, A.-H., Bloch, J.S., Nitschké, M., Santambrogio, L., Kerjaschki, D., Sixt, M., and Halin, C. (2016). Intralymphatic CCL21

Promotes Tissue Egress of Dendritic Cells through Afferent Lymphatic Vessels. Cell Reports *14*, 1723–1734.

235. Sabine, A., and Petrova, T.V. (2014). Interplay of mechanotransduction, FOXC2, connexins, and calcineurin signaling in lymphatic valve formation. Adv Anat Embryol Cell Biol *214*, 67–80.

236. Sabine, A., Bovay, E., Demir, C.S., Kimura, W., Jaquet, M., Agalarov, Y., Zangger, N., Scallan, J.P., Graber, W., Gulpinar, E., et al. (2015). FOXC2 and fluid shear stress stabilize postnatal lymphatic vasculature. J. Clin. Invest. *125*, 3861–3877.

237. Sabine, A., Saygili Demir, C., and Petrova, T.V. (2016). Endothelial cell responses to biomechanical forces in lymphatic vessels. Antioxid. Redox Signal.

238. Sanders, K.M., Ward, S.M., and Koh, S.D. (2014). Interstitial Cells: Regulators of Smooth Muscle Function. Physiological Reviews *94*, 859–907.

239. Sandmann, and Unger L-and T-type calcium channel blockade -the efficacy of the calcium channel antagonist mibefradil. J Clin Basic Cardiol *2*, 187–201.

240. Sather, W.A., and McCleskey, E.W. (2003). Permeation and selectivity in calcium channels. Annu. Rev. Physiol. *65*, 133–159.

241. Satoh, H. (1995). Role of T-type Ca2+ channel inhibitors in the pacemaker depolarization in rabbit sino-atrial nodal cells. Gen. Pharmacol. *26*, 581–587.

242. Scallan, J.P., and Davis, M.J. (2013a). Genetic removal of basal nitric oxide enhances contractile activity in isolated murine collecting lymphatic vessels. J Physiol *591*, 2139–2156.

243. Scallan, J.P., Wolpers, J.H., and Davis, M.J. (2013b). Constriction of isolated collecting lymphatic vessels in response to acute increases in downstream pressure. J. Physiol. (Lond.) *591*, 443–459.

244. Scallan, J., Huxley, V.H., and Korthuis, R.J. (2010). Capillary Fluid Exchange: Regulation, Functions, and Pathology (San Rafael (CA): Morgan & Claypool Life Sciences).

245. Scallan, J.P., Hill, M.A., and Davis, M.J. (2016). Lymphatic Vascular Integrity is Disrupted in a Mouse Model of Diabetes: Dual Regulation by Nitric Oxide. FASEB J *30*, 950.9-950.9.

246. Schäfer, S., Ferioli, S., Hofmann, T., Zierler, S., Gudermann, T., and Chubanov, V. (2016). Mibefradil represents a new class of benzimidazole TRPM7 channel agonists. Pflugers Arch. *468*, 623–634.

247. Schaffer, S.W., and Li, M. (2014). T-type Calcium Channels in Basic and Clinical Science (Springer).

248. Schmid-Schonbein, G.W. (1990). Microlymphatics and lymph flow. Physiological Reviews *70*, 987–1028.

249. Seisenberger, C., Specht, V., Welling, A., Platzer, J., Pfeifer, A., Kühbandner, S., Striessnig, J., Klugbauer, N., Feil, R., and Hofmann, F. (2000). Functional embryonic cardiomyocytes after disruption of the L-type alpha1C (Cav1.2) calcium channel gene in the mouse. J. Biol. Chem. *275*, 39193–39199.

250. Sergeant, G.P., Thornbury, K.D., McHale, N.G., and Hollywood, M.A. (2006). Interstitial cells of Cajal in the urethra. J Cell Mol Med *10*, 280–291.

251. Sevick-Muraca, E.M., Kwon, S., and Rasmussen, J.C. (2014). Emerging lymphatic imaging technologies for mouse and man. J. Clin. Invest. *124*, 905–914.

252. Shen, Z., Li, C., Frieler, R.A., Gerasimova, A.S., Lee, S.J., Wu, J., Wang, M.M., Lumeng, C.N., Brosius, F.C., Duan, S.Z., et al. (2012). Smooth muscle protein 22 alpha-Cre is expressed in myeloid cells in mice. Biochem Biophys Res Commun *422*, 639–642.

253. Sheng, S., Perry, C.J., and Kleyman, T.R. (2002). External nickel inhibits epithelial sodium channel by binding to histidine residues within the extracellular domains of alpha and gamma subunits and reducing channel open probability. J. Biol. Chem. *277*, 50098–50111.

254. Shirasawa, Y., and Benoit, J.N. (2003). Stretch-induced calcium sensitization of rat lymphatic smooth muscle. American Journal of Physiology - Heart and Circulatory Physiology *285*, H2573–H2577.

255. Shuba, Y.M. (2014). Models of calcium permeation through T-type channels. Pflugers Arch. *466*, 635–644.

256. SoRelle, R. (1998). Withdrawal of Posicor From Market. Circulation *98*, 831–832.

257. Souza-Smith, F.M., Kerut, E.K., Breslin, J.W., and Molina, P.E. (2015). Mechanisms of Acute Alcohol Intoxication-Induced Modulation of Cyclic Mobilization of [Ca^{2+}] in Rat Mesenteric Lymphatic Vessels. Lymphat Res Biol *13*, 93–99.

258. Stanton, A.W.B., Modi, S., Mellor, R.H., Levick, J.R., and Mortimer, P.S. (2009). Recent advances in breast cancer-related lymphedema of the arm: lymphatic pump failure and predisposing factors. Lymphat Res Biol *7*, 29–45.

259. Stockand, J., Sultan, A., Molony, D., DuBose, T., and Sansom, S. (1993). Interactions of cadmium and nickel with K channels of vascular smooth muscle. Toxicol. Appl. Pharmacol. *121*, 30–35.

260. Strege, P.R., Bernard, C.E., Ou, Y., Gibbons, S.J., and Farrugia, G. (2005). Effect of mibefradil on sodium and calcium currents. Am. J. Physiol. Gastrointest. Liver Physiol. *289*, G249-253.

261. Suy, R., Thomis, S., and Fourneau, I. (2016). The discovery of lymphatic system in the seventeenth century. Part I: the early history. Acta Chir. Belg. 1–7.

262. Svenningsen, P., Andersen, K., Thuesen, A.D., Shin, H.-S., Vanhoutte, P.M., Skøtt, O., Jensen, B.L., Hill, C., and Hansen, P.B.L. (2014). T-type Ca2+ channels facilitate NO-formation, vasodilatation and NO-mediated modulation of blood pressure. Pflugers Arch - Eur J Physiol *466*, 2205–2214.

263. Swartz, M.N. (2004). Cellulitis. New England Journal of Medicine *350*, 904–912.

264. Swartz, M.A., and Lund, A.W. (2012). Lymphatic and interstitial flow in the tumour microenvironment: linking mechanobiology with immunity. Nat. Rev. Cancer *12*, 210–219.

265. Sweet, D.T., Jiménez, J.M., Chang, J., Hess, P.R., Mericko-Ishizuka, P., Fu, J., Xia, L., Davies, P.F., and Kahn, M.L. (2015). Lymph flow regulates collecting lymphatic vessel maturation in vivo. Journal of Clinical Investigation *125*, 2995–3007.

266. Szabó, G., and Magyar, Z. (1967). Effect of increased systemic venous pressure on lymph pressure and flow. Am. J. Physiol. *212*, 1469–1474.

267. Taylor, A.E. (1990). The lymphatic edema safety factor: the role of edema dependent lymphatic factors (EDLF). Lymphology *23*, 111–123.

268. Telinius, N., Mohanakumar, S., Majgaard, J., Kim, S., Pilegaard, H., Pahle, E., Nielsen, J., de Leval, M., Aalkjaer, C., Hjortdal, V., et al. (2014a). Human lymphatic vessel contractile activity is inhibited in vitro but not in vivo by the calcium channel blocker nifedipine. J Physiol *592*, 4697–4714.

269. Telinius, N., Kim, S., Pilegaard, H., Pahle, E., Nielsen, J., Hjortdal, V., Aalkjaer, C., and Boedtkjer, D.B. (2014b). The contribution of K+ channels to human thoracic duct contractility. American Journal of Physiology - Heart and Circulatory Physiology *307*, H33–H43.

270. Telinius, N., Majgaard, J., Kim, S., Katballe, N., Pahle, E., Nielsen, J., Hjortdal, V., Aalkjaer, C., and Boedtkjer, D.B. (2015). Voltage-gated sodium channels contribute to action potentials and spontaneous contractility in isolated human lymphatic vessels. J Physiol *593*, 3109–3122.

271. Thangaswamy, S., Bridenbaugh, E.A., and Gashev, A.A. (2012). Evidence of Increased Oxidative Stress in Aged Mesenteric Lymphatic Vessels. Lymphat Res Biol *10*, 53–62.

272. Thomas-MacLean, R., Miedema, B., and Tatemichi, S.R. (2005). Breast cancer-related lymphedema. Can Fam Physician *51*, 247.

273. Toland, H.M., McCloskey, K.D., Thornbury, K.D., McHale, N.G., and Hollywood, M.A. (2000). Ca(2+)-activated Cl(-) current in sheep lymphatic smooth muscle. Am. J. Physiol., Cell Physiol. *279*, C1327-1335.

274. Trzewik, J., Mallipattu, S.K., Artmann, G.M., Delano, F.A., and Schmid-Schönbein, G.W. (2001). Evidence for a second valve system in lymphatics: endothelial microvalves. FASEB J *15*, 1711–1717.

275. Uebele, V.N., Gotter, A.L., Nuss, C.E., Kraus, R.L., Doran, S.M., Garson, S.L., Reiss, D.R., Li, Y., Barrow, J.C., Reger, T.S., et al. (2009). Antagonism of T-type calcium channels inhibits high-fat diet-induced weight gain in mice. J. Clin. Invest. *119*, 1659–1667.

276. Unno, N., Nishiyama, M., Suzuki, M., Yamamoto, N., Inuzuka, K., Sagara, D., Tanaka, H., and Konno, H. (2008). Quantitative Lymph Imaging for Assessment of Lymph Function using Indocyanine Green Fluorescence Lymphography. European Journal of Vascular and Endovascular Surgery *36*, 230–236.

277. Unthank, J.L., and Bohlen, H.G. (1988). Lymphatic pathways and role of valves in lymph propulsion from small intestine. Am. J. Physiol. *254*, G389-398.

278. Van Helden, D.F. (1993). Pacemaker potentials in lymphatic smooth muscle of the guinea-pig mesentery. J. Physiol. (Lond.) *471*, 465–479.

279. Vasioukhin, V., Degenstein, L., Wise, B., and Fuchs, E. (1999). The magical touch: Genome targeting in epidermal stem cells induced by tamoxifen application to mouse skin. Proc Natl Acad Sci U S A *96*, 8551–8556.

280. Verheijck, E.E., Ginneken, A.C.G. van, Wilders, R., and Bouman, L.N. (1999). Contribution of L-type Ca2+current to electrical activity in sinoatrial nodal myocytes of rabbits. American Journal of Physiology - Heart and Circulatory Physiology *276*, H1064–H1077.

281. Wang, W., Nepiyushchikh, Z., Zawieja, D.C., Chakraborty, S., Zawieja, S.D., Gashev, A.A., Davis, M.J., and Muthuchamy, M. (2009). Inhibition of myosin light chain phosphorylation

decreases rat mesenteric lymphatic contractile activity. Am. J. Physiol. Heart Circ. Physiol. *297*, H726-734.

282. Weid, P.-Y. von der, Cho, E.-B., Kratofil, R., and Lee, S. (2015). Involvement of TRPM4 in Stretch-Induced Modulation of Lymphatic Pumping. FASEB J *29*, 633.4.

283. von der Weid, P.-Y. (1998). ATP-sensitive K+ channels in smooth muscle cells of guinea-pig mesenteric lymphatics: role in nitric oxide and β-adrenoceptor agonist-induced hyperpolarizations. Br J Pharmacol *125*, 17–22.

284. von der Weid, P.-Y., Rahman, M., Imtiaz, M.S., and van Helden, D.F. (2008). Spontaneous transient depolarizations in lymphatic vessels of the guinea pig mesentery: pharmacology and implication for spontaneous contractility. Am. J. Physiol. Heart Circ. Physiol. *295*, H1989-2000.

285. von der Weid, P.-Y., Rehal, S., Dyrda, P., Lee, S., Mathias, R., Rahman, M., Roizes, S., and Imtiaz, M.S. (2012). Mechanisms of VIP-induced inhibition of the lymphatic vessel pump. J. Physiol. (Lond.) *590*, 2677–2691.

286. von der Weid, P.-Y., Lee, S., Imtiaz, M.S., Zawieja, D.C., and Davis, M.J. (2014). Electrophysiological Properties of Rat Mesenteric Lymphatic Vessels and their Regulation by Stretch. Lymphat Res Biol *12*, 66–75.

287. Weiss, M., Burgard, C., Baumeister, R., Strobl, F., Rominger, A., Bartenstein, P., Wallmichrath, J., Frick, A., and Notohamiprodjo, M. (2014). Magnetic resonance imaging versus lymphoscintigraphy for the assessment of focal lymphatic transport disorders of the lower limb: first experiences. Nuklearmedizin *53*, 190–196.

288. Weitman, E.S., Aschen, S.Z., Farias-Eisner, G., Albano, N., Cuzzone, D.A., Ghanta, S., Zampell, J.C., Thorek, D., and Mehrara, B.J. (2013). Obesity impairs lymphatic fluid transport and dendritic cell migration to lymph nodes. PLoS ONE *8*, e70703.

289. Wigle, J.T., and Oliver, G. (1999). Prox1 Function Is Required for the Development of the Murine Lymphatic System. Cell *98*, 769–778.

290. Wiig, H., and Swartz, M.A. (2012). Interstitial fluid and lymph formation and transport: physiological regulation and roles in inflammation and cancer. Physiol. Rev. *92*, 1005–1060.

291. Wiig, H., Schröder, A., Neuhofer, W., Jantsch, J., Kopp, C., Karlsen, T.V., Boschmann, M., Goss, J., Bry, M., Rakova, N., et al. (2013). Immune cells control skin lymphatic electrolyte homeostasis and blood pressure. J. Clin. Invest. *123*, 2803–2815.

292. Zamponi, G.W., Bourinet, E., and Snutch, T.P. (1996). Nickel block of a family of neuronal calcium channels: subtype- and subunit-dependent action at multiple sites. J. Membr. Biol. *151*, 77–90.

293. Zawieja, D.C. (1996). Lymphatic microcirculation. Microcirculation *3*, 241–243.

294. Zawieja, D.C. (2009). Contractile physiology of lymphatics. Lymphat Res Biol *7*, 87–96.

295. Zawieja, D.C., von der Weid, P.-Y., and Gashev, A.A. (2011). Microlymphatic Biology. In Comprehensive Physiology, (John Wiley & Sons, Inc.)

296. Zhang, W., and Liu, H.T. (2002). MAPK signal pathways in the regulation of cell proliferation in mammalian cells. Cell Res *12*, 9–18.

297. Zhang, R., Taucer, A.I., Gashev, A.A., Muthuchamy, M., Zawieja, D.C., and Davis, M.J. (2013). Maximum shortening velocity of lymphatic muscle approaches that of striated muscle. Am. J. Physiol. Heart Circ. Physiol. *305*, H1494-1507.

298. Zhang, X., Anderson, J.W., and Fedida, D. (1997). Characterization of Nifedipine Block of the Human Heart Delayed Rectifier, hKv1.5. J Pharmacol Exp Ther *281*, 1247–1256.

299. Zhao, Y., Londono, P., Cao, Y., Sharpe, E.J., Proenza, C., O'Rourke, R., Jones, K.L., Jeong, M.Y., Walker, L.A., Buttrick, P.M., et al. (2015). High-efficiency reprogramming of fibroblasts into cardiomyocytes requires suppression of pro-fibrotic signalling. Nat Commun *6*, 8243.

300. Zhong, X., Liu, J.R., Kyle, J.W., Hanck, D.A., and Agnew, W.S. (2006). A profile of alternative RNA splicing and transcript variation of CACNA1H, a human T-channel gene candidate for idiopathic generalized epilepsies. Hum. Mol. Genet. *15*, 1497–1512.

301. Zolla, V., Nizamutdinova, I.T., Scharf, B., Clement, C.C., Maejima, D., Akl, T., Nagai, T., Luciani, P., Leroux, J.-C., Halin, C., et al. (2015). Aging-related anatomical and biochemical changes in lymphatic collectors impair lymph transport, fluid homeostasis, and pathogen clearance. Aging Cell *14*, 582–594.

302. Zuther, J.E. (2009). Lymphedema Management: The Comprehensive Guide for Practitioners (Thieme).

303. Zweifach, B.W., and Prather, J.W. (1975). Micromanipulation of pressure in terminal lymphatics in the mesentery. Am. J. Physiol. *228*, 1326–1335.

304. "Lymphedema and lymphatic diseases affect millions and concern us all" http://lymphaticnetwork.org/living-with-lymphedema/lymphedema-and-lymphatic-diseases-affect-millions-and-concern-us-all/. Accessed January 17 2017.

305. "TTA-A2, a blocker of T-type Cav channels" http://www.alomone.com/p/tta-a2/t-140/7. Accessed January 17 2017.

Title: Some consequences of capillary permeability to macromolecules: Starling's hypothesis reconsidered

Author: E. M. Renkin

Publication: Am J Physiol- Heart and Circulatory Physiology

Publisher: The American Physiological Society

Date: May 1, 1986

Permission Not Required

Permission is not required for this type of use.

JOHN WILEY AND SONS LICENSE TERMS AND CONDITIONS

Dec 27, 2016

This Agreement between Kim To ("You") and John Wiley and Sons ("John Wiley and Sons") consists of your license details and the terms and conditions provided by John Wiley and Sons and Copyright Clearance Center.

License Number	4017300994376
License date	Dec 27, 2016
Licensed Content Publisher	John Wiley and Sons
Licensed Content Publication	Journal of Physiology
Licensed Content Title	The impact of splice isoforms on voltage-gated calcium channel α1 subunits
Licensed Content Author	Karin Jurkat-Rott,Frank Lehmann-Horn
Licensed Content Date	Feb 1, 2004
Licensed Content Pages	11
Type of use	Dissertation/Thesis
Requestor type	University/Academic
Format	Electronic
Portion	Figure/table
Number of figures/tables	1
Original Wiley figure/table number(s)	Figure 1
Will you be translating?	No
Title of your thesis / dissertation	Role of T-type Ca channels in the lymphatic pacemaking
Expected completion date	Feb 2017
Expected size (number of pages)	200
Requestor Location	Kim To 1 Hospital Dr. COLUMBIA, MO 65201 United States Attn: Kim To
Publisher Tax ID	EU826007151
Billing Type	Invoice
Billing Address	Kim To 1 Hospital Dr. COLUMBIA, MO 65201

ELSEVIER LICENSE
TERMS AND CONDITIONS

Dec 27, 2016

This Agreement between Kim To ("You") and Elsevier ("Elsevier") consists of your license details and the terms and conditions provided by Elsevier and Copyright Clearance Center.

License Number	4017310146709
License date	Dec 27, 2016
Licensed Content Publisher	Elsevier
Licensed Content Publication	Trends in Pharmacological Sciences
Licensed Content Title	Use of transgenic mice to study voltage-dependent Ca2+ channels
Licensed Content Author	James N. Muth,Gyula Varadi,Arnold Schwartz
Licensed Content Date	1 October 2001
Licensed Content Volume Number	22
Licensed Content Issue Number	10
Licensed Content Pages	7
Start Page	526
End Page	532
Type of Use	reuse in a thesis/dissertation
Intended publisher of new work	other
Portion	figures/tables/illustrations
Number of figures/tables/illustrations	1
Format	both print and electronic
Are you the author of this Elsevier article?	No
Will you be translating?	No
Order reference number	
Original figure numbers	1
Title of your thesis/dissertation	Role of T-type Ca channels in the lymphatic pacemaking
Expected completion date	Feb 2017
Estimated size (number of pages)	200
Elsevier VAT number	GB 494 6272 12
Requestor Location	Kim To 1 Hospital Dr.

ELSEVIER LICENSE
TERMS AND CONDITIONS

Dec 27, 2016

This Agreement between Kim To ("You") and Elsevier ("Elsevier") consists of your license details and the terms and conditions provided by Elsevier and Copyright Clearance Center.

License Number	4017310146709
License date	Dec 27, 2016
Licensed Content Publisher	Elsevier
Licensed Content Publication	Trends in Pharmacological Sciences
Licensed Content Title	Use of transgenic mice to study voltage-dependent Ca2+ channels
Licensed Content Author	James N. Muth,Gyula Varadi,Arnold Schwartz
Licensed Content Date	1 October 2001
Licensed Content Volume Number	22
Licensed Content Issue Number	10
Licensed Content Pages	7
Start Page	526
End Page	532
Type of Use	reuse in a thesis/dissertation
Intended publisher of new work	other
Portion	figures/tables/illustrations
Number of figures/tables/illustrations	1
Format	both print and electronic
Are you the author of this Elsevier article?	No
Will you be translating?	No
Order reference number	
Original figure numbers	1
Title of your thesis/dissertation	Role of T-type Ca channels in the lymphatic pacemaking
Expected completion date	Feb 2017
Estimated size (number of pages)	200
Elsevier VAT number	GB 494 6272 12
Requestor Location	Kim To 1 Hospital Dr.

JOHN WILEY AND SONS LICENSE TERMS AND CONDITIONS

Jan 11, 2017

This Agreement between Kim To ("You") and John Wiley and Sons ("John Wiley and Sons") consists of your license details and the terms and conditions provided by John Wiley and Sons and Copyright Clearance Center.

License Number	4025790090334
License date	Jan 11, 2017
Licensed Content Publisher	John Wiley and Sons
Licensed Content Publication	Journal of Physiology
Licensed Content Title	Distinct roles of L- and T-type voltage-dependent Ca2+ channels in regulation of lymphatic vessel contractile activity
Licensed Content Author	Stewart Lee,Simon Roizes,Pierre-Yves von der Weid
Licensed Content Date	Oct 30, 2014
Licensed Content Pages	19
Type of use	Dissertation/Thesis
Requestor type	University/Academic
Format	Print and electronic
Portion	Figure/table
Number of figures/tables	8
Original Wiley figure/table number(s)	Figure 8
Will you be translating?	No
Title of your thesis / dissertation	Role of T-type Ca channels in the lymphatic pacemaking
Expected completion date	Feb 2017
Expected size (number of pages)	200
Requestor Location	Kim To 1 Hospital Dr. COLUMBIA, MO 65201 United States Attn: Kim To
Publisher Tax ID	EU826007151
Billing Type	Invoice
Billing Address	Kim To 1 Hospital Dr. COLUMBIA, MO 65201

VITA

Kim To received a Pharmacy degree in Ho Chi Minh City, Vietnam. She then obtained a Master's degree in Angers, France. She joined the PhD program in the Department of Medical Pharmacology and Physiology at the University of Missouri, in the USA. In Dr. Michael Davis' laboratory, she had the opportunity to study about the lymphatic vessels. She plans to graduate in May 2017. After graduation, she hopes to be able to apply the skills and experience in her next career move.